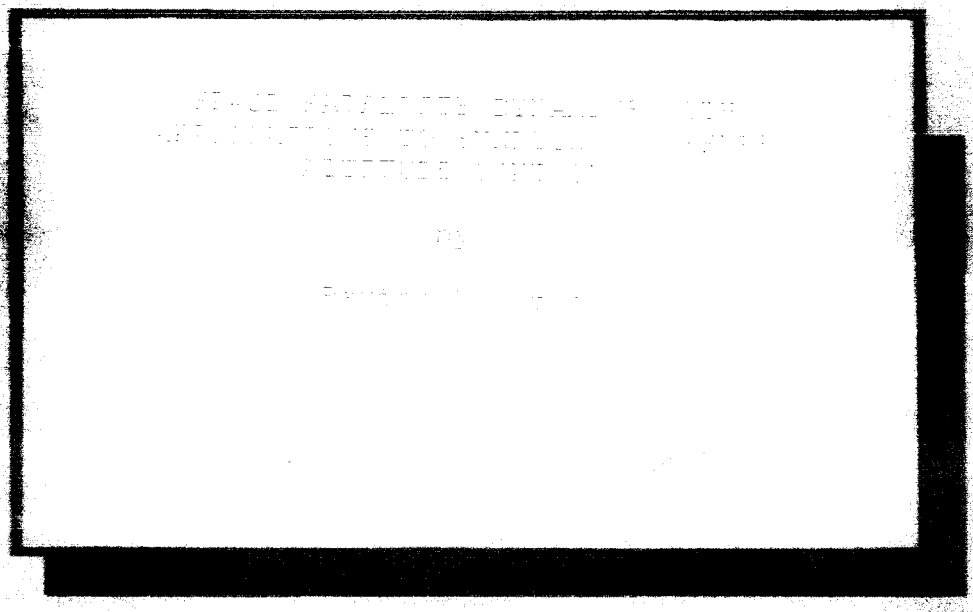

CENTER FOR SPACE RESEARCH
MASSACHUSETTS INSTITUTE OF TECHNOLOGY

SPACE SATELLITE DYNAMICS WITH APPLICATIONS TO SUNLIGHT PRESSURE ATTITUDE CONTROL

by

Barton W. Stuck

CSR T-72-2 June 1972

SPACE SATELLITE DYNAMICS WITH APPLICATIONS TO SUNLIGHT PRESSURE ATTITUDE CONTROL

by

Barton William Stuck

Submitted to the Department of Electrical Engineering on May 19, 1972 in partial fulfillment of the requirements for the Degree of Doctor of Science.

ABSTRACT

A research program into three aspects of space satellite dynamics has been carried out.

First, a four-dimensional space-time formulation of Newtonian mechanics is developed. This theory allows a new physical interpretation of the conservation theorems of mechanics first derived rigorously by Noether. The formulation has turned out to be similar to that in a forgotten 1923 paper by E. Cartan. However, the work presented here offers much greater physical insight into the underlying mathematical structure of Newtonian mechanics than that of Cartan.

Second, a new concept for estimating the three angles which specify the orientation in space of a rigid body is presented. Two separate methods for implementing this concept are discussed, one based on direction cosines, the other on quaternions. Two examples are discussed: constant orientation in space, and constant rate of change of the three angles with time. The behavior of each method in the absence of noise is discussed. Fokker-Planck equations are derived for the aposteriori probability density functions for estimation error in the presence of noise. Steady state error statistics for the case of constant rate of change of the three angles with time for a quaternion implementation are explicitly derived.

Third, two synchronous equatorial orbit communication satellite designs which use sunlight pressure to control their attitude are analyzed. Each design is equipped with large reflecting surfaces, called solar sails, which can be canted in different directions to generate torques to correct pointing errors. The total equations of motion for each design are derived, and then linearized about a nominal trajectory; a theoretical analysis of the linearized equations is carried out. A specific control law is discussed. Disturbance torques are shown to be negligible compared to attitude control torques. Computer simulation of the total equations of motion verified the theoretical analysis of the linearized equations.

New directions in space satellite dynamics research are sketched.

THESIS SUPERVISOR: John V. Harrington
TITLE: Professor of Electrical Engineering
Professor of Aeronautics and Astronautics

ACKNOWLEDGMENTS

It is a pleasure to acknowledge the many helpful comments and suggestions made by my thesis supervisor Professor John V. Harrington and the thesis readers Professor Roger Brockett and Professor Arthur Baggeroer. Their comments and suggestions were the most valuable aspect of my graduate education.

In particular, it was at the suggestion of Professor Harrington that solar pressure space satellite attitude control dynamics were investigated. I am especially grateful to him for the tremendous freedom allowed throughout this program to pursue many interesting side issues indirectly related to this problem. Professor Brockett suggested applying modern mathematical disciplines such as differential geometry and Lie groups and Lie algebras to problems arising in space satellite dynamics. Professor Baggeroer was extremely helpful in pointing out all the detailed problems that must be carefully defined and explored in estimating the orientation in space of a satellite. All of these gentlemen were very generous with their own time, constantly being available on the spur of a moment to thrash out new ideas.

Computer time was provided by the M.I.T. Laboratory for Nuclear Science. Computer programming assistance was provided by the computer programming staff of the Laboratory for Nuclear Science, as well as the M.I.T. Computation Center. Dr. Pete Smith of the M.I.T. Lincoln Laboratory had several very helpful suggestions related to the computer simulation of the dynamics of the two space satellites described in Chapter Four.

The M.I.T. Electrical Engineering Department provided financial support throughout this research program in the form of a Teaching Assistantship, except for the summer of 1971 and the spring term of 1972, when I held an N.S.F. Traineeship.

TABLE OF CONTENTS

LIST OF FIGURES

Notation

A_k	Surface Area of Face k of antenna k = 1, . . . , 6
$\underline{A}$	Linear Time-Invariant System 3 x 3 Feedback Gain Matrix
a_k	Cant Angle of Solar Sail k k=1, . . . , 6
$\underline{a}_s$	Deterministic Roll-Pitch-Yaw Angles . . . (s_x, s_y, s_z)
$\underline{a}_n$	Random Process Roll-Pitch-Yaw Angles . . . (n_x, n_y, n_z)
$\underline{a}_r$	Received Roll-Pitch-Yaw Angles . . . $(x_r, y_r, z_r) = \underline{a}_s + \underline{a}_n$
$\underline{a}$	Vector used to Generate Roll-Pitch-Yaw Angle Estimates . . . (x, y, z)
$\underline{a}$	Roll-Pitch-Yaw Angle Estimates . . . (x, y, z)
α	Angle Between Fixed +x-Axis and Instantaneous Axis of Rotation
B	Absorptivity of all Antenna Surfaces
$\underline{B}$	Error Amplification Matrix
b_k	Pitch Angle of Solar Sail k k=1, . . . , 6
β	Angle Between Fixed +y-Axis and Instantaneous Axis of Rotation
c	Speed of Light in Vacuum
γ	Angle Between Fixed +z-Axis and Instantaneous Axis of Rotation
$\underline{D}_i^b$	Direction Cosine Matrix from Body-Fixed to Inertial Axes
$\underline{D}_b^e$	Direction Cosine Matrix from Earth-Pointing to Body-Fixed Axes
$\underline{D}_s^e$	Direction Cosine Matrix from Earth-Pointing to Sun-Pointing Axes
$\underline{D}_{nom}^I$	Design I Nominal Direction Cosine Matrix
$\underline{D}_{nom}^{II}$	Design II Nominal Direction Cosine Matrix
$\underline{D}_r$	Received or Observed Direction Cosine Matrix
$\underline{D}$	Estimate of $\underline{D}_r$

$\underline{d}$	Difference between Actual and Estimated Angles... $(d_x, d_y, d_y) = \underline{d} = \underline{a}_s - \underline{\hat{a}}$
$\underline{\delta}$	Perturbations away from Steady State Angle Estimates... $(\delta x, \delta y, \delta z)$
d_{ij}	Element in Row i, Column j of Direction Cosine Matrix $\underline{D}$
$\underline{E}$	Direction Cosine Error Matrix... $\underline{D}_r \underline{D}^T$
$\underline{E}'$	Direction Cosine Error Matrix, Relating Earth-Pointing Axes to Actual Antenna Fixed Axes
	Emissivity of a Surface
	Rotational Errors about x, y, z Axes = (e_x, e_y, e_z)
	Rotational Errors about Actual Antenna-Fixed Axes with Respect to Earth-Pointing Axes
$\underline{e}'$	Demodulated and Low-Pass-Filtered Phase Estimation Errors
$\underline{e}_1(kT)$	Discrete Samples of Satellite Rotational Errors with Respect to Nominal Sun-Pointing Axes = $(e_x(kT), e_y(kT), e_z(kT))$ $k=1,2,...$
$\underline{e}_2(kT)$	Discrete Samples of Derivative of $\underline{e}_1(kT)$
$\underline{e}_3(kT)$	Discrete Samples of Derivative of $\underline{e}_2(kT)$
$\underline{F}$	Forces = (F_x, F_y, F_z)
$\underline{f}$	Frequencies or Rates of Change of $\underline{a}_s$ with Respect to Time = (f_x, f_y, f_z)
h	Distance Between Solar Panels and Satellite Center of Mass
I	Intensity of Sunlight in Equatorial Synchronous Earth Orbit
$\hat{i}$	X-Axis Unit Quaternion
$\underline{I}_I$	Total Inertia Tensor of Design I
$\underline{I}_{II}$	Total Inertia Tensor of Design II
$\underline{I}_a$	Antenna Inertia Tensor in Antenna-Fixed Axes
$\underline{I}_{ab}$	Antenna Inertia Tensor in Body-Fixed Axes

$\underline{I}_{pm}$ Principal Axis Solar Panel Inertia Tensor

$\underline{I}_{pk}$ Center of Mass of Solar Panel k (k=1,2) Inertia Tensor with Respect to Satellite Center of Mass

$\underline{I}_{p}$ Solar Panel Inertia Tensor

$\underline{I}_{sat}$ Satellite Inertia Tensor

$\hat{j}$ Y-Axis Unit Quaternion

$\hat{k}$ Z-Axis Unit Quaternion

$\underline{K}$ Amplification Gains of $\underline{e}_2(kT) = (k_x, k_y, k_z)$

$\underline{L}_{x}$ 3 x 3 Skew Symmetric Matrix Associated with x-Axis Rotations

$\underline{L}_{y}$ 3 x 3 Skew Symmetric Matrix Associated with y-Axis Rotations

$\underline{L}_{z}$ 3 x 3 Skew Symmetric Matrix Associated with z-Axis Rotations

L Lagrangian

l_s Distance from Point where Solar Sail is Attached to Solar Panel to Sail Center of Pressure

M_{sat} Total Mass of Satellite

$\underline{N}_{sails}$ Solar Sail Torque = (N_x, N_y, N_z)

$\underline{N}_{ant \rightarrow panel}$ Reaction Torque of Antenna on a Solar Panel

$\underline{N}_{panel \rightarrow ant}$ Reaction Torque of a Solar Panel on Antenna

$\underline{N}^a_{body}$ Sail Torque in Body-Fixed Axes for Correcting x-Axis Rotational Errors

$\underline{N}^b_{body}$ Sail Torque in Body-Fixed Axes for Correcting y-Axis Rotational Errors

$\underline{N}^c_{body}$ Sail Torque in Body-Fixed Axes for Correcting z-Axis Rotational Errors

$\underline{N}^e_{gravity\ gradient}$ Gravity Gradient Torques in Earth-Pointing Axes

$N_x/2$ x-Axis Amplification Noise Spectral Density Height

$N_y/2$ y-Axis Amplification Noise Spectral Density Height

$N_z/2$ z-Axis Amplification Noise Spectral Density Height

$\underline{n}$ Additive Amplification Noise... (n_x, n_y, n_z)

$\underline{n}_k$ Unit Normal Vector to Solar Sail k k=1,...6

$\underline{\varphi}_r$ Phase Angles of $\underline{a}_r$, $\underline{a}_r = \underline{f}t + \underline{\varphi}_r$, $\underline{\varphi}_r = (\varphi_{rx}, \varphi_{ry}, \varphi_{rz})$

$\hat{\underline{\varphi}}$ Phase Angle Estimates of $\underline{\varphi}_r$, $\hat{\underline{\varphi}} = (\hat{\varphi}_x, \hat{\varphi}_y, \hat{\varphi}_z)$

$\underline{p}$ Linear Momentum of Point Mass = (p_x, p_y, p_z, m)

p Aposteriori Probability Density Function of $\underline{a}$

$\underline{q}$ Quaternion... ai+bj+ck+d(1)

q^+ Quaternion Conjugate...-ai-bj-ck+d(1)

$\underline{q}_r$ Received Quaternion

$\underline{q}$ Estimated Quaternion

r Radius of Gyration of Solar Panels in Design I About Shaft

$\underline{s}$ Sum of $\underline{a}_r$ and $\underline{a}$, $\underline{a}_r + \hat{\underline{a}} = (s_x, s_y, s_z)$

$\underline{W}_i^b$ Skew Symmetric Matrix Representation of $\underline{w}_i^b$

$\underline{W}_b^a$ Skew Symmetric Matrix Representation of $\underline{w}_b^a$

$\underline{W}_{nom}$ Skew Symmetric Matrix Representation of $\underline{w}_{nom}$

$\underline{W}$ Skew Symmetric Matrix Representation $\underline{w}$

$\underline{w}$ Angular Velocity (w_x, w_y, w_z)

$\underline{w}_p$ Solar Panel Angular Velocity

$\underline{w}_b^a$ Antenna Angular Velocity in Body-Fixed Axes

$\underline{w}_{nom}$ Nominal Satellite Angular Velocity

$\underline{w}_i^b$ Angular Velocity of Satellite with Respect to Inertial Coordinates

w Amount of Rotation about Instantaneous Axis of Rotation

Vectors are denoted by an underlined lower case letter, e.g., $\underline{x}$, and are assumed to be column vectors. Matrices are denoted by an underlined upper case letter, e.g., $\underline{W}$, with W_{ij} representing the element in row i, column j of $\underline{W}$. All vectors and matrices appearing here have real valued elements i.e., elements in R^1.

Chapter One

Introduction

1.1. Introductory Remarks

In 1958 the first communication satellite (SCORE) was placed in earth orbit. Since that time, dozens of communication satellites have been launched into space and are currently being used for commercial and governmental communication between points scattered across the face of the earth.

One fundamental problem in communication satellite design is control of satellite orientation. This report describes the results of a three fold research program into space satellite dynamics. The first and second phases deal with aspects of deterministic and stochastic rigid body mechanics, respectively. The third phase builds on the first two, and involves the analysis of two specific satellite designs which use sunlight pressure for attitude control.

1.2. Scope of the Research Program

1.2.1. Theoretical Rigid Body Mechanics

The first phase of the research program was devoted to applications of differential geometry, tensor algebra and calculus, and Lie groups and Lie algebras to problems in space satellite dynamics. The main result was the development of a four-dimensional space-time formulation of Newtonian mechanics. This theory is a complete self-consistent set of ten equations; four of the equations deal with linear momentum, while the other six are concerned with angular momentum. Many mechanics treatises often ignore three of the angular momentum equations; this is not surprising, since information

contained in these three equations is also contained in the linear momentum equations, making these equations to a certain extent redundant. However, by including these three additional equations, a new physical interpretation of the ten conservation theorems of mechanics due to Noether arises in a very natural simple manner. Noether's approach to the conservation theorems was based on a Lagrangian formulation of mechanics plus some subtle variational arguments; the same theorems follow quite naturally and simply by formulating Newtonian mechanics in space-time. No attempt is made to achieve mathematical rigor in developing this theory of mechanics; rather, the emphasis is on physical insight and intuitive arguments, coupled with the requirement the theory be consistent with experimental observations.

1.2.2. Estimation Theory

The second phase of the research program touched on a problem in estimation theory: given noisy measurements of the orientation in space of a rigid body, estimate the three angles which define this orientation.

Is attitude estimation really a problem in space satellite dynamics? Yes, in fact in many present day satellites, attitude estimation is the chief limitation in controlling the spatial orientation of these designs; the reader should consult the bibliography for specific examples. One approach to attitude estimation is to linearize the equations of motion about a nominal trajectory, and then apply linear filtering theory to the linearized equations of motion. The actual implementation of this approach can be very complex. In addition, this approach ignores the structure implicit in the equations of motion which describe how orientations in space change with time.

The method presented here is analogous to a phase-locked loop, in that it estimates the three angles defining the spatial orientation of a rigid body using an estimation procedure resembling that of a phase-locked loop. This method takes advantage of the structure implicit in the equations of motion, and for the two examples considered here (constant orientation in space, and constant rate of change of the angles with time) is quite simple to implement compared to an approach based on linearization of the equations about a nominal trajectory.

The chief question left unanswered is what is the optimal or best method for processing noisy sensor measurements in order to estimate spatial orientation. The method presented here works well for the two examples considered; however, it is still not clear how well the optimal estimation procedure would perform compared to the method discussed in this report, and what if anything is lost using the method described here or a method based on Kalman filtering.

1.2.3. Solar Pressure Attitude Control

The attitude control dynamics of two specific satellites which use sunlight pressure to generate attitude control torques are analyzed in the last phase of the research program.

Why use sunlight pressure for attitude control? At synchronous altitude the largest disturbance torque on many present day communication satellites is due to sunlight pressure (NASA(63)); since it is such a nuisance, perhaps it can be used to aid rather than hinder attitude control. By canting large reflecting surfaces, called solar sails here, in specified directions, it appears to be

possible to control the orientation of two specific designs with as great an accuracy as any other presently existing method.

All of these statements are based on paper-and-pencil analysis plus extensive computer simulation of each design. Clearly, this is no substitute for an actual test in space of these ideas. Some attempt was made to include technological constraints into the designs described here, and all computer simulations were carried out with hopefully realistic numbers for all parameters; however, many engineering problems were ignored, on the grounds that they did not critically affect the attitude control dynamics of each design. Thus, the research program has merely indicated that solar pressure attitude control of synchronous orbit communication satellites might be feasible, but the question still deserves more discussion.

1.3. Background

The reader is referred to the bibliography for material that was found to be especially helpful in one or more aspects of the present research program.

In particular, Goldstein(10) provides sufficient background in classical rigid body mechanics, while Abraham(1) provides a much more modern treatment of mechanics. Nelson(20), Flanders(7), Greub(11), and Warner(27) provide sufficient background material in tensor algebra, as it is used in the first part of this research program.

Van Trees(47), Viterbi(48) and Jazwinski(39) are excellent references in estimation theory and phase-locked-loop techniques. Ito(36) and McKean(41,44) provide a more modern and mathematically rigorous approach to the characterization of noisy measurements of spatial orientation.

To gain some idea of present day attitude control techniques that are used, the reader is referred to Likins(58), Fleischer(55) and Much et al(62). The NASA publication on radiation pressure torques, including both sunlight pressure torques as well as thermal torques, is a good introduction to the practical aspects of solar pressure attitude control disturbances(NASA(63)).

Chapter Two

Four-Dimensional Space-Time Newtonian Mechanics

2.1 Introduction

In this chapter, a novel, simple and elegant space-time formulation of Newtonian mechanics is developed. The main mathematical tool used to develop this theory is the exterior product, a generalization of the cross product between two vectors from 3 to 4 dimensions. Using this tool, a complete and self-consistent set of equations of motion for a single particle are developed; four equations deal with time derivatives of linear momentum, while the other six are time derivatives of angular momentum. The first four, Newton's laws, are the fundamental equations of motion; the six angular momentum equations follow as a natural consequence of the four linear momentum equations.

The formulation presented here offers a new simple physical interpretation of the ten conservation theorems of mechanics, theorems dealing with ten quantities that do not change with time when no forces are present. These theorems were shown by Noether(21) to be the only possible conservation theorems; however, her arguments, based on a Lagrangian formulation of mechanics, involve some subtle variational techniques viz.a.viz. the ten independent parameters governing transformations from one space-time coordinate frame to another. On the other hand, these ten theorems follow quite directly and simply from the ten equations to be presented here.

The theory is complete and self-consistent, in that no more equations of motion can be found than those presented here, provided the only

mathematical operations allowed are the exterior product and differentiation with respect to time. Many treatises on mechanics hav overlooked three of the angular momentum equations to be presented here, and concentrated on the four fundamental linear momentum equations, often leaving the impression these three angular momentum equations do not even exist. After this work had been completed, the author searched the literature and was able to find only one forgotten paper by Cartan(3) which even intimated there might be ten equations of motion for Newtonian mechanics (see Appendix). However, Cartan's work is very different in spirit from that found here. In this chapter, a series of intuitive and physical arguments are presented to develop a natural and correct approach to Newtonian mechanics, at the expense of mathematical rigor. Cartan's treatment contains more mathematical rigor, but is missing much of the physical flavor found in the arguments here; moreover, he is extremely terse on why there should be ten equations of motion for Newtonian mechanics. Since the three forgotten angular momentum equations contain no new information than that found in the four linear momentum equations, it is perhaps not surprising they have been forgotten.

It is straightforward to extend these equations to include effects due to special relativity in a natural manner, unlike other relativistic theories of mechanics known to the author; this issue will be dealt with elsewhere.

2.2. Kinematics of a Single Particle

This section is concerned with describing the position of a single particle, in space and time with respect to a reference coordinate. Space and time together make up the arena in which the dynamics of the single particle can take place. The particle is assumed to have positive mass M, but occupies such an infinitesimal volume of space at any instant of time that it can be considered a point in space-time with mass, or a point mass. Four independent numbers are needed to describe the position in space and time of the particle: three to specify its position, in space, and one to describe the instant of time the particle is at that position.

An interesting question now arises: given the space-time coordinates of a particle in a reference coordinate frame, called frame A (arbitrarily), how do these coordinates relate to the particle's coordinates in a different reference frame, labeled frame B (again arbitrarily)? It is assumed both frames have a standard orthonormal rectangular right-handed set of basis vectors for the three space coordinates; the unit vector associated with time is assumed orthogonal to the three space basis vectors. The relationship between the particle's coordinates in frames A and B is (Goldstein(10)):

$$\begin{bmatrix} x_B \\ y_B \\ z_B \\ t_B \end{bmatrix} = \begin{bmatrix} d_{11} & d_{12} & d_{13} & v_x \\ d_{21} & d_{22} & d_{23} & v_y \\ d_{31} & d_{32} & d_{33} & v_z \\ 0 & 0 & 0 & 1 \end{bmatrix} \begin{bmatrix} x_A \\ y_A \\ z_A \\ t_A \end{bmatrix} + \begin{bmatrix} x_o \\ y_o \\ z_o \\ t_o \end{bmatrix}$$

where (x_A, y_A, z_A, t_A) and (x_B, y_B, z_B, t_B) are the coordinates of the point mass in space-time in frames A and B respectively.

The physical interpretation of the various parameters in this coordinate transformation is now discussed:

i) (x_o, y_o, z_o, t_o)--when $(x_A = 0,\ y_A = 0,\ z_A = 0,\ t_A = 0)$, then $(x_B = x_o,\ y_B = y_o,\ z_B = z_o,\ t_B = t_o)$, where (x_o, y_o, z_o, t_o) are all assumed constant. Thus, the space-time origin of frame B is displaced from the space-time origin of frame A by (x_o, y_o, z_o, t_o)

ii) (v_x, v_y, v_z)--when $(x_A = 0,\ y_A = 0,\ z_A = 0,\ t_A = t_A)$, then $(x_B = x_o + v_x t_A,\ y_B = y_o + v_y t_B,\ z_B = z_o + v_z t_z,\ t_B = t_A + t_o)$. This means the spatial part of the space-time origin of frame B is displaced from the spatial component of the space-time of frame A by the sum of (x_o, y_o, z_o) and $(v_x t_A, v_y t_A, v_z t_B)$. The first term is part of the displacement discussed in i); the second term is called a translation. The time components t_A and t_B are related by a displacement in time, t_o.

Unlike (x_o, y_o, z_o, t_o), (v_x, v_y, v_z) are assumed to be functions of time.

iii) $(d_{11}, d_{12}, d_{13}, d_{21}, d_{22}, d_{23}, d_{32}, d_{33})$--these nine parameters have six constraints associated with them:

$$\begin{bmatrix} d_{11} & d_{12} & d_{13} \\ d_{21} & d_{22} & d_{23} \\ d_{31} & d_{32} & d_{33} \end{bmatrix} \begin{bmatrix} d_{11} & d_{21} & d_{31} \\ d_{12} & d_{22} & d_{32} \\ d_{13} & d_{23} & d_{33} \end{bmatrix} = \begin{bmatrix} 1 & 0 & 0 \\ 0 & 1 & 0 \\ 0 & 0 & 1 \end{bmatrix}$$

$$\left.\begin{array}{ll} d_{11}^2 + d_{12}^2 + d_{13}^2 = 1 & d_{11}d_{21} + d_{12}d_{22} + d_{13}d_{23} = 0 \\ d_{21}^2 + d_{22}^2 + d_{23}^2 = 1 & d_{11}d_{31} + d_{12}d_{32} + d_{13}d_{33} = 0 \\ d_{31}^2 + d_{32}^2 + d_{33}^2 = 1 & d_{21}d_{31} + d_{22}d_{32} + d_{23}d_{33} = 0 \end{array}\right\} \text{six constraints}$$

where d_{11} represents the projection of a unit vector directed along frame A's x-axis onto frame B's x-axis, d_{12} the projection of a unit vector directed along frame A's y-axis onto frame B's x-axis, and so on. Since there are a total of nine parameters with six constraints, there are only three independent parameters associated the d_{ij}'s, $i, j = 1, 2, 3$. To emphasize that there are only three independent parameters, the matrix of d_{ij}'s $i\ j = 1, 2, 3$ is decomposed into the product of three matrices, each parameterized by one independent variable, each representing a rotation in space about some axis:

$$2.3)\quad \begin{bmatrix} d_{11} & d_{12} & d_{13} \\ d_{21} & d_{22} & d_{23} \\ d_{31} & d_{32} & d_{33} \end{bmatrix} = \exp(a_1 \underline{L}_1)\, \exp(a_2 \underline{L}_2)\, \exp(a_3 \underline{L}_3) \qquad \begin{matrix} -\pi < a_1, a_2, a_3 \leq \pi \\ \underline{L}_1 \neq \underline{L}_2, \underline{L}_2 \neq \underline{L}_3 \end{matrix}$$

$$\underline{L}_1, \underline{L}_2, \underline{L}_3 \in \{\underline{L}_x, \underline{L}_y, \underline{L}_z\} \qquad \underline{L}_x = \begin{bmatrix} 0 & 0 & 0 \\ 0 & 0 & -1 \\ 0 & 1 & 0 \end{bmatrix} \quad \underline{L}_y = \begin{bmatrix} 0 & 0 & 1 \\ 0 & 0 & 0 \\ -1 & 0 & 0 \end{bmatrix} \quad \underline{L}_z = \begin{bmatrix} 0 & -1 & 0 \\ 1 & 0 & 0 \\ 0 & 0 & 0 \end{bmatrix}$$

where $\mathrm{Exp}(a_k \underline{L}_k)$ $k = 1, 2, 3$ is defined as a matrix exponential.

Thus, the ten independent variables, $a_1, a_2, a_3, v_x, v_y, v_z, x_o, y_o, z_o, t_o$ completely describe the relationship between space-time coordinates in frame B with respect to those of frame A.

2.3. Exterior Algebra

In order to discuss Newtonian mechanics in four dimensions, the notion of a cross product between two vectors must be extended from three to four dimensions. This extension is called an exterior product. The treatment here will concentrate on the algebraic properties of the exterior product; for much more detailed discussions of exterior algebra, the reader should consult Flanders(7), Warner(27), Nelson(20) or Greub(11). Exterior products will be defined in very general terms with respect to a finite dimensional vector space; the special case of a four dimensional vector space, space-time, will be used as a concrete non-trivial illustration of these general properties.

Let V be a real n-dimensional vector space, with an orthonormal set of basis vectors $\{dx_1, \ldots, dx_n\}$ with respect to some coordinate frame.

Associated with this vector space is a space of zero-dimensional vectors, the space of all real scalar functions of the n coordinates (usually these functions are assumed to be continuous and infinitely differentiable, but these properties will not be needed here). This zero-dimensional vector space is denoted $\Lambda^0(V)$, and has a basis vector $\{1\}$. Next, there exists an n-dimensional vector space, with the same basis as V, denoted $\Lambda^1(V)$. Third, there exists an $\frac{1}{2}\, n(n-1)$ dimensional vector space associated with V, denoted $\Lambda^2(V)$, consisting of all vectors $v \in \Lambda^2(V)$ of the form

$$2.4) \qquad v = \sum_{i=1}^{n} \sum_{j=1}^{n} v_{ij} \, (dx_i \wedge dx_j) \qquad v_{ij} \in \mathbb{R}^1$$

where "$\wedge$" is the exterior product. The exterior product must obey the following four constraints:

i) $(c_1 v_1 + c_2 v_2) \wedge u = c_1 (v_1 \wedge u) + c_2 (v_2 \wedge u)$

ii) $v \wedge (d_1 u_1 + d_2 u_2) = d_1 (v \wedge u_1) + d_2 (v \wedge u_2)$

iii) $v \wedge v = 0$

iv) $v \wedge u + u \wedge v = 0$

$$v = \sum_{i=1}^{n} v_i dx_i \,, \quad v_1 = \sum_{i=1}^{n} v_i^1 dx_i \,, \quad v_2 = \sum_{i=1}^{n} v_i^2 dx_i \qquad v_i^1, v_i^2, v_i \in \mathbb{R}^1 \;\; \forall i, i=1 \ldots n$$

$$u = \sum_{j=1}^{n} u_j dx_j \,, \quad u_1 = \sum_{j=1}^{n} u_j^1 dx_j \,, \quad u_2 = \sum_{j=1}^{n} u_j^2 dx_j \qquad u_j^1, u_j^2, u_j \in \mathbb{R}^1 \;\; \forall j, j=1 \ldots n$$

Thus, a basis for $\Lambda^2(V)$ is $\{dx_i \wedge dx_j \,;\, i,j = 1, \ldots n\}$ subject to the constraints of exterior multiplication; there are $\frac{1}{2}\, n(n-1)$ vectors in this basis for $\Lambda^2(V)$.

By induction, the above rules can be extended to vector spaces $\Lambda^p(V)$, where $2 \leq p \leq n$. Each vector v in $\Lambda^p(V)$ can be written as

$$2.5) \quad v = \underbrace{\sum_{i=1}^{n} \sum_{j=1}^{n} \cdots \sum_{l=1}^{n}}_{p \text{ SUMS}} v_{ij\cdots l} \underbrace{dx_i \wedge dx_j \wedge \cdots \wedge dx_l}_{p \text{ PRODUCTS}}$$

Vectors in $\Lambda^p(V)$ are subject to the following conditions

i) $(av + bu) \wedge v_2 \wedge \cdots \wedge v_p = a(v \wedge v_2 \wedge \cdots \wedge v_p) + b(v \wedge v_2 \wedge \cdots \wedge v_p)$

$v_1 \wedge (av + bu) \wedge v_3 \wedge \cdots \wedge v_p = a(v_1 \wedge v \wedge v_3 \wedge \cdots \wedge v_p) + b(v_1 \wedge v \wedge v_3 \wedge \cdots \wedge v_p)$

$v_1 \wedge v_2 \wedge \cdots \wedge v_{p-1} \wedge (av + bu) = a(v_1 \wedge \cdots \wedge v_{p-1} \wedge v) + b(v_1 \wedge \cdots \wedge v_{p-1} \wedge u)$

ii) $v_1 \wedge \cdots \wedge v_p = 0$ IF FOR SOME PAIR OF INDICES $i \neq j$, $v_i = v_j$ FOR $i, j = 1 \cdots p$

iii) $v_1 \wedge \cdots \wedge v_p$ CHANGES SIGN IF FOR SOME PAIR OF ADJACENT v_i's, ARE INTERCHANGED

where $u, v, v_1, \ldots, v_p \in \Lambda^1(V)$ $\quad a, b \in \mathbb{R}^1$

As an example, consider the four dimensional space-time vector space discussed earlier, with an orthonormal rectangular set of basis vectors, {dx, dy, dz, dt}. Associated with this vector space are a total of five vector spaces, defined according to the exterior multiplication rules of exterior algebra:

Vector Space	Basis Vectors
$\Lambda^0(V)$	1
$\Lambda^1(V)$	dx, dy, dz, dt
$\Lambda^2(V)$	$dy \wedge dz, dz \wedge dx, dx \wedge dy, dt \wedge dx, dt \wedge dy, dt \wedge dz$
$\Lambda^3(V)$	$dy \wedge dz \wedge dt, dz \wedge dx \wedge dt, dx \wedge dy \wedge dt, dx \wedge dy \wedge dz$
$\Lambda^4(V)$	$dx \wedge dy \wedge dz \wedge dt$

The physical interpretation of these basis vectors is of interest:

i) $\Lambda^0(V)$ -- $\{1\}$ is a scalar real number, with neither magnitude nor direction in space-time

ii) $\Lambda^1(V)$ -- $\{dx, dy, dz, dt\}$ are basis vectors with both magnitude and direction, e.g., dx has a "one-dimensional magnitude" of +1 in the +x-direction

iii) $\Lambda^2(V)$ -- $\{dy \wedge dz, dz \wedge dx, dx \wedge dy, dt \wedge dx, dt \wedge dy, dt \wedge dz\}$ have both magnitude and direction, e.g., $dy \wedge dz$ has a "two-dimensional magnitude" of +1 in the "y-wedge-z" direction, while dt dx has a "two-dimensional magnitude" of +1 in the "t-wedge-x" direction, where "wedge" denotes exterior product and not the ordinary three dimensional vector cross product

iv) $\Lambda^3(V)$ -- $\{dy \wedge dz \wedge dt, dz \wedge dx \wedge dt, dx \wedge dy \wedge dt, dx \wedge dy \wedge dz\}$ have both magnitude and direction, e.g., $dy \wedge dz \wedge dt$ has a "three-dimensional magnitude" of +1 in the "y-wedge z-wedge-t" direction, while $dx \wedge dy \wedge dz$ has a "three-dimensional magnitude" of +1 in the "x-wedge-y-wedge-z" direction

v) $\Lambda^4(V)$ -- $\{dx \wedge dy \wedge dz \wedge dt\}$ has a "four dimensional magnitude" of +1 in the "x-wedge-y-wedge-z-wedge-t" direction.

2.4. Newtonian Space-Time Mechanics of a Single Particle

This section derives the ten space-time equations of motion of a single particle the space-time coordinates of the particle are

2.6) $\begin{bmatrix} x_o \\ y_o \\ z_o \\ t_o \end{bmatrix}$ = space-time coordinates of a single particle

The velocity of the particle is defined to be the derivative with respect to time of the space-time coordinates:

2.7) $\frac{d}{dt} \begin{bmatrix} x_o \\ y_o \\ z_o \\ t_o \end{bmatrix} \triangleq \begin{bmatrix} u_x \\ u_y \\ u_z \\ 1 \end{bmatrix}$ = velocity of a single particle

The linear momentum of the particle is defined to be its mass in times its velocity:

2.8) $m \frac{d}{dt} \begin{bmatrix} x_o \\ y_o \\ z_o \\ t_o \end{bmatrix} = \begin{bmatrix} mu_x \\ mu_y \\ mu_z \\ m \end{bmatrix} \triangleq \begin{bmatrix} p_x \\ p_y \\ p_z \\ m \end{bmatrix}$ = linear momentum of a single particle

Newton postulated that the time rate of change of the linear momentum of a single particle equals the forces acting on the particle:

2.9) $\frac{d}{dt} \begin{bmatrix} p_x \\ p_y \\ p_z \\ m \end{bmatrix} = \begin{bmatrix} F_x \\ F_y \\ F_z \\ 0 \end{bmatrix}$

Where $(F_x, F_y, F_z, 0)$ are forces acting on the x-, y-, z- and t- components of the linear momentum, respectively, and these equations assume the linear momentum and forces are computed in a special coordinate frame, an inertial frame, which is defined (albeit circularly) as a coordinate frame in which the linear momentum equations of motion can be written in the form above.

The moment about the space-time origin of the linear momentum can be found using the exterior product:

$$(x_o dx + y_o dy + z_o dz + t_o dt) \wedge (p_x dx + p_y dy + p_z dz + m dt) =$$

$$2.10) \quad (y_o p_z - z_o p_y) dy \wedge dz + (z_o p_x - x_o p_z) dz \wedge dx + (x_o p_y - y_o p_x) dx \wedge dy +$$

$$(t_o p_x - m x_o) dt \wedge dx + (t_o p_y - m y_o) dt \wedge dy + (t_o p_z - m z_o) dt \wedge dz$$

The first three terms, along $dy \wedge dz, dz \wedge dx$ and $dx \wedge dy$, are called here space-like angular momentum components, because they arise from purely spatial exterior products. The final three terms, along $dt \wedge dx, dt \wedge dy, dt \wedge dz$ are called here time-like angular momentum components, because they arise from a mixture of space-time exterior products. All six terms together make up what is called here the total angular momentum of the particle.

Using the four equations of motion for linear momentum, the time rates of change of the six angular momentum components are:

$$2.11) \quad \frac{d}{dt}(y_o p_z - z_o p_y) = u_y (m u_z) - u_z (m u_y) + y_o F_z - z_o F_y = y_o F_z - z_o F_y$$

$$2.12) \quad \frac{d}{dt}(z_o p_x - x_o p_z) = u_z (m u_x) - u_x (m u_z) + z_o F_x - x_o F_z = z_o F_x - x_o F_z$$

$$2.13) \quad \frac{d}{dt}(x_o p_y - y_o p_x) = u_x (m u_y) - u_y (m u_x) + x_o F_y - y_o F_x = x_o F_y - y_o F_x$$

$$2.14) \quad \frac{d}{dt}(t_o p_x - m x_o) = t_o F_x + (m u_x) - (m u_x) - \left(\frac{dm}{dt}\right) x_o = t_o F_x$$

2.15) $\frac{d}{dt}(t_o p_y - m y_o) = t_o F_y + (m u_y) - (m u_y) - \left(\frac{dm}{dt}\right) y_o = t_o F_y$

2.16) $\frac{d}{dt}(t_o p_z - m z_o) = t_o F_z + (m u_z) - (m u_z) - \left(\frac{dm}{dt}\right) z_o = t_o F_z$

Next, all possible exterior products of $(x_o\, dx + y_o\, dy + z_o\, dz + t_o\, dt)$ and $(p_x dx + p_y\, dy + p_z\, dz + m\, dt)$ taken three at a time are computed, and all eight such products are found to be zero. Thus, there are no further quantities than the four components of linear momentum and six components of angular momentum in mechanics, given all that is computed are exterior products of space-time vectors describing position and linear momentum, and their time derivatives.

What if no forces act on the particle? If $F_x = F_y = F_z = 0$, then all components of the linear and angular momentum are constant. Note that while it is obvious from these ten equations that quantities such as p_x or $(y_o\, p_z - z_o\, p_y)$ are now constant, it is also obvious that $(t_o\, p_x - m x_o)$ is constant; the first two constants appear in many texts on mechanics, but the last one is mentioned rarely.

Noether[21] derived these ten conserved quantities from the Lagrangian L of the particle, assuming no forces act on the particle, where

$$L = \frac{1}{2}\, m(u_x^2 + u_y^2 + u_z^2)$$

through an argument based on techniques used in calculus of variations. Recall that four number specify the position of a particle in space-time; if this position is perturbed slightly, the new position will be a function of the old position as well as the ten independent parameters defining the transformation from the old to the new position. This transformation is

2.17)
$$\begin{bmatrix} x_o \\ y_o \\ z_o \\ t_o \end{bmatrix}_{new} = \begin{bmatrix} 1 & -\Delta a_z & \Delta a_y & \Delta v_x \\ +\Delta a_z & 1 & -\Delta a_x & \Delta v_y \\ -\Delta a_y & \Delta a_x & 1 & \Delta v_z \\ 0 & 0 & 0 & 1 \end{bmatrix} \begin{bmatrix} x_o \\ y_o \\ z_o \\ t_o \end{bmatrix}_{old} + \begin{bmatrix} \Delta x \\ \Delta y \\ \Delta z \\ \Delta t \end{bmatrix}$$

assuming

$$|\Delta x| \ll 1,\ |\Delta y| \ll 1,\ |\Delta z| \ll 1,\ |\Delta t| \ll 1$$

$$|\Delta a_x| \ll 1,\ |\Delta a_y| \ll 1,\ |\Delta a_z| \ll 1$$

$$|\Delta v_x| \ll 1,\ |\Delta v_y| \ll 1,\ |\Delta v_z| \ll 1$$

Associated with each independent parameter, according to Noether, there is a conserved quantity

Parameter	Conserved Quantity
Δx	p_x
Δy	p_y
Δz	p_z
Δt	E
Δa_x	$y_o p_z - z_o p_y$
Δa_y	$z_o p_x - x_o p_z$
Δa_z	$x_o p_y - y_o p_x$
Δv_x	$t_o p_x - m x_o$
Δv_y	$t_o p_y - m y_o$
Δv_z	$t_o p_z - m z_o$

where E is the kinetic energy of the particle,

$$E = L = \frac{1}{2m}\left[p_x^2 + p_y^2 + p_z^2\right] = \frac{1}{2}m\left(u_x^2 + u_y^2 + u_z^2\right)$$

Note that since p_x, p_y, p_z and E are constant, m must be constant. Note further that E equals the Lagrangian L; Noether demanded that the ten independent parameters not perturb the Lagrangian, but due to the fact that the kinetic energy and Lagrangian are identical here, perhaps missed a more fundamental observation: m is constant, a fact that arises quite naturally from a space-time formulation of mechanics.

2.5. Space-Time Equations of Motion of a Single Rigid Body

This chapter concludes with a derivation of the ten space-time equations of motion for a single rigid body. A single rigid body may be viewed as finite collection of small bodies, each occupying a small but finite volume of space at any instant of time, and fixed rigidly with respect to all the other small bodies comprising the rigid body. "Small" in this context means the volume occupied by each body comprises many thousands of atoms of whatever substance the rigid body is made of, while at the same time this volume is much less than total volume of the rigid body. The sketch below shows a typical rigid body decomposed into N small bodies.

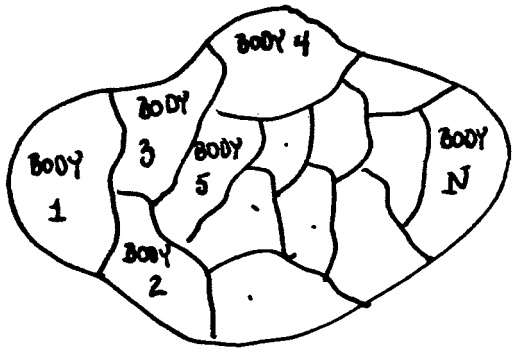

Figure 2.1
A single rigid body broken down into N rigid bodies

The space-time coordinates, in an inertial frame, of the k^{th} mass are (x_k, y_k, z_k, t_k). The equations of motion for this mass, assuming it is a point mass, are:

$$2.18) \quad \frac{d}{dt} p_{xk} = F^E_{xk} + \sum_{j=1}^{N} F^j_{xk} \, s_{jk}$$

$$2.19) \quad \frac{d}{dt} p_{yk} = F^E_{yk} + \sum_{j=1}^{N} F^j_{yk} \, s_{jk}$$

2.20) $$\frac{d}{dt} p_{zk} = F^E_{zk} + \sum_{j=1}^{N} F^j_{zk} s_{jk}$$

2.21) $$\frac{d}{dt} m_k = 0$$

2.22) $$\frac{d}{dt}(y_k p_{zk} - z_k p_{yk}) = (y_k F^E_{zk} - z_k F^E_{yk}) + \sum_{j=1}^{N} (y_k F^j_{zk} - z_k F^j_{yk}) s_{jk}$$

2.23) $$\frac{d}{dt}(z_k p_{xk} - x_k p_{zk}) = (z_k F^E_{xk} - x_k F^E_{zk}) + \sum_{j=1}^{N} (z_k F^j_{xk} - x_k F^j_{zk}) s_{jk}$$

2.24) $$\frac{d}{dt}(x_k p_{yk} - y_k p_{xk}) = (x_k F^E_{yk} - y_k F^E_{xk}) + \sum_{j=1}^{N} (x_k F^j_{yk} - y_k F^j_{xk}) s_{jk}$$

2.25) $$\frac{d}{dt}(t_k p_{xk} - m_k x_k) = t_k \left\{ F^E_{xk} + \sum_{j=1}^{N} F^j_{xk} s_{jk} \right\}$$

2.26) $$\frac{d}{dt}(t_k p_{yk} - m_k y_k) = t_k \left\{ F^E_{yk} + \sum_{j=1}^{N} F^j_{yk} s_{jk} \right\}$$

2.27) $$\frac{d}{dt}(t_k p_{zk} - m_k z_k) = t_k \left\{ F^E_{zk} + \sum_{j=1}^{N} F^j_{zk} s_{jk} \right\}$$

where

2.28) $$m_k \cdot \frac{d}{dt} \begin{bmatrix} x_k \\ y_k \\ z_k \\ t_k \end{bmatrix} = \begin{bmatrix} p_{xk} \\ p_{yk} \\ p_{zk} \\ m_k \end{bmatrix} \qquad k = 1 \ldots N$$

and

F^E_{xk}, F^E_{yk}, F^E_{zk} = x-, y-, and z-components, respectively, of external forces acting on mass k

F^{j}_{xk}, F^{j}_{yk}, F^{j}_{zk} = x-, y-, and z-components, respectively, of constraint or reaction force of mass j acting mass k

$$s_{kj} = \begin{cases} 1 & \text{if mass k is adjacent to mass j} \\ 0 & \text{if mass k is not adjacent to mass j} \end{cases}$$

If all equations for the x-component of the linear momentum are added,

$$\frac{d}{dt}\left(\sum_{k=1}^{N} p_{xk}\right) = \left(\sum_{k=1}^{N} F^{E}_{xk}\right) + \left(\sum_{k=1}^{N}\sum_{j=1}^{N} F^{j}_{xk}\, s_{jk}\right)$$

defining

2.29) $$P_x = \sum_{k=1}^{N} p_{xk}$$

2.30) $$F^{E}_{x} = \sum_{k=1}^{N} F^{E}_{xk}$$

and realizing the reaction force of mass k on mass j is equal and opposite to the reaction force of mass j on mass k,

2.31) $$F^{j}_{xk} = -F^{k}_{xj}$$

so

2.32) $$\sum_{k=1}^{N}\sum_{j=1}^{N} F^{j}_{xk}\, s_{jk} = 0$$

This equation can be written simply as

2.33) $$\frac{d}{dt} P_x = F^{E}_{x}$$

By adding up all the other equations for the linear momentum, component by components, it is easy to see

2.34) $\frac{d}{dt} p_y = F^E_y \qquad p_y \triangleq \sum_{k=1}^{N} p_{yk} \;, \qquad F^E_y \triangleq \sum_{k=1}^{N} F^E_{yk}$

2.35) $\frac{d}{dt} p_z = F^E_z \qquad p_z \triangleq \sum_{k=1}^{N} p_{zk} \;, \qquad F^E_z \triangleq \sum_{k=1}^{N} F^E_{zk}$

2.36) $\frac{d}{dt} M = 0 \qquad M = \sum_{k=1}^{N} m_k$

To proceed further, it is useful to define the center-of-mass of the body. This is a set of coordinates, $(x_{cm}, y_{cm}, z_{cm}, t_{cm})$, where

2.37) $x_{cm} \triangleq \frac{1}{M} \left\{ \sum_{k=1}^{N} m_k x_k \right\}$

2.38) $y_{cm} \triangleq \frac{1}{M} \left\{ \sum_{k=1}^{N} m_k y_k \right\}$

2.39) $z_{cm} \triangleq \frac{1}{M} \left\{ \sum_{k=1}^{N} m_k z_k \right\}$

2.40) $t_{cm} \triangleq \frac{1}{M} \left\{ \sum_{k=1}^{N} m_k t_k \right\} = t_j \qquad j = 1 \ldots N$

Note that time is assumed identical through the body, at all space-time coordinates. It is also useful to define coordinates with respect to the center of mass:

2.41) $x_{k/cm} = x_k - x_{cm}$

2.42) $y_{k/cm} = y_k - y_{cm}$

2.43) $z_{k/cm} = z_k - z_{cm}$

2.44) $t_{k/cm} = t_k - t_{cm} = 0$

Then in terms of center-of-mass coordinates, the linear momentum equations of motion become:

2.45a) $\frac{d}{dt}(P_x) = F^E_x$ 2.45b) $P_x = M \frac{d}{dt}(x_{cm})$

2.46a) $\frac{d}{dt}(P_y) = F^E_y$ 2.46b) $P_y = M \frac{d}{dt}(y_{cm})$

2.47a) $\frac{d}{dt}(P_z) = F^E_z$ 2.47b) $P_z = M \frac{d}{dt}(z_{cm})$

2.48) $\frac{d}{dt} M = 0$

Adding up the angular momentum equations of motion, component by component, it is straightforward to show

2.49) $\frac{d}{dt}(t_{cm} P_x - M x_{cm}) = t_{cm} F^E_x$

2.50) $\frac{d}{dt}(t_{cm} P_y - M y_{cm}) = t_{cm} F^E_y$

2.51) $\frac{d}{dt}(t_{cm} P_z - M z_{cm}) = t_{cm} F^E_z$

2.52) $\frac{d}{dt}\left\{ \sum_{k=1}^{N} [y_k P_{zk} - z_k P_{yk}] \right\} = \sum_{k=1}^{N} [y_k F^E_{zk} - z_k F^E_{yk}]$

2.53) $\frac{d}{dt}\left\{ \sum_{k=1}^{N} [z_k P_{xk} - x_k P_{zk}] \right\} = \sum_{k=1}^{N} [z_k F^E_{xk} - x_k F^E_{zk}]$

2.54) $\frac{d}{dt}\left\{ \sum_{k=1}^{N} [x_k P_{yk} - y_k P_{xk}] \right\} = \sum_{k=1}^{N} [x_k F^E_{yk} - y_k F^E_{xk}]$

These ten equations, (2.45)-(2.54) are the ten space-time equations of motion for a single rigid body. Note that the time-like component of the angular

momentum is a function of center-of-mass variables alone, as is the linear momentum, while the space-like component of the angular momentum depends both on center-of-mass variables and coordinates with respect to the center of mass.

The equations of motion decouple into two sets of equations, one describing motion of the center of mass (equations (2.45)-2.51)), the other motion about the center of mass (equations (2.52), (2.53), (2.54)). Since the motion of the center of mass in space can be described by six first order differential equations, three of the equations (in (2.45) - (2.51)) are redundant; typically, equations (2.49), (2.50), (2.51) are ignored, since they contain no more information about how external forces act on the center of mass than equations (2.45a), (2.46a), (2.47a). In fact, the motion of the center of mass is completely described by

2.45b) $\frac{d}{dt} X_{cm} = \frac{1}{M} P_x$

2.46b) $\frac{d}{dt} y_{cm} = \frac{1}{M} P_y$

2.47b) $\frac{d}{dt} z_{cm} = \frac{1}{M} P_z$

2.45a) $\frac{d}{dt} P_x = F^E_x$ OR 2.49) $\frac{d}{dt}(t_{cm} P_x - M X_{cm}) = t_{cm} F^E_x$

2.46a) $\frac{d}{dt} P_y = F^E_y$ OR 2.50) $\frac{d}{dt}(t_{cm} P_y - M y_{cm}) = t_{cm} F^E_y$

2.47a) $\frac{d}{dt} P_z = F^E_z$ OR 2.51) $\frac{d}{dt}(t_{cm} P_z - M z_{cm}) = t_{cm} F^E_z$

APPENDIX

After the work described in Chapter II was completed, a thorough literature search was undertaken to see whether a similar four-dimensional space-time formulation of Newtonian mechanics had been presented elsewhere. To the best of the author's knowledge, there is only one earlier work that is similar to the theory presented in Chapter II:

> "Sur les Variétés à Connexion Affine et la Théorie de la Relativité Généralisée," É. Cartan, Annales Scientifiques de l'École Normale Superieure, Series 3, Volume 40, 1923

Since this paper has apparently been forgotten, the three pages of the article relevant to the work described in Chapter II are included here so that the reader may compare the two developments for himself.

elles sont identiquement vérifiées s'il n'y a pas de pression; dans le cas général elles donnent

$$p_{zy} - p_{yz} = 0,$$
$$p_{xz} - p_{zx} = 0,$$
$$p_{yx} - p_{xy} = 0.$$

11. On peut représenter les résultats précédents au moyen d'une notation vectorielle simple. Désignons par les lettres

$$\mathbf{e}_0, \quad \mathbf{e}_1, \quad \mathbf{e}_2, \quad \mathbf{e}_3$$

les quatre vecteurs d'Univers qui ont respectivement pour composantes

$$1, \quad 0, \quad 0, \quad 0;$$
$$0, \quad 1, \quad 0, \quad 0;$$
$$0, \quad 0, \quad 1, \quad 0;$$
$$0, \quad 0, \quad 0, \quad 1.$$

Les quatre derniers sont des vecteurs d'espace. Avec ces notations la « quantité de mouvement-masse » d'un point matériel de masse m est représentée par

$$m\left(\mathbf{e}_0 + \frac{dx}{dt}\mathbf{e}_1 + \frac{dy}{dt}\mathbf{e}_2 + \frac{dz}{dt}\mathbf{e}_3\right).$$

Si nous convenons encore de désigner par une lettre $\mathbf{m}$ un point d'Univers (t, x, y, z), la dérivée $\frac{d\mathbf{m}}{dt}$ de ce point par rapport au temps est le vecteur d'Univers de composantes

$$1, \quad \frac{dx}{dt}, \quad \frac{dy}{dt}, \quad \frac{dz}{dt};$$

on voit que la « quantité de mouvement-masse » d'un point matériel est représentée par la notation

$$m\frac{d\mathbf{m}}{dt}.$$

Les points et les vecteurs (libres) sont des *formes géométriques* du premier degré. On peut considérer aussi des formes géométriques du second degré, qui représentent des systèmes de vecteurs *glissants*. On désigne par $[\mathbf{m}\mathbf{m}']$ le vecteur glissant qui a pour origine le point d'Univers $\mathbf{m}$ et pour extrémité le point d'Univers $\mathbf{m}'$. Ce vecteur glissant a dix coordonnées plückériennes qui sont les déterminants

du deuxième ordre formés avec le Tableau

$$\begin{matrix} 1 & t & x & y & z, \\ 1 & t' & x' & y' & z' \end{matrix}$$

on a évidemment

$$[\mathbf{m}'\mathbf{m}] = -[\mathbf{m}\,\mathbf{m}].$$

De même on désignera par $|\mathbf{me}|$ le vecteur glissant obtenu en portant à partir du point d'Univers $\mathbf{m}$ un vecteur équipollent à un vecteur donné $\mathbf{e}$; les dix coordonnées pluckériennes de ce vecteur glissant sont formées avec le Tableau

$$\begin{matrix} 1 & t & x & y & z, \\ 0 & \lambda & \xi & \eta & \zeta, \end{matrix}$$

où figurent dans la seconde ligne les composantes du vecteur $\mathbf{e}$. Enfin la notation $|\mathbf{ee}'|$ désignera le *bivecteur* dont les dix coordonnées sont formées avec le Tableau

$$\begin{matrix} 0 & \lambda & \xi & \eta & \zeta, \\ 0 & \lambda' & \xi' & \eta' & \zeta', \end{matrix}$$

des composantes des deux vecteurs libres $\mathbf{e}$ et $\mathbf{e}'$.

Dans chacun des cas précédents le vecteur glissant ou le bivecteur considéré peut être regardé comme le produit (extérieur) des deux facteurs, qui sont des formes géométriques du premier degré (point ou vecteur libre). Le produit de deux formes géométriques quelconques du premier degré satisfait à la loi distributive, mais change de signe avec l'ordre des facteurs.

12. Le vecteur glissant qui a pour origine le point d'Univers $\mathbf{m}$ qui représente un point matériel donné à un instant donné, et qu'on obtient en portant à partir de ce point sa « quantité de mouvement-masse », a pour expression

$$m\left[\mathbf{m}\,\frac{d\mathbf{m}}{dt}\right],$$

et l'équation

$$\frac{d}{dt}\left\{m\left[\mathbf{m}\,\frac{d\mathbf{m}}{dt}\right]\right\} = |\mathbf{F}|,$$

où $\mathbf{F}$ représente le vecteur glissant « force », contient, en même temps que le principe fondamental de la Dynamique, le théorème des

moments cinétiques; elle condense en effet les dix équations

$$\frac{dm}{dt} = 0,$$

$$\frac{d}{dt}\left(m\frac{dx}{dt}\right) = X,$$

$$\frac{d}{dt}\left(m\frac{dy}{dt}\right) = Y,$$

$$\frac{d}{dt}\left(m\frac{dz}{dt}\right) = Z,$$

$$\frac{d}{dt}\left(mt\frac{dx}{dt} - mx\right) = tX,$$

$$\frac{d}{dt}\left(mt\frac{dy}{dt} - my\right) = tY,$$

$$\frac{d}{dt}\left(mt\frac{dz}{dt} - mz\right) = tZ,$$

$$\frac{d}{dt}\left(my\frac{dz}{dt} - mz\frac{dy}{dt}\right) = yZ - zY,$$

$$\frac{d}{dt}\left(mz\frac{dx}{dt} - mx\frac{dz}{dt}\right) = zX - xZ,$$

$$\frac{d}{dt}\left(mx\frac{dy}{dt} - my\frac{dx}{dt}\right) = xY - yX.$$

13. Revenons à la Mécanique des milieux continus. Désignons par **G** le vecteur glissant qui représente l'élément à trois dimensions de « quantité de mouvement-masse » et par **F** le vecteur glissant qui représente la force de volume élémentaire. *Les équations de la Mécanique sont condensées dans la formule*

$$\mathbf{G}' = [dt\,\mathbf{F}]. \tag{6}$$

On a du reste ici

$$\mathbf{G} = [\mathbf{m}\mathbf{e}_0]\mathbf{H} + [\mathbf{m}\mathbf{e}_1]\mathbf{H}_x + [\mathbf{m}\mathbf{e}_2]\mathbf{H}_y + [\mathbf{m}\mathbf{e}_3]\mathbf{H}_z,$$

$$\mathbf{F} = [\mathbf{m}\mathbf{e}_1]X\,dx\,dy\,dz + [\mathbf{m}\mathbf{e}_2]Y\,dx\,dy\,dz + [\mathbf{m}\mathbf{e}_3]Z\,dx\,dy\,dz.$$

Le calcul de $\mathbf{G}'$ peut se faire en tenant compte de l'équation

$$d\mathbf{m} = \mathbf{e}_0\,dt + \mathbf{e}_1\,dx + \mathbf{e}_2\,dy + \mathbf{e}_3\,dz;$$

il donne

$$\begin{aligned}\mathbf{G}' = {} & [\mathbf{m}\mathbf{e}_0]\mathbf{H}' + [\mathbf{m}\mathbf{e}_1]\mathbf{H}'_x + [\mathbf{m}\mathbf{e}_2]\mathbf{H}'_y + [\mathbf{m}\mathbf{e}_3]\mathbf{H}'_z \\ & + [\mathbf{e}_0\mathbf{e}_1][dt\,\mathbf{H}_x - dx\,\mathbf{H}] + [\mathbf{e}_0\mathbf{e}_2][dt\,\mathbf{H}_y - dy\,\mathbf{H}] - [\mathbf{e}_0\mathbf{e}_3][dt\,\mathbf{H}_z - dz\,\mathbf{H}] \\ & + [\mathbf{e}_2\mathbf{e}_3][dy\,\mathbf{H}_z - dz\,\mathbf{H}_y] + [\mathbf{e}_3\mathbf{e}_1][dz\,\mathbf{H}_x - dx\,\mathbf{H}_z] + [\mathbf{e}_1\mathbf{e}_2][dx\,\mathbf{H}_y - dy\,\mathbf{H}_x].\end{aligned}$$

Chapter III

Attitude Estimation

A new concept for estimating the three angles which specify the orientation in space of a rigid body is now presented. The estimation procedure is analogous to phase-locked loop phase estimation: an observed function of the unknown angles is modulated by a function of the estimated angles, the resultant function is filtered by a linear time-invariant system, and the system outputs are the angle estimates. Two separate methods for implementing this concept are discussed, one based on direction cosines, the other on quaternions. No attempt is made to show that the particular estimation method presented here is an optimum method, in the sense of minimizing an error criteria. The aim of this chapter is to present a working technique that offers potential savings in hardware, in certain cases, over, for example, methods based on Kalman filtering (see Jazwinski(31)).

Before beginning the actual description of the attitude estimation procedure developed in this research program it is perhaps instructive to survey those features common to any estimation problem. Those features are three in number: 1) a parameter space, a space on which the parameters to be estimated are well defined, 2) an observation space, where functions of the parameters, corrupted by noise, can be observed, and 3) two mappings, one from the parameter space to the observation space which defines the functions to be observed in terms of the parameters and noise, and one from the observation space to the parameter space, which defines an estimation

procedure, a method for processing observations in order to estimate the desired parameters. For the problems to be discussed here, the parameter space is a real three dimensional Euclidean vector space in which three angles take on their values. The observation space is a real Euclidean vector space. The mapping from the parameter space to the observation space can be done in many ways, but only two will be discussed here, a direction cosine mapping and a quaternion mapping; each of these mappings may be viewed as an exponential mapping of the three angles from the parameter space to the observation space, loosely speaking. For both mappings, observations are functions of sines and cosines of the unknown angles, as well as noise. The estimation procedure, the mapping from the observation space back to the parameter space, is the subject of this chapter.

In order to assess the worth of the estimation procedure, one approach would be to define an error criteria, a measure of how much the actual parameters differ from their estimates. The error criteria considered in this chapter, often implicitly, is the difference between the actual value of an actual value of an angle and its estimate. An optimum estimation procedure minimizes the error criteria to its smallest possible value, assuming the error criteria actually has a minimum and that an optimum estimation rule actually exists; the question of optimum estimation will not be addressed in this chapter.

3.1. Attitude Characterization

This section discusses two methods for specifying the spatial orientation of a rigid body, direction cosines and quaternions. The material presented

here is largely tutorial; Goldstein(10) is an excellent reference for material on direction cosines, while Whittaker(28) is fine for quaternions.

3.1.1. Direction Cosines

Consider two right handed cartesian coordinate frames in $\mathbb{R}^3$ with the same origin labeled A and B. Assume that when frame A is rotated about some axis, eventually it will coincide with frame B (see Euler's Theorem-Whittaker, p.2). If an arbitrary vector has coordinates $\underline{r}_A = (x_A, y_A, z_A)$ in frame A. and $\underline{r}_B = (x_B, y_B, z_B)$ in frame B, then it is well known

$$3.1) \quad \begin{bmatrix} x_B \\ y_B \\ z_B \end{bmatrix} = \begin{bmatrix} d_{11} & d_{12} & d_{13} \\ d_{21} & d_{22} & d_{23} \\ d_{31} & d_{32} & d_{33} \end{bmatrix} \begin{bmatrix} x_A \\ y_A \\ z_A \end{bmatrix}, \quad \underline{r}_B = \underline{D}\underline{r}_A$$

where $\underline{D}$ is the direction cosine matrix from frame A to frame B. The physical interpretation of the elements in $\underline{D}$ is simple; e.g., d_{13} is the projection of a unit vector along the z-axis in frame A onto the x-axis in frame B. The elements in $\underline{D}$ are constrained by

$$3.2) \quad \underline{D}\,\underline{D}^T = \underline{D}^T\underline{D} = \underline{I}$$

where $\underline{D}^T$ is the transpose of $\underline{D}$. Since there are six constraints in this matrix equation,

$$d_{11}^2 + d_{12}^2 + d_{13}^2 = 1 \qquad d_{11}\,d_{21} + d_{12}\,d_{22} + d_{13}\,d_{23} = 0$$

$$d_{21}^2 + d_{22}^2 + d_{23}^2 = 1 \qquad d_{11}\,d_{31} + d_{12}\,d_{32} + d_{13}\,d_{33} = 0$$

$$d_{31}^2 + d_{32}^2 + d_{33}^2 = 1 \qquad d_{21}\,d_{31} + d_{22}\,d_{32} + d_{23}\,d_{33} = 0$$

while $\underline{D}$ contains nine parameters total, $\underline{D}$ can be characterized by three independent parameters. These three parameters are angles, denoted by a three-tuple $\underline{a} = (a_1, a_2, a_3)$, represent rotations about x, y, or z axes:

3.3) $\underline{D} = \mathrm{EXP}(a_1 \underline{L}_1)\ \mathrm{EXP}(a_2 \underline{L}_2)\ \mathrm{EXP}(a_3 \underline{L}_3) \quad -\pi < a_k \leq \pi \quad k = 1,2,3 \quad \underline{L}_1 \neq \underline{L}_2, \underline{L}_2 \neq \underline{L}_3$

$\underline{L}_1, \underline{L}_2, \underline{L}_3 \in \{\underline{L}_x, \underline{L}_y, \underline{L}_z\}$

$$\underline{L}_x = \begin{bmatrix} 0 & 0 & 0 \\ 0 & 0 & -1 \\ 0 & 1 & 0 \end{bmatrix} \quad \underline{L}_y = \begin{bmatrix} 0 & 0 & 1 \\ 0 & 0 & 0 \\ -1 & 0 & 0 \end{bmatrix} \quad \underline{L}_z = \begin{bmatrix} 0 & -1 & 0 \\ 1 & 0 & 0 \\ 0 & 0 & 0 \end{bmatrix}$$

In all cases, $\underline{D}$ is specified by the three independent angles a_1, a_2, a_3. However if either

i) $\underline{L}_1 = \underline{L}_3$ AND $a_2 = \pi K \quad K = 0, \pm 1, \pm 2, \ldots$

or ii) $\underline{L}_1 \neq \underline{L}_3$ AND $a_2 = \frac{\pi}{2} + l\pi \quad l = 0, \pm 1, \pm 2, \ldots$

then $\underline{D}$ can be shown to be composed of sines and cosines of $(a_1 + a_3)$ or sines and cosines of $(a_1 - a_3)$, depending on the exact choice of $\underline{L}_1$ and $\underline{L}_3$ in terms of $\{\underline{L}_x, \underline{L}_y, \underline{L}_z\}$. In this case $\underline{D}$ is "singular," in that specifying only two independent parameters, a_2 and either $(a_1 + a_3)$ or $(a_1 - a_3)$ uniquely determines $\underline{D}$.

If coordinate frame A is rotating relative to frame B, then the direction cosines from A to B change with time. The derivative of $\underline{D}$ with respect to time is

$$\frac{d}{dt}\underline{D} = \left[\dot{a}_1 \underline{L}_1 + e^{a_1 \underline{L}_1} \dot{a}_2 \underline{L}_2 e^{-a_1 \underline{L}_1} + e^{a_1 \underline{L}_1} e^{a_2 \underline{L}_2} \dot{a}_3 \underline{L}_3 e^{-a_2 \underline{L}_2} e^{-a_1 \underline{L}_1}\right] \underline{D}$$

$$\frac{d}{dt}\underline{D} = \underline{W}\,\underline{D}, \quad \underline{W} = \dot{a}_1 \underline{L}_1 + e^{a_1 \underline{L}_1} \dot{a}_2 \underline{L}_2 e^{-a_1 \underline{L}_1} + e^{a_1 \underline{L}_1} e^{a_2 \underline{L}_2} \dot{a}_3 \underline{L}_3 e^{-a_2 \underline{L}_2} e^{-a_1 \underline{L}_1}$$

$$\underline{W} = \begin{bmatrix} 0 & -w_z & w_y \\ w_z & 0 & -w_x \\ -w_y & w_x & 0 \end{bmatrix} \qquad \underline{w} = \begin{bmatrix} w_x \\ w_y \\ w_z \end{bmatrix}$$

where $\underline{w}$ is called the angular velocity of frame B with respect to frame A.

3.1.2. Quaternions

A second way of characterizing a rotation in space is by a quaternion. A quaternion q may be viewed as a four-tuple (with one constraint)

3.5) $$\underset{\sim}{q} = a\hat{i} + b\hat{j} + c\hat{k} + d(1)$$

where $\hat{i}$, $\hat{j}$, $\hat{k}$ and 1 are unit quaternions, which multiply according to the rules of quaternion multiplication:

$$\hat{i}\hat{j} = -\hat{j}\hat{i} = \hat{k} \qquad 1\hat{i} = \hat{i}1 = \hat{i} \qquad \hat{i}^2 = \hat{j}^2 = \hat{k}^2 = -1$$

$$\hat{j}\hat{k} = -\hat{k}\hat{j} = \hat{i} \qquad 1\hat{j} = \hat{j}1 = \hat{j} \qquad 1^2 = 1$$

$$\hat{k}\hat{i} = -\hat{i}\hat{k} = \hat{j} \qquad 1\hat{k} = \hat{k}1 = \hat{k}$$

The conjugate of a quaternion $\underline{q}$, denoted $\underline{q}^+$, is defined to be

3.6) $$\underline{q}^+ = -a\hat{i} - b\hat{j} - c\hat{k} + d(1)$$

The four parameters of a quaternion are constrained:

3.7) $$\underline{q}\,\underline{q}^+ = \underline{q}^+\underline{q} = a^2 + b^2 + c^2 + d^2 = 1$$

Since any rotation in space is a rotation about some axis, a quaternion may be viewed with respect to a reference coordinate frame as

3.8) $$\underset{\sim}{q} = \cos\left(\frac{\omega}{2}\right) + \sin\left(\frac{\omega}{2}\right)\left[\hat{i}\cos\alpha + \hat{j}\cos\beta + \hat{k}\cos\gamma\right]$$

where at any instant of time the rotation is about a unit length vector, called the instantaneous axis of rotation, and

$\cos\alpha$ = projection of instantaneous axis of rotation onto x-axis of reference frame

$\cos\beta$ = projection of instantaneous axis of rotation onto y-axis of reference frame

$\cos\gamma$ = projection of instantaneous axis of rotation onto z-axis of reference frame

w = amount of rotation (in radians) about instantaneous axis of rotation

Using the power series definition of an exponential plus the rules of quaternion multiplication, this can be rewritten as

3.9) $$\underline{q} = \text{EXP}\left\{ \frac{w}{2}\left[\hat{i}\cos\alpha + \hat{j}\cos\beta + \hat{k}\cos\gamma \right] \right\}$$

If $w = w_o + 2\pi n$, physically this represents a rotation of w_o radians about the instantaneous axis of rotation. Note that

$$\underline{q} = \cos\left(\frac{w}{2}\right) + \sin\left(\frac{w}{2}\right)\left[\hat{i}\cos\alpha + \hat{j}\cos\beta + \hat{k}\cos\gamma \right]\}$$

3.10) $$\underline{q} = (-1)^n \left\{ \cos\left(\frac{w_o}{2}\right) + \sin\left(\frac{w_o}{2}\right)\left[\hat{i}\cos\alpha + \hat{j}\cos\beta + \hat{k}\cos\gamma \right] \right\} = (-1)^n \underline{q}_o$$

WHERE $$\underline{q}_o = \cos\left(\frac{w_o}{2}\right) + \sin\left(\frac{w_o}{2}\right)\left[\hat{i}\cos\alpha + \hat{j}\cos\beta + \hat{k}\cos\gamma \right]$$

that is, both $\underline{q}_o$ (if n is even) and $-\underline{q}_o$ (if n is odd) represent the same rotation in space. This fact is reflected in how quaternions transform vectors in frame A to vectors in frame B. If an arbitrary vector has coordinates $\underline{r}_A = (x_A, y_A, z_A)$ in frame A, and $\underline{r}_B = (x_B, y_B, z_B)$ in frame B, where frame A and B are related by a rotation about some axis, then

3.11) $$\underline{r}_B = \underline{q}\,\underline{r}_A\,\underline{q}^+$$

Since this can also be written as

3.12) $$\underline{r}_B = (-\underline{q})\,\underline{r}_A\,(-\underline{q}^+)$$

a quaternion is a point on a sphere in Euclidean four-space, but the rotation that quaternion represents must be considered as two antipodal points (a, b, c, d) and (-a, -b, -c, -d), on that sphere.

If coordinate frame A rotates relative to frame B, then the quaternion relating those two frames changes with time; it can be shown (Whittaker(28), p. 16)

3.13) $$\frac{d}{dt}\begin{bmatrix} a \\ b \\ c \\ d \end{bmatrix} = \frac{1}{2}\begin{bmatrix} 0 & -w_z & w_u & w_x \\ w_z & 0 & -w_x & w_y \\ -w_y & w_x & 0 & w_z \\ -w_x & -w_y & -w_y & 0 \end{bmatrix}\begin{bmatrix} a \\ b \\ c \\ d \end{bmatrix}, \quad \underline{w} = \begin{bmatrix} w_x \\ w_y \\ w_z \end{bmatrix}$$

where $\underline{w}$ is the angular velocity of B with respect to A.

3.2. Attitude Estimation With Direction Cosines

3.2.1. Deterministic Attitude Estimation

3.2.1.1. Model

A block diagram for a system which estimates the three angles which specify the orientation of a rigid body from direction cosine measurements is shown below (without any noise sources):

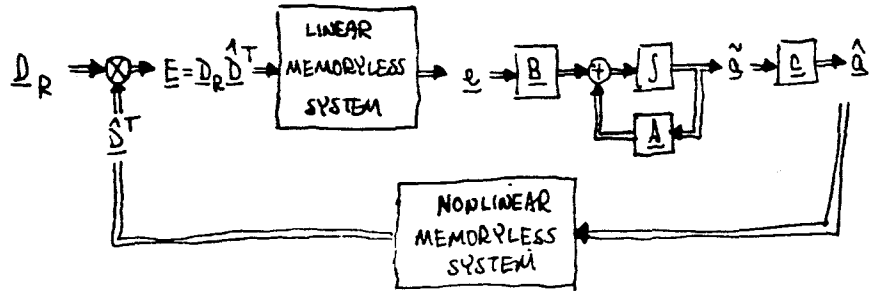

FIGURE 3.1
DIRECTION COSINE ATTITUDE ESTIMATION CONSTANT ORIENTATION IN SPACE

It is assumed:

1) all components of $\underline{D}_R$, the received direction cosine matrix, are observable

2) $\underline{D}_R$ and $\hat{\underline{D}}$, the received and estimated direction cosine matrices, respectively, are each described by three roll-pitch-yaw angles, $\underline{a}_R$ and $\underline{a}$, respectively

3.14) $$\underline{D}_R = \exp(x_R \underline{L}_x) \exp(y_R \underline{L}_y) \exp(z_R \underline{L}_z) \qquad \underline{a}_R = (x_R, y_R, z_R)$$

3.15) $$\hat{\underline{D}} = \exp(\hat{x} \underline{L}_x) \exp(\hat{y} \underline{L}_y) \exp(\hat{z} \underline{L}_z) \qquad \hat{\underline{a}} = (\hat{x}, \hat{y}, \hat{z})$$

where

$$\underline{L}_x = \begin{bmatrix} 0 & 0 & 0 \\ 0 & 0 & -1 \\ 0 & 1 & 0 \end{bmatrix}, \quad \underline{L}_y = \begin{bmatrix} 0 & 0 & 1 \\ 0 & 0 & 0 \\ -1 & 0 & 0 \end{bmatrix}, \quad \underline{L}_z = \begin{bmatrix} 0 & -1 & 0 \\ 1 & 0 & 0 \\ 0 & 0 & 0 \end{bmatrix}$$

$\underline{E}$ results from postmultiplying $\underline{D}_R$ by $\hat{\underline{D}}^T$, the transpose (denoted with a "T") of $\hat{\underline{D}}$.

3.16) $$\underline{E} = \underline{D}_R \hat{\underline{D}}^T = \begin{bmatrix} E_{11} & E_{12} & E_{13} \\ E_{21} & E_{22} & E_{23} \\ E_{31} & E_{32} & E_{33} \end{bmatrix}$$

If each of the six angles is small compared to one, then $\underline{E}$ can be approximated:

3.17) $$\underline{E} \cong \begin{bmatrix} 1 & -(z_r - \hat{z}) & (y_r - \hat{y}) \\ (z_r - \hat{z}) & 1 & -(x_r - \hat{x}) \\ -(y_r - \hat{y}) & (x_r - \hat{x}) & 1 \end{bmatrix} \qquad \begin{matrix} |x_r| \ll 1 & |\hat{x}| \ll 1 \\ |y_r| \ll 1 & |\hat{y}| \ll 1 \\ |z_r| \ll 1 & |\hat{z}| \ll 1 \end{matrix}$$

The 3 x 1 error vector $\underline{e}$ may be defined as

$$
\begin{aligned}
e_x &= E_{32}(M_x) - E_{23}(1-M_x) \qquad 0 \le M_x \le 1 \\
3.18) \qquad e_y &= E_{13}(M_y) - E_{31}(1-M_y) \qquad 0 \le M_y \le 1 \\
e_z &= E_{21}(M_z) - E_{12}(1-M_z) \qquad 0 \le M_z \le 1
\end{aligned}
$$

Each error component may be chosen in many ways; it is not obvious that one choice is better than any other choice. Only two will be considered here, to provide a concrete example for discussion, and to simplify algebraic manipulation:

$$
\begin{aligned}
e_x &= E_{32} & \qquad e_x &= -E_{23} \\
3.19) \qquad e_y &= E_{13} & 3.20) \qquad e_y &= -E_{31} \\
e_z &= E_{21} & e_z &= -E_{12}
\end{aligned}
$$

The error vector $\underline{e}$ is used as an input to a linear time-invariant system which generates angle estimates, $\hat{\underline{a}}$,

$$
\begin{aligned}
\dot{\tilde{\underline{a}}} &= \underline{A}\,\tilde{\underline{a}} + \underline{B}\,\underline{e} \qquad \tilde{\underline{a}}(t_o) = \tilde{\underline{a}}_o \\
3.21 \qquad \hat{\underline{a}} &= \underline{C}\,\tilde{\underline{a}}
\end{aligned}
$$

where $\underline{A}$, $\underline{B}$, and $\underline{C}$ are 3 x 3 matrices, $\tilde{\underline{a}}$ and $\hat{\underline{a}}$ are 3 x 1 vectors. For the two examples to be considered, $\underline{A} = \underline{0}$, so this system is a pure integrator. The angle estimates are then used to generate $\underline{D}^T$, closing the loop The intuitive operation of the loop is simple: postmultiplying $\underline{D}_R$ by $\underline{D}^T$ undoes the rotation represented by $\underline{D}_R$; the negative feedback of the loop eventually zeroes $\underline{e}$, eventually making $\underline{E}$ the identity matrix and $\hat{\underline{a}} = \underline{a}_R$. For future reference the off diagonal elements of $\underline{E}$ are now explicitly spelled out:

3.22a) $E_{12} = s(y_r)\,c(z_r-\hat{z})\,s(\hat{x})\,s(\hat{y}) - s(z_r-\hat{z})\,c(y_r)\,c(\hat{x})\,c(\hat{y}) - s(y_r)\,s(\hat{x})\,c(\hat{y})$

3.22b) $E_{13} = -c(y_r)\,c(z_r-\hat{z})\,c(\hat{x})\,s(\hat{y}) - c(y_r)\,s(z_r-\hat{z})\,s(\hat{x}) + s(y_r)\,c(\hat{x})\,c(\hat{y})$

3.22c) $E_{21} = c(\hat{y})\{s(x_r)\,s(y_r)\,c(z_r-\hat{z}) + c(x_r)\,s(z_r-\hat{z})\} - s(x_r)\,c(y_r)\,s(\hat{y})$

3.22d) $E_{23} = -c(\hat{x})\,s(\hat{y})\{s(y_r)\,s(x_r)\,c(z_r-\hat{z}) + c(x_r)\,s(z_r-\hat{z})\} - s(x_r)\,c(y_r)\,c(\hat{x})\,c(\hat{y})$
$+ s(\hat{x})\{c(y_r)\,c(z_r-\hat{z}) - s(x_r)\,s(y_r)\,s(z_r-\hat{z})\}$

3.22e) $E_{31} = c(\hat{y})\{s(x_r)\,s(z_r-\hat{z}) - s(y_r)\,c(x_r)\,c(z_r-\hat{z})\} + c(x_r)\,c(y_r)\,s(\hat{y})$

3.22f) $E_{32} = s(\hat{x})\,s(\hat{y})\{s(x_r)\,s(z_r-\hat{z}) - s(y_r)\,c(x_r)\,c(z_r-\hat{z})\} - s(\hat{x})\,c(\hat{y})\,c(x_r)\,c(y_r)$
$+ c(\hat{x})\{s(y_r)\,c(x_r)\,s(z_r-\hat{z}) + s(x_r)\,c(z_r-\hat{z})\}$

where sine and cosine have been abreviated to s and c, respectively. To carry the analysis further, two examples are now examined in detail.

3.2.1.2. Example 1--Constant Orientation in Space

Throughout this section $\underline{a}_R$ is assumed constant but unknown. If

$$\underline{A} = \begin{bmatrix} 0 & 0 & 0 \\ 0 & 0 & 0 \\ 0 & 0 & 0 \end{bmatrix} \quad \underline{B} = \begin{bmatrix} B_x & 0 & 0 \\ 0 & B_y & 0 \\ 0 & 0 & B_z \end{bmatrix} \quad \underline{C} = \begin{bmatrix} 1 & 0 & 0 \\ 0 & 1 & 0 \\ 0 & 0 & 1 \end{bmatrix}$$

3.23) $\dot{\hat{\underline{a}}} = \underline{B}\cdot\underline{e}\,(\underline{a}_R, \hat{\underline{a}}) \qquad \hat{\underline{a}}(t_o) = \hat{\underline{a}}_o$

If (3.19) is used for $\underline{e}$, these three equations can be written out explicitly:

3.24)
$$\dot{\hat{x}} = B_x\{s(\hat{x})\,s(\hat{y})[s(x_r)\,s(z_r-\hat{z}) - s(y_r)\,c(x_r)\,c(z_r-\hat{z})] - s(\hat{x})\,c(\hat{y})\,c(x_r)\,c(y_r)$$
$$+ c(\hat{x})[s(y_r)\,c(x_r)\,s(z_r-\hat{z}) + s(x_r)\,c(z_r-\hat{z})]\}$$
$$\dot{\hat{y}} = B_y\{-c(y_r)\,c(z_r-\hat{z})\,c(\hat{x})\,s(\hat{y}) - c(y_r)\,s(z_r-\hat{z})\,s(\hat{x}) + s(y_r)\,c(\hat{x})\,c(\hat{y})\}$$
$$\dot{\hat{z}} = B_z\{c(\hat{y})[s(x_r)\,s(y_r)\,c(z_r-\hat{z}) + c(x_r)\,s(z_r-\hat{z})] - s(x_r)\,c(y_r)\,s(\hat{y})\}$$

The figure below shows a sampled-input, discrete-time approximation to these equations

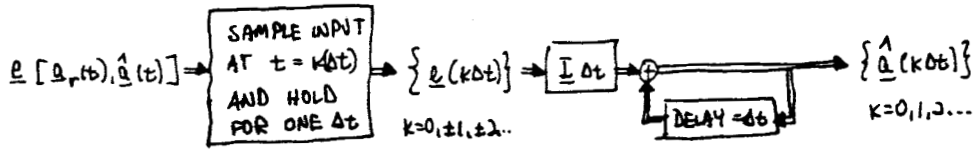

FIGURE 3.2

SAMPLED-INPUT SYSTEM -- DISCRETE-TIME APPROXIMATION TO IDEAL CONTINUOUS-TIME INTEGRATION

The figures on the following page show the results of a computer simulation of the equations above using the discrete time filter (Figure 3.3 $\hat{\underline{a}}_o = 0$, $\underline{a}_R = (60^o, 45^o, 30^o)$; Figure 3.4 $\hat{\underline{a}}_o = \underline{0}$, $\underline{a}_R = (-60^o, -45^o, -30^o)$) with $\Delta t = 0.1$ seconds in each case, and $B_x = B_y = B_z = 1$.

The next step is a linearized analysis of these equations. If $\underline{a}_r = (60^o, 45^o, 30^o)$, and if it is assumed

$$\hat{x} = 60^o + \delta x \qquad |\delta x| \ll 1$$

3.25) $$\hat{y} = 45^o + \delta y \qquad |\delta y| \ll 1$$

$$\hat{z} = 30^o + \delta z \qquad |\delta z| \ll 1$$

then using the approximations $\sin a \cong a$, $\cos a \cong 1$ for $|a| \ll 1$, and keeping terms to first order only, it can be shown that

FIGURE 3.3-3.4
DIRECTION COSINE ATTITUDE ESTIMATION--COMPUTER SIMULATION
ESTIMATED ANGLES VS TIME

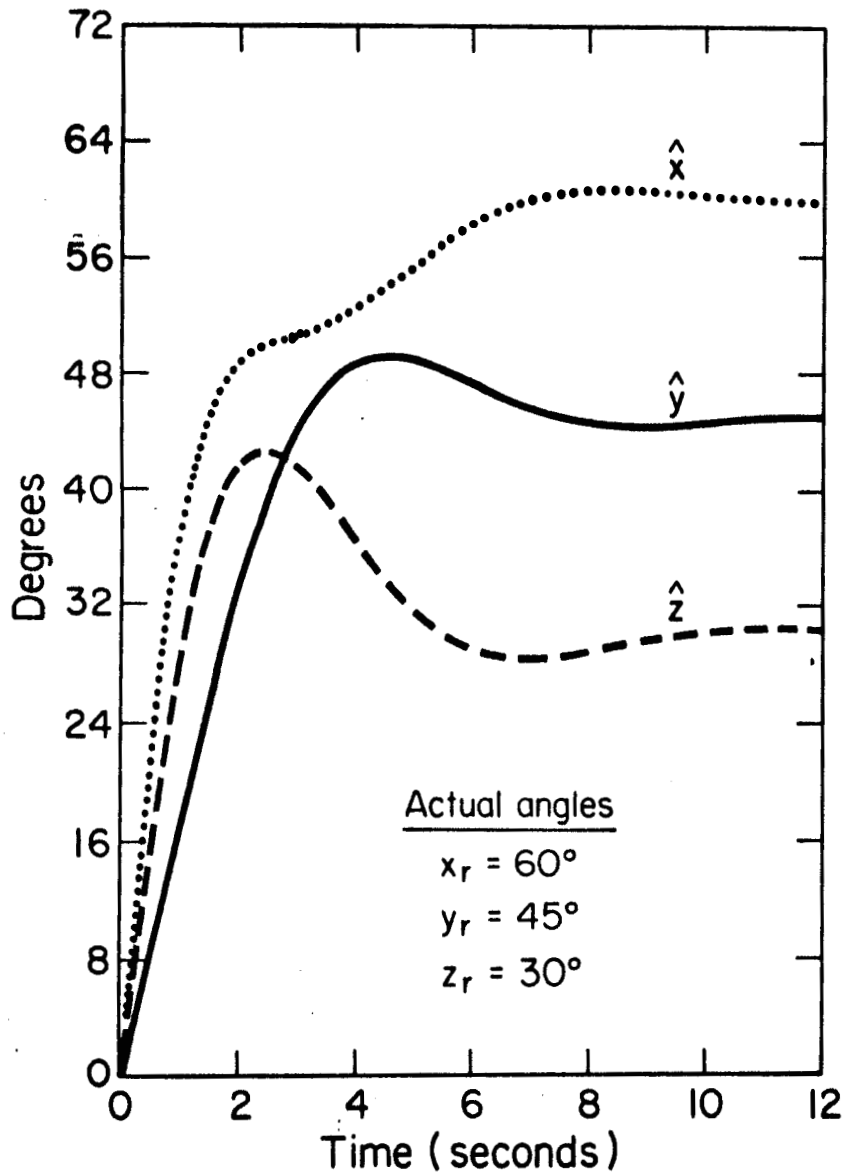

FIGURE 3.3

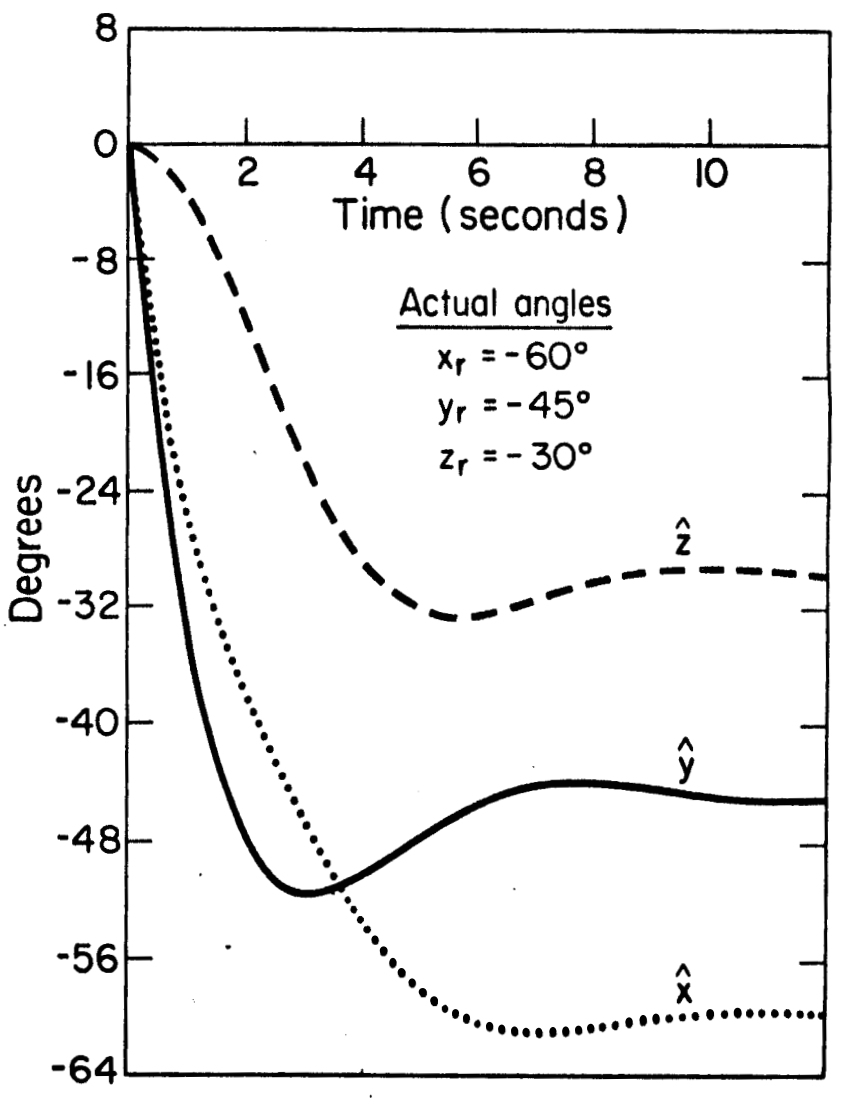

FIGURE 3.4

3.26)
$$\dot{\delta x} \cong -B_x$$
$$\dot{\delta y} \cong -B_y$$
$$\dot{\delta z} \cong -B_z$$

Note that estimation errors can be nulled out faster than in Figure 3.4 (where $B_x = B_y = B_z = 1$) by choosing $B_x >> 1$, $B_y >> 1$, $B_z >> 1$. A word of caution is in order: strictly speaking, this linearized analysis is valid only for $|\delta x| << 1$, $|\delta y| << 1$, $|\delta z| << 1$ while Figure 3.4 shows that near t = 0 there approximations are not valid. As long as estimation errors are less than 10°, i.e., t > 6 seconds in Figure 3.4, the linearized analysis provides good agreement with simulation results.

If instead of equation (3.19), equation (3.20) is chosen for $\underline{e}$, the results of both the computer simulations and linearized analysis are identical to those just discussed.

The stable states of equation (3.23) were investigated next.

First, the steady state solutions to (3.23) were found; if (3.19) is used for $\underline{e}$, the steady state solutions are

3.27)

$\hat{x} = x_r + a\pi$	$\hat{x} = -x_r + a\pi$	$\hat{x} = x_r + a\pi$
$\hat{y} = y_r + b\pi$ (b EVEN, c EVEN)	$\hat{y} = y_r + b\pi$ (b EVEN, c ODD)	$\hat{y} = -y_r + b\pi$ (b ODD, c ODD)
$\hat{z} = z_r + c\pi$	$\hat{z} = z_r + c\pi$	$\hat{z} = z_r + c\pi$

where (a, b, c) are integers, while if (3.17) is used for $\underline{e}$, the steady state solutions are

3.28)

$\hat{x} = x_r + a\pi$	$\hat{x} = -x_r + a\pi$	$\hat{x} = -x_r + a\pi$
$\hat{y} = y_r + b\pi$ (b EVEN, c EVEN)	$\hat{y} = -y_r + b\pi$ (b EVEN, c ODD)	$\hat{y} = y_r + b\pi$ (b ODD, c EVEN)
$\hat{z} = z_r + c\pi$	$\hat{z} = z_r + c\pi$	$\hat{z} = z_r + c\pi$

As a check on these solutions, $\underline{a}_R$ was held fixed, and the M.I.T. Computation Center Fortran IV Subroutine "NONLIN" was used to solve $\underline{e}(\underline{a}_R, \hat{\underline{a}}) = \underline{0}$, with a grid of initial trial solutions for $\hat{\underline{a}}$. No more solutions were found in this way than those above; clearly, this is no guarantee all the steady state solutions are known.

To illustrate this point, a different choice of $\underline{e}$ was made:

$$3.29) \qquad \begin{aligned} e_x &= \tfrac{1}{2}(E_{32} - E_{23}) \\ e_y &= \tfrac{1}{2}(E_{13} - E_{31}) \\ e_z &= \tfrac{1}{2}(E_{21} - E_{12}) \end{aligned}$$

A paper-and-pencil solution to $\underline{e} = \underline{0}$ yielded results similar to those in equations (3.27) and (3.28). However, using this $\underline{e}$, when $a_{rx} = 60^\circ$, $a_{ry} = 45^\circ$, $a_{rz} = 30^\circ$, "NONLIN" showed that $\underline{e} = \underline{0}$ when $\hat{a}_x = 188.88^\circ$, $\hat{a}_y = 209.75^\circ$, $\hat{a}_z = 39.13^\circ$, as well as at the expected solutions.

The stable states can be found by linearizing the equations of motion about the steady state solutions above, and then perturbing the equations away from the steady state solutions to see if solutions to the linearized equations are stable or unstable. To be more explicit, denote a steady state solution as (x_{ss}, y_{ss}, z_{ss}), and assume the estimates are perturbed slightly from this solution:

$$3.30) \qquad \begin{aligned} \hat{x} &\cong x_{ss} + \delta x \qquad |\delta x| \ll 1 \qquad \dot{\hat{x}} \cong \dot{\delta x} \\ \hat{y} &\cong y_{ss} + \delta y \qquad |\delta y| \ll 1 \qquad \dot{\hat{y}} \cong \dot{\delta y} \\ \hat{z} &\cong z_{ss} + \delta z \qquad |\delta z| \ll 1 \qquad \dot{\hat{z}} \cong \dot{\delta z} \end{aligned}$$

Expand $\underline{e}$ in a Taylor series about (x_{ss}, y_{ss}, z_{ss}), ignoring second and higher order terms:

$$
\begin{aligned}
e_x(\hat{x},\hat{y},\hat{z}) &\cong e_x(x_{ss},y_{ss},z_{ss}) + \left.\frac{\partial e_x}{\partial \hat{x}}\right|_{ss}\delta x + \left.\frac{\partial e_x}{\partial \hat{y}}\right|_{ss}\delta y + \left.\frac{\partial e_x}{\partial \hat{z}}\right|_{ss}\delta z \\
e_y(\hat{x},\hat{y},\hat{z}) &\cong e_y(x_{ss},y_{ss},z_{ss}) + \left.\frac{\partial e_y}{\partial \hat{x}}\right|_{ss}\delta x + \left.\frac{\partial e_y}{\partial \hat{y}}\right|_{ss}\delta y + \left.\frac{\partial e_y}{\partial \hat{z}}\right|_{ss}\delta z \\
e_z(\hat{x},\hat{y},\hat{z}) &\cong e_z(x_{ss},y_{ss},z_{ss}) + \left.\frac{\partial e_z}{\partial \hat{x}}\right|_{ss}\delta x + \left.\frac{\partial e_z}{\partial \hat{y}}\right|_{ss}\delta y + \left.\frac{\partial e_z}{\partial \hat{z}}\right|_{ss}\delta z
\end{aligned}
\qquad 3.31)
$$

Then in terms of perturbed variables $(\delta x, \delta y, \delta z)$, equation (3.10) becomes

$$
\frac{d}{dt}\begin{bmatrix}\delta x\\ \delta y\\ \delta z\end{bmatrix} = \begin{bmatrix}\frac{\partial}{\partial \hat{x}}e_x & \frac{\partial}{\partial \hat{y}}e_x & \frac{\partial}{\partial \hat{z}}e_x\\ \frac{\partial}{\partial \hat{x}}e_y & \frac{\partial}{\partial \hat{y}}e_y & \frac{\partial}{\partial \hat{z}}e_y\\ \frac{\partial}{\partial \hat{x}}e_z & \frac{\partial}{\partial \hat{y}}e_z & \frac{\partial}{\partial \hat{z}}e_z\end{bmatrix}_{ss}\begin{bmatrix}\delta x\\ \delta y\\ \delta z\end{bmatrix} \qquad 3.32)
$$

where $\underline{e}\,(x_{ss}, y_{ss}, z_{ss}) = \underline{0}$ and "ss" means "evaluated at $\hat{x} = x_{ss}$, $\hat{y} = y_{ss}$, $\hat{z} = z_{ss}$." Note that the eigenvalues of the linearized system can be determined by the steady state solutions. For example, if (3.19) is used for $\underline{e}$, one set of steady state solutions is

$$
\begin{aligned}
\hat{x} &= x_r + a\pi \\
\hat{y} &= -y_r + b\pi \qquad b \text{ odd}, c \text{ odd} \\
\hat{z} &= z_r + c\pi
\end{aligned}
$$

It can be shown that if $x_r = y_r = z_r = 0$, none of these steady state solutions are stable, but if $x_r = \pi$, $y_r = z_r = 0$, then a stable steady state solution exists for a, b, c all odd. The figure on the next page shows the result of a computer simulation of equation (3.24) with $B_x = B_y = B_z = 1$, and

$$
\begin{aligned}
\hat{x}_0 &= 0^\circ \qquad & x_r &= 120^\circ \\
\hat{y}_0 &= 0^\circ \qquad & y_r &= 105^\circ \\
\hat{z}_0 &= 0^\circ \qquad & z_r &= 90^\circ
\end{aligned}
$$

Clearly the stable steady-state solution to this simulation is

$$
\begin{aligned}
\hat{x} &= -60^\circ = x_r + (-1)\pi \\
\hat{y} &= 75^\circ = -y_r + (1)\pi \\
\hat{z} &= -90^\circ = z_r + (-1)\pi
\end{aligned}
$$

DIRECTION COSINE ATTITUDE ESTIMATION
COMPUTER SIMULATION RESULTS
ANGLE ESTIMATES VS TIME

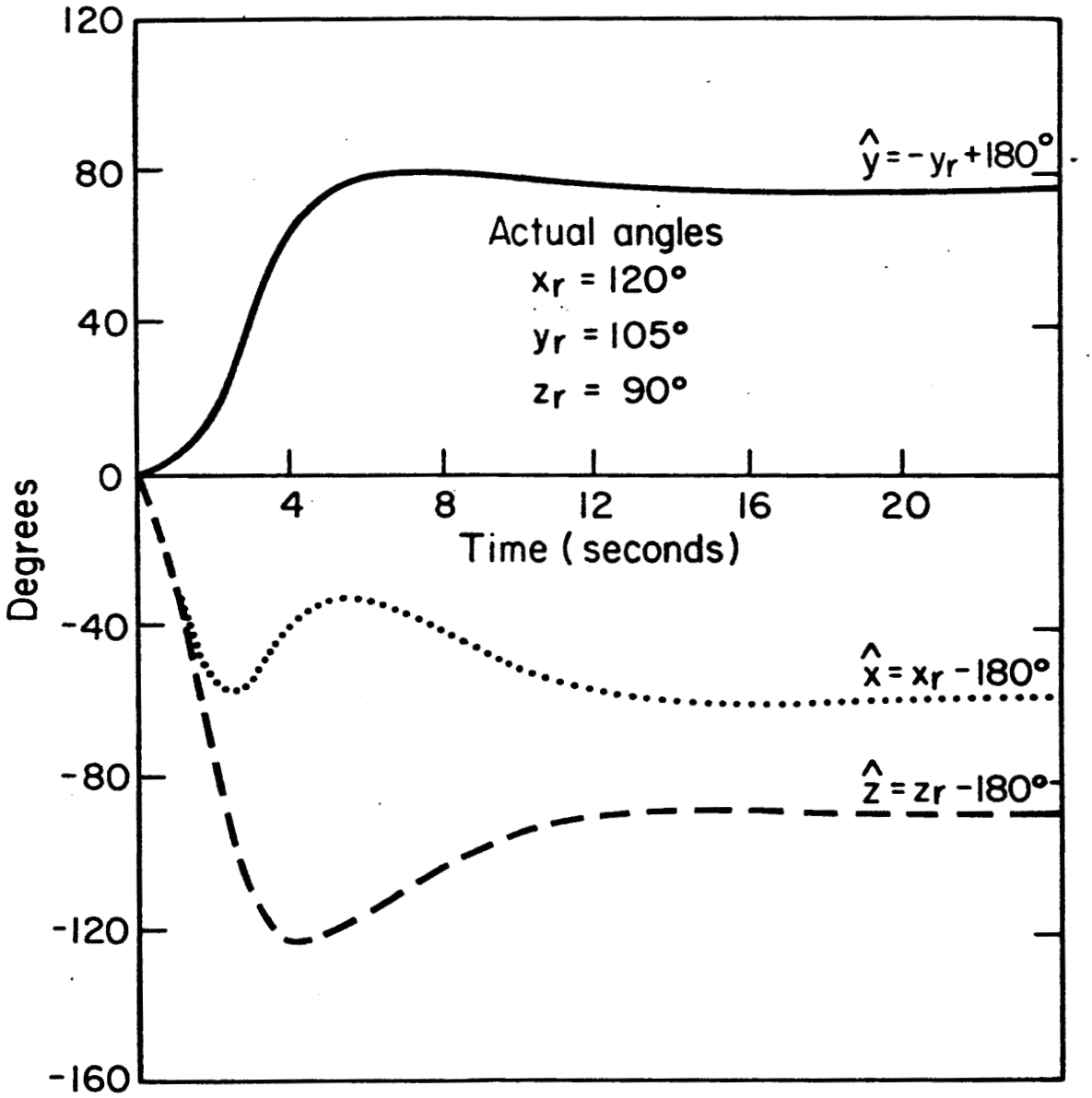

FIGURE 3.5

3.2.1.3. Constant Rate of Change of Roll-Pitch-Yaw Angles

Throughout this section, $\underline{a}_r$ and $\hat{\underline{a}}$ are assumed to be of the form

$$\left.\begin{aligned} a_{rx} &= f_x t + \varphi_{rx} & \hat{a}_x &= f_x t + \hat{\varphi}_x \\ a_{ry} &= f_y t + \varphi_{ry} & \hat{a}_y &= f_y t + \hat{\varphi}_y \\ a_{rz} &= f_z t + \varphi_{rz} & \hat{a}_z &= f_z t + \hat{\varphi}_z \end{aligned}\right\} \quad \begin{aligned} \underline{a}_r &= \underline{f} t + \underline{\varphi}_r \\ \hat{\underline{a}} &= \underline{f} t + \hat{\underline{\varphi}} \end{aligned}$$

where $\underline{f} = (f_x, f_y, f_z)$ are known and constant, $\underline{\varphi}_r = (\varphi_{rx}, \varphi_{ry}, \varphi_{rz})$ are unknown and constant, and $\hat{\underline{\varphi}} = (\hat{\varphi}_x, \hat{\varphi}_y, \hat{\varphi}_z)$ are estimates of $\underline{\varphi}_r = (\varphi_{rx}, \varphi_{ry}, \varphi_{rz})$. The reader is cautioned not to confuse this set of circumstances with a constant angular velocity; from Goldstein(10), angular velocity in terms of roll-pitch-yaw angles can be shown to be

$$\begin{bmatrix} w_x \\ w_y \\ w_z \end{bmatrix} = \begin{bmatrix} 1 & 0 & 0 \\ 0 & \cos a_{rx} & -\sin a_{rx} \\ 0 & \sin a_{rx} & \cos a_{rx} \end{bmatrix} \begin{bmatrix} \cos a_{ry} & 0 & \sin a_{ry} \\ 0 & 1 & 0 \\ -\sin a_{ry} & 0 & \cos a_{ry} \end{bmatrix} \begin{bmatrix} 0 \\ 0 \\ -\dot{a}_{rz} \end{bmatrix}$$

$$+ \begin{bmatrix} 1 & 0 & 0 \\ 0 & \cos a_{rx} & -\sin a_{rx} \\ 0 & \sin a_{rx} & \cos a_{rx} \end{bmatrix} \begin{bmatrix} 0 \\ -\dot{a}_{ry} \\ 0 \end{bmatrix} + \begin{bmatrix} -\dot{a}_{rx} \\ 0 \\ 0 \end{bmatrix}.$$

Only under special circumstances (e.g., $f_x = f_y = 0$) does constant rate of change of roll-pitch-yaw angles reduce to constant angular velocity.

The system block diagram is slightly modified to take this into account:

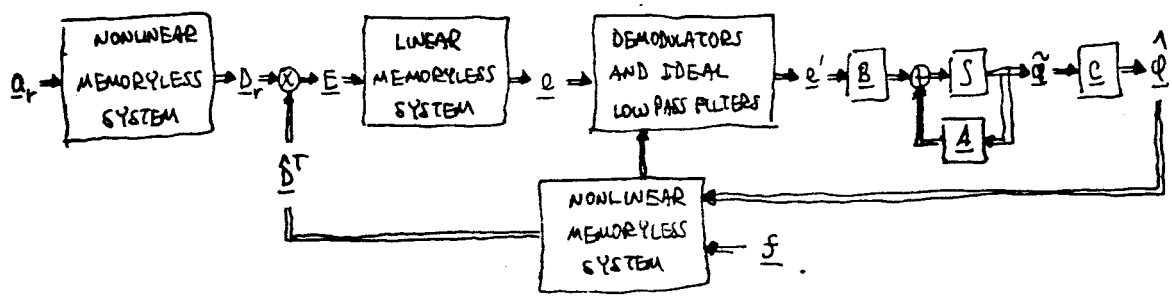

The only change from the earlier system is a processor which demodulates and filters $\underline{e}(\underline{\varphi}, \underline{\varphi}_r, \hat{\underline{\varphi}}, t)$ to give $\underline{e}'(\underline{\varphi}_r, \hat{\underline{\varphi}})$. If $\underline{e}$ is given by (3.16), then a possible processor is:

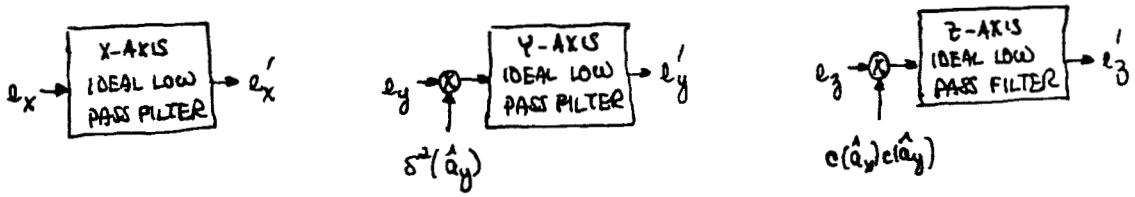

FIGURE 3.7

DIRECTION COSINE ATTITUDE ESTIMATION
DEMODULATORS AND LOW PASS FILTERS
CONSTANT RATE OF CHANGE OF ROLL-PITCH-YAW ANGLES

Each low pass filter is assumed ideal, passing signals at zero frequency without attenuation, but perfectly blocking signals outside this band from passing.

The demodulated and low pass filtered error, $\underline{e}'$, is used as the input to the linear time invariant system:

$$\dot{\tilde{\underline{\varphi}}} = \underline{A}\,\tilde{\underline{\varphi}} + \underline{B}\,\underline{e}' \qquad \tilde{\underline{\varphi}}(t_0) = \tilde{\underline{\varphi}}_0$$

3.33)

$$\hat{\underline{\varphi}} = \underline{C}\,\tilde{\underline{\varphi}}$$

For the example above, $\underline{e}'$ is

$$e_x' = \frac{1}{8}\left[-2\delta(d_y - d_x - d_z) - 2\delta(d_y - d_x + d_z) + \delta(d_x + d_y) + 2\delta(d_x + d_z) + 2\delta(d_x - d_z)\right]$$

$$e_y' = \frac{1}{8}\left[\delta(d_y + d_z) + \delta(d_y - d_z)\right]$$

$$e_z' = \frac{1}{8}\left[\delta(d_z + d_x) + \delta(d_z - d_x)\right]$$

$$d_x = \varphi_{rx} - \hat{\varphi}_x \qquad d_y = \varphi_{ry} - \hat{\varphi}_y \qquad d_z = \varphi_{rz} - \hat{\varphi}_z$$

The linearized analysis of these equations is straightforward: if $\underline{\varphi}_r = \underline{0}$, then $\underline{d} = -\hat{\underline{\varphi}}$ and if $|\varphi_x| \ll 1, |\varphi_y| \ll 1, |\varphi_z| \ll 1$, then to first order in $\hat{\underline{\varphi}}$

$$\dot{\hat{e}}_x \cong \frac{1}{8}\left[3\hat{e}_y - 9\hat{e}_x\right]$$
$$\dot{\hat{e}}_y \cong \frac{1}{8}\left[2\hat{e}_y\right]$$
$$\dot{\hat{e}}_z \cong -\frac{1}{8}\left[2\hat{e}_z\right]$$

If

$$\underline{B} = B\begin{bmatrix} 8/9 & -6 & 0 \\ 0 & -4 & 0 \\ 0 & 0 & 4 \end{bmatrix}, \quad \underline{A} = \underline{0}, \quad \underline{C} = \underline{I}$$

then

3.34)
$$\dot{\hat{\varphi}}_x \cong -B\hat{\varphi}_x \qquad \hat{\varphi}_x(t) \cong \hat{\varphi}_{x0}\, e^{-B(t-t_0)}$$
$$\dot{\hat{\varphi}}_y \cong -B\hat{\varphi}_y \qquad \hat{\varphi}_y(t) \cong \hat{\varphi}_{y0}\, e^{-B(t-t_0)} \qquad t \geq t_0$$
$$\dot{\hat{\varphi}}_z \cong -B\hat{\varphi}_z \qquad \hat{\varphi}_z(t) \cong \hat{\varphi}_{z0}\, e^{-B(t-t_0)}$$

That is, for small initial errors this system will estimate the correct phases. The steady state solutions can be discussed for this example just as in the previous example. No computer simulation of the equations of motion was carried out.

3.2.2. Stochastic Attitude Estimation

3.2.2.1. Model

A block diagram which includes noise sources is shown below, virtually identical with that in Figure 3.1:

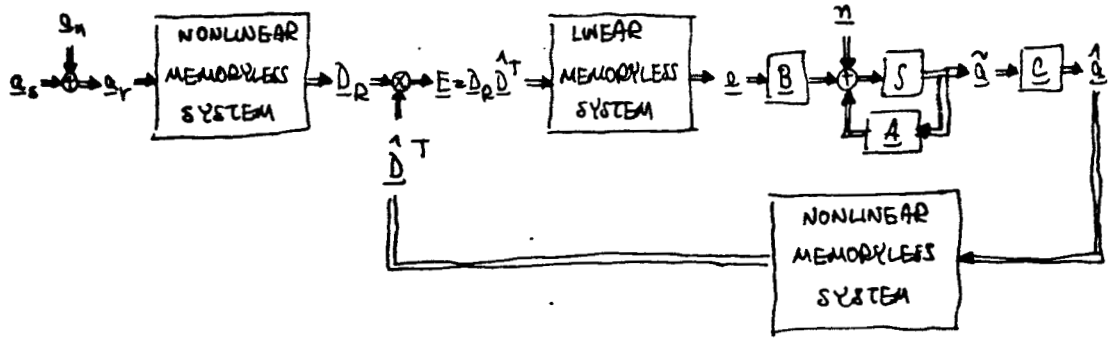

Two noise sources are evident:

1) $\underline{a}_n$, noise generated by sensor measurements, assumed added to the true angles $\underline{a}_s$

2) $\underline{n}$, noise generated by modulation and amplification of sensor measurements.

The received direction cosines are:

3.35) $$\underline{D}_R = \exp[(\tilde{s}_x + n'_x)\underline{L}_x]\exp[(\tilde{s}_y + n'_y)\underline{L}_y]\exp[(\tilde{s}_z + n'_z)\underline{L}_z]$$

i.e., products of exponentials of random processes. Ito (36) and McKean (41) have done some preliminary work in characterizing this particular process. However, the problem considered here, finding the aposteriori probability density of $\hat{\underline{a}}$, is apparently still unsolved. From here on, $\underline{a}_n$ is assumed $\underline{0}$, while $\underline{n}$ is assumed to the only source of uncertainty in estimating $\underline{a}_s$ given $\underline{D}_R$. This is an ad hoc assumption, done only in the hope of making the new problem analytically tractable.

3.2.2.2. Fokker-Planck Analysis

For example one, including amplifier noise $\underline{n}$ but not sensor noise $\underline{a}_n$, (3.23) becomes

$$\begin{aligned}
\dot{\hat{x}} &= B_x e_x(\hat{\underline{a}}, \underline{a}_r = \underline{a}_s) + n_x \\
\dot{\hat{y}} &= B_y e_y(\hat{\underline{a}}, \underline{a}_r = \underline{a}_s) + n_y \\
\dot{\hat{z}} &= B_z e_z(\hat{\underline{a}}, \underline{a}_r = \underline{a}_s) + n_z
\end{aligned} \qquad E(\underline{n}) = \underline{0}, E[\underline{n}(t)\underline{n}^T(s)] = \frac{1}{2}\delta(t-s)\begin{bmatrix} N_x & 0 & 0 \\ 0 & N_y & 0 \\ 0 & 0 & N_z \end{bmatrix}$$

where $\underline{n}$ is assumed to a zero-mean white Gauss-Markov random process, uncorrelated between axes.

It is straightforward to derive the Fokker-Planck equation for the aposteriori density function of $\underline{\hat{a}}(t)$, given $\underline{e} + \underline{n}$ from an initial time t_o to the present time t (see Viterbi (48)):

3.37) $$\frac{\partial}{\partial t} p = -\frac{\partial}{\partial \hat{\alpha}}(B_x \ell_x p) - \frac{\partial}{\partial \hat{\beta}}(B_y \ell_y p) - \frac{\partial}{\partial \hat{\gamma}}(B_z \ell_z p) + \frac{1}{2}\left[\frac{N_x}{2}\frac{\partial^2 p}{\partial \hat{\alpha}^2} + \frac{N_y}{2}\frac{\partial^2 p}{\partial \hat{\beta}^2} + \frac{N_z}{2}\frac{\partial^2 p}{\partial \hat{\gamma}^2}\right]$$

$$p = p(\underline{\hat{a}}(t) \mid \underline{e}, \underline{n}, [t_o, t])$$

This equation has an initial condition, in that $\underline{\hat{a}}(t_o)$ is known: $p(\underline{\hat{a}}(t_o)) = \delta(\underline{\hat{a}} - \underline{\hat{a}}_o)$. Since $\underline{e}$ is periodic in each component, p has a boundary condition:

$$p(\underline{\hat{a}}(t) \mid \underline{e}, \underline{n}, [t_o, t)) = p(\underline{\hat{a}}(t) + (a2\pi, b2\pi, c2\pi) \mid \underline{e}, \underline{n}, [t_o, t)), a, b, c \text{ integers}$$

This boundary condition suggests a possible approach to either solving the Fokker-Planck equation or approximating a solution is to expand the probability density in a Fourier series for each of the three estimated angles; this approach was never seriously investigated.

Either equation (3.19) or (3.20) can be used for $\underline{e}$; in neither case was it possible to solve the Fokker Planck equation explicitly.

For example two, again including amplifier noise $\underline{n}$ but ignoring sensor noise $\underline{a}_n$, (3.33) becomes ($\beta = 1$)

3.38)
$$\dot{\hat{\psi}}_x = 2s(d_y - d_x - d_z) - 2s(d_y - d_x + d_z) + s(d_x + d_y) + 2s(d_x + d_z) + 2s(d_x - d_z) + n_x$$
$$\dot{\hat{\psi}}_y = -s(d_y + d_z) - s(d_y - d_z) + n_y$$
$$\dot{\hat{\psi}}_z = s(d_z + d_x) + s(d_z - d_x) + n_z$$

$$E(\underline{n}) = \underline{0} \qquad E(\underline{n}(t)\underline{n}^T(s)) = \frac{1}{2}\delta(t-s) \begin{bmatrix} N_x & 0 & 0 \\ 0 & N_y & 0 \\ 0 & 0 & N_z \end{bmatrix}$$

The Fokker-Planck equation is identical in form to that in equation (3.37), with identical boundary conditions and initial conditions. Again, it was impossible to solve this equation explicitly for the aposteriori probability density function of $\underline{a}$.

3.2.2.3. Angle Estimate Skipping

Recall that without noise present many steady-state solutions exist for the two examples discussed. With noise present, it is possible for the systems discussed here to skip from one steady-state solution to another, with the skip caused by a burst of noise; computer simulations were carried out to observe this skipping, and showed it indeed does occur.

There are two ways for the estimated angles to skip: first, any estimated angle may increase by a multiple of 2π radians; second, all the angle estimates may hop from one type of steady-state solution to an entirely different one (cf. the three different types of steady-state solutions in equations (3.27) - (3.28)). The first case corresponds to a rotation in space about some axis by a multiple of 2π radians; physically, this corresponds to no change in the estimate of orientation in space. The second case does correspond to a change in the estimate of spatial orientation. The only approach known for investigating these two cases is to check the stability of steady-state solutions in the absence of noise, as was discussed in sections 3.2.1.2-3. Bounds on how frequently an angle estimate might skip are not known at the present time.

3.3. Attitude Estimation With Quaternions

3.3.1. Deterministic Attitude Estimation

Because of algebraic complexity encountered in using direction cosines, as well as the inability to solve the Fokker-Planck equation for the aposteriori statistics of $\underline{a}$, the same attitude estimation method was implemented with quaternions rather than direction cosines. This implementation is now discussed.

3.3.1.1. Model

A block diagram for a system which estimates three roll-pitch-yaw angles which specify the orientation of a rigid body from quaternion measurements is shown below (without any noise sources):

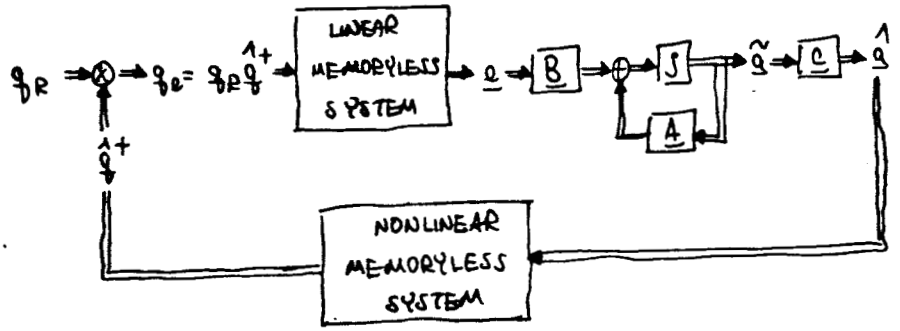

FIGURE 3.9
QUATERNION ATTITUDE ESTIMATION
CONSTANT ORIENTATION IN SPACE

It is assumed:

1) all components of $\underline{q}_r$, the received quaternion, are observable
2) $\underline{q}_r$ and $\hat{\underline{q}}$, the received and estimated quaternions, respectively, are each described by three roll-pitch-yaw angles, $\underline{a}_r$ and $\hat{\underline{a}}$, respectively.

3.39) $\underline{q}_r = [c(x_r/2)+\hat{i}\,s(y_r/2)]\,[c(y_r/2)+\hat{j}\,s(y_t/2)][c(z_r/2)+\hat{k}\,s(z_r/2)]$

3.40) $\hat{\underline{q}} = [c(\hat{x}/2)+\hat{i}\,s(\hat{x}/2)]\,[c(\hat{y}/2)+\hat{j}\,s(\hat{y}/2)]\,[c(\hat{z}/2)+\hat{k}\,s(\hat{z}/2)]$

where $(1,\hat{i},\hat{j},\hat{k})$ are unit quaternions which multiply according to the rules of quaternion multiplication. $\underline{q}_r$ is postmultiplied by $\underline{q}^+$, the quaternion conjugate of $\underline{q}$ (denoted with a "+"), which produces an error quaternion, $\underline{q}_e$

3.41) $\underline{q}_e = \underline{q}_r\,\underline{q}^+ = e_x\hat{i}+e_y\hat{j}+e_z\hat{k}+e_w$

If each of the estimated angles as well as the actual angles has magnitude much less than unity, $\underline{q}_e$ can be approximated

3.42) $e_x \tilde{=} (x_r - \hat{x})/2$, $e_y \tilde{=} (y_r - \hat{y})/2$, $e_z \tilde{=} (z_r - \hat{z})/2$ $\quad e_w \tilde{=} 1$

Unlike the direction cosine case, $\underline{e}$ can be chosen here in only one way, $\underline{e} = (e_x, e_y, e_z)$.

$\underline{e} = (e_x, e_y, e_z)$ is used as an input to a linear time-invariant system which generates $\underline{a}$:

$$\dot{\tilde{\underline{a}}} = \underline{A}\tilde{\underline{a}} + \underline{B}\underline{e}$$

3.43) $$\hat{\underline{a}} \tilde{=} \underline{C}\tilde{\underline{a}}$$

$\hat{\underline{a}}$ is then used to generate $\underline{q}^+$, closing the loop. The intuitive operation of a quaternion "phase-locked-loop" is identical to that of a direction cosine "phase-locked-loop": postmultiplying $\underline{q}_r$ by $\underline{q}^+$ undoes the rotation represented by $\underline{q}_r$; the loop negative feedback action nulls $\underline{e}$ to zero, eventually making $\underline{q}_e = 1$ and $\underline{a}_r = \hat{\underline{a}}$. For future reference the components of $\underline{e}$ are explicitly stated:

3.44a) $e_x = s(d_x/2)c(d_y/2)c(d_z/2)+c(d_x/2)s(s_y/2)s(d_z/2)$ $\quad s_x = x_r + \hat{x}$ $\quad d_x = x_r - \hat{x}$

3.44b) $e_y = c(s_x/2)s(d_y/2)c(d_z/2)-s(d_x/2)c(s_y/2)s(d_z/2)$ $\quad s_y = y_r + \hat{y}$ $\quad d_y = y_r - \hat{y}$

3.44c) $e_z = c(s_x/2)c(s_y/2)s(d_z/2)+s(s_x/2)s(d_y/2)c(d_z/2)$ $\quad s_z = z_r + \hat{z}$ $\quad d_z = z_r - \hat{z}$

To proceed further, the two examples discussed in the direction cosine case are re-examined.

3.3.1.2. Example 1--Constant Orientation in Space

Throughout this section, $\underline{a}_r$ is assumed constant but unknown. If

$$\underline{A} = \begin{bmatrix} 0 & 0 & 0 \\ 0 & 0 & 0 \\ 0 & 0 & 0 \end{bmatrix} \qquad \underline{B} = \begin{bmatrix} B_x & 0 & 0 \\ 0 & B_y & 0 \\ 0 & 0 & B_z \end{bmatrix} \qquad \underline{C} = \begin{bmatrix} 1 & 0 & 0 \\ 0 & 1 & 0 \\ 0 & 0 & 1 \end{bmatrix}$$

then equations (3.43) and (3.44) can be combined:

$$\begin{aligned} \dot{\hat{x}} &= \{s(d_x/2)c(d_y/2)c(d_z/2)+c(d_x/2)s(s_y/2)s(d_z/2)\}B_x \qquad x(t_o) = x_o \\ \dot{\hat{y}} &= \{c(s_x/2)s(d_y/2)c(d_z/2)-s(d_x/2)c(s_y/2)s(d_z/2)\}B_y \qquad y(t_o) = y_o \\ \dot{\hat{z}} &= \{c(s_x/2)c(s_y/2)s(d_z/2)+s(s_x/2)s(d_y/2)c(d_z/2)\}B_z \qquad z(t_o) = z_o \end{aligned} \tag{3.45}$$

This discrete-time sampled-input approximation in Figure 3.2 was used to approximate these equations; the figures on the next page are the results of two computer simulations (Figure 3.10, $x_r = 60^\circ$, $y_r = 45^\circ$, $z_r = 30^\circ$, $\underline{a}_o = \underline{0}^\circ$ and Figure 3.11, $x_r = 60^\circ$, $y_r = 45^\circ$, $z_r = -30^\circ$, $\underline{a}_o = \underline{0}^\circ$) with $\Delta t = 0.2$ seconds and $B_x = B_y = B_z = 1$.

The linearized analysis, assuming $\underline{a}_r = (60^\circ, 45^\circ, 30^\circ)$, and $\hat{\underline{q}} = (x_r+\delta x, y_r+\delta y, z_r+\delta z)$ with $|\delta x|\ll 1, |\delta y|\ll 1, |\delta z|\ll 1$, to first order in $\delta x, \delta y, \delta z$ shows

QUATERNION ATTITUDE ESTIMATION
COMPUTER SIMULATION RESULTS

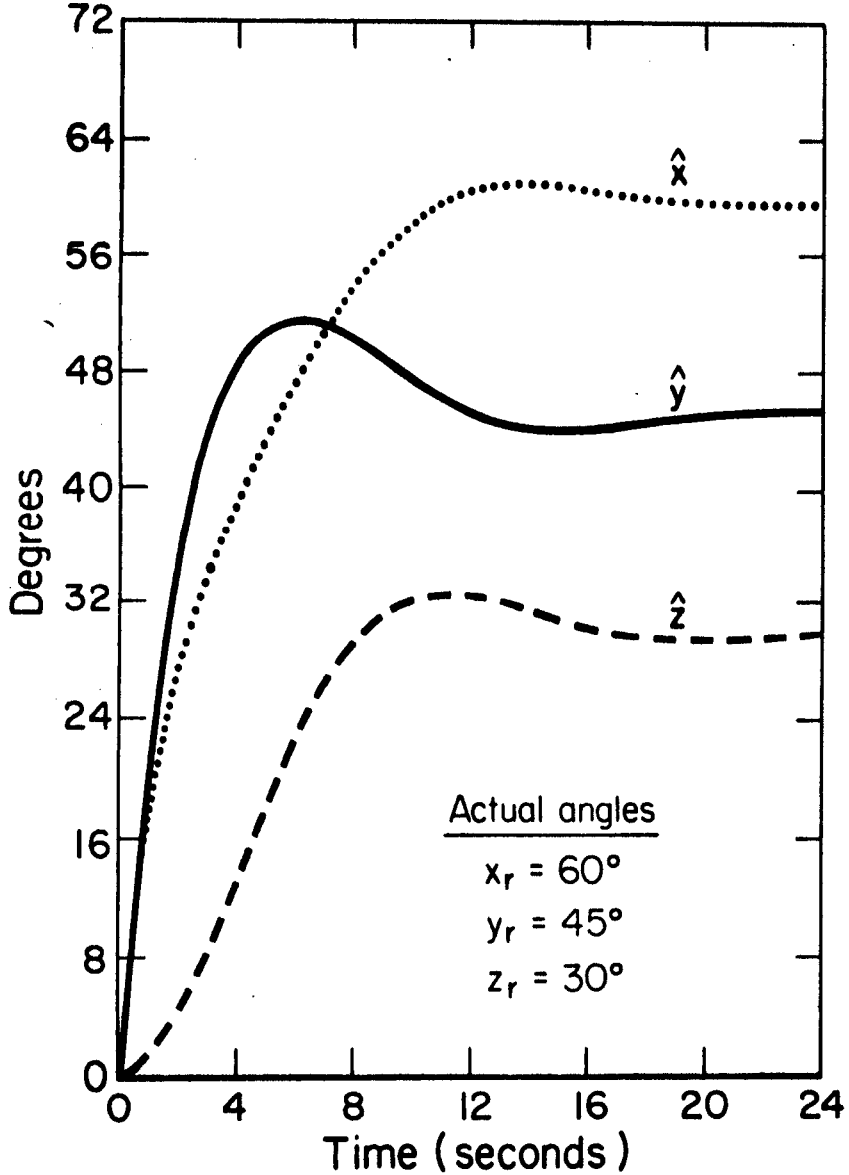

FIGURE 3.10

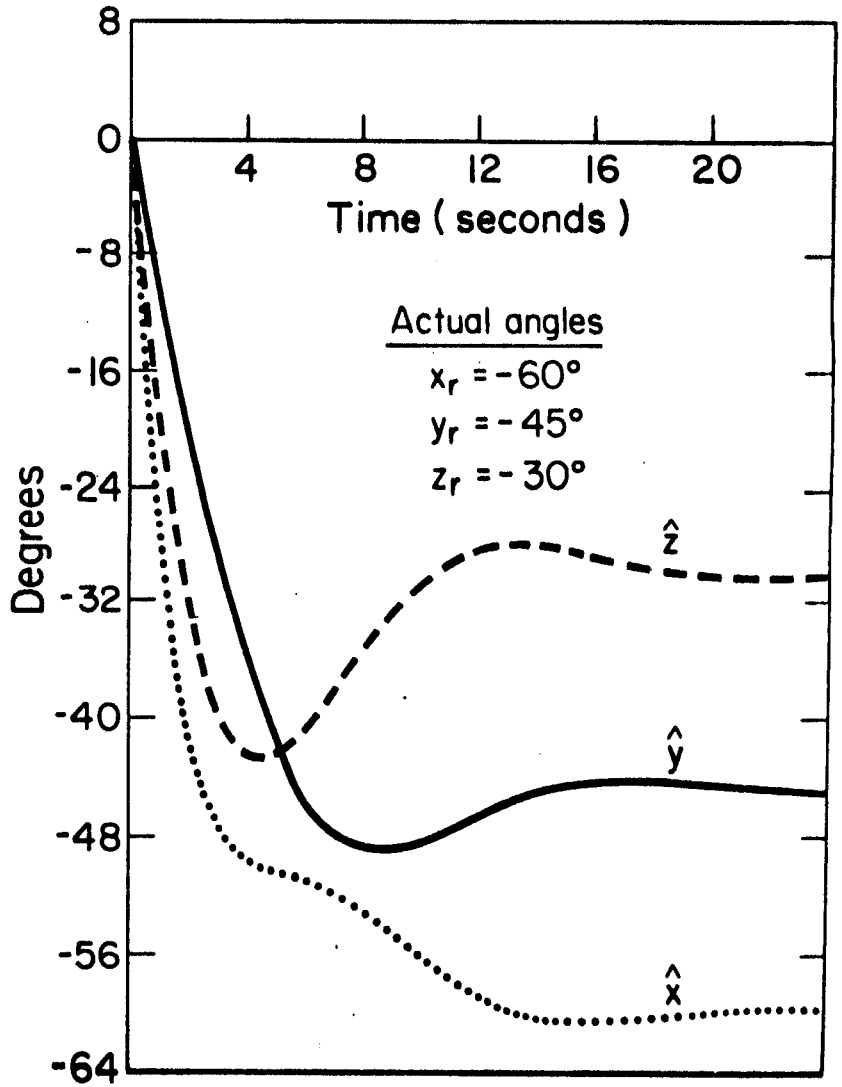

FIGURE 3.11

$$
\begin{aligned}
\dot{\delta x} &\cong B_x\left[-\tfrac{1}{2}\delta x - \tfrac{\sqrt{3}}{4}\delta y\right] & \delta x(t) &\cong e^{-\frac{1}{2}B_x(t-t_0)}\,\delta x_0 \\
\dot{\delta y} &\cong B_y\left[-\tfrac{1}{4}\delta y\right] & \delta y(t) &\cong e^{-\frac{1}{4}B_y(t-t_0)}\,\delta y_0 \qquad t \geq t_0 \\
\dot{\delta z} &\cong B_z\left[-\tfrac{1}{4}\delta y - \tfrac{\sqrt{3}}{8}\delta z\right] & \delta z(t) &\cong e^{-\frac{\sqrt{3}}{8}B_z(t-t_0)}\,\delta z_0
\end{aligned}
\tag{3.46}
$$

The steady state solutions to $\underline{e} = (e_x, e_y, e_z) = \underline{0}$ are

$$
\begin{aligned}
x &= x_r + \pi a & & & x &= x_r + a\pi \\
y &= y_r + \pi b & & a,b,c \text{ even;} & y &= -y_r + b\pi \qquad a,b,c \text{ odd} \\
z &= z_r + \pi c & & & z &= z_r + c\pi
\end{aligned}
$$

Again, an analysis similar to that in Section (3.2.1.2) must be carried out to determine which states are stable and which are not. For example, a computer simulation of these equations was carried out for

$$
\begin{aligned}
\hat{x}_o &= 0^o & x_r &= 120^o \\
\hat{y}_o &= 0^o & y_r &= 105^o \\
\hat{z}_o &= 0^o & z_r &= 90^o
\end{aligned}
$$

and the results were similar to those in Figure 3.6, with the steady state (denoted ss) angle estimates being

$$
\begin{aligned}
\hat{x}_{ss} &= -60^o \cong x_r + a\pi \\
\hat{y}_{ss} &= 75^o \cong -y_r + b\pi \qquad a,b,c \text{ odd} \\
\hat{z}_{ss} &= -90^o \cong z_r + c\pi
\end{aligned}
$$

3.3.1.3. Example 2--Constant Rate of Change of Roll-Pitch-Yaw Angles

In this section $\underline{a}_r = \underline{f}\,t + \underline{\varphi}_r$, and $\underline{a} = \underline{f}\,t + \hat{\underline{\varphi}}$, where $\underline{f}$ is known and constant, $\underline{\varphi}_r$ is unknown and constant, and $\hat{\underline{\varphi}}$ is estimate of $\underline{\varphi}_r$. The block diagram of the attitude estimation system becomes

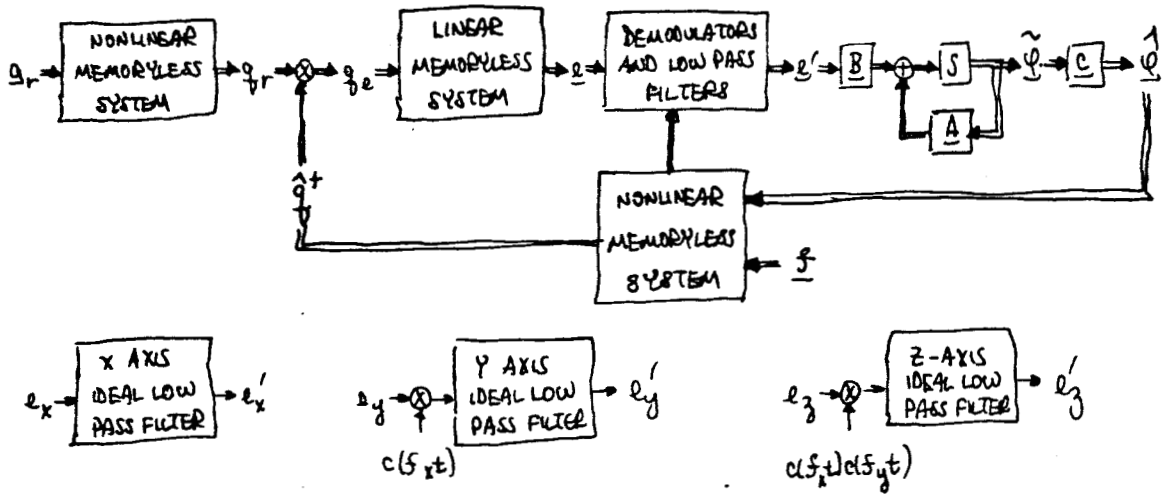

FIGURE 3.12

QUATERNION ATTITUDE ESTIMATION -- CONSTANT RATE OF CHANGE OF ROLL-PITCH-YAW ANGLES

If $\underline{e}' = (e'_x, e'_y, e'_z)$ is the input to the linear time invariant system

$$\underline{A} = \underline{0} \quad B = \begin{bmatrix} B_x & 0 & 0 \\ 0 & B_y & 0 \\ 0 & 0 & B_z \end{bmatrix} \quad \underline{C} = \underline{I}$$

then the equations for $\hat{\underline{\varphi}}$ are

$$\begin{aligned}
\dot{\hat{\varphi}}_x &= B_x \left\{ s[(\varphi_{rx} - \hat{\varphi}_x)/2]\, c[(\varphi_{ry} - \hat{\varphi}_y)/2]\, c[(\varphi_{rz} - \hat{\varphi}_z)/2] \right\} \qquad \hat{\varphi}_x(t_0) = \hat{\varphi}_{x0} \\
\dot{\hat{\varphi}}_y &= B_y \left\{ c[(\varphi_{rx} + \hat{\varphi}_x)/2]\, s[(\varphi_{ry} - \hat{\varphi}_y)/2]\, c[(\varphi_{rz} - \hat{\varphi}_z)/2] \right\} \qquad \hat{\varphi}_y(t_0) = \hat{\varphi}_{y0} \\
\dot{\hat{\varphi}}_z &= B_z \left\{ c[(\varphi_{rx} + \hat{\varphi}_x)/2]\, c[(\varphi_{ry} + \hat{\varphi}_y)/2]\, s[(\varphi_{rz} - \hat{\varphi}_z)/2] \right\} \qquad \hat{\varphi}_z(t_0) = \hat{\varphi}_{z0}
\end{aligned} \tag{3.47}$$

The linearized analysis of these equations (assuming $\underline{\varphi}_r = \underline{0}$, and $|\hat{\varphi}_x| << 1$, $|\hat{\varphi}_y| << 1$, $|\hat{\varphi}_z| << 1$) is identical to that in (3.36). The steady state solutions, which are also the stable solutions, are

$$\hat{\varphi}_x = \varphi_{rx} + 2\pi a$$
$$\hat{\varphi}_y = \varphi_{ry} + 2\pi b \qquad a, b, c \text{ INTEGERS}$$
$$\hat{\varphi}_z = \varphi_{rz} + 2\pi c$$

3.48)

3.3.2. Stochastic Attitude Estimation

3.3.2.1. Model

A block diagram which includes noise sources is shown below,

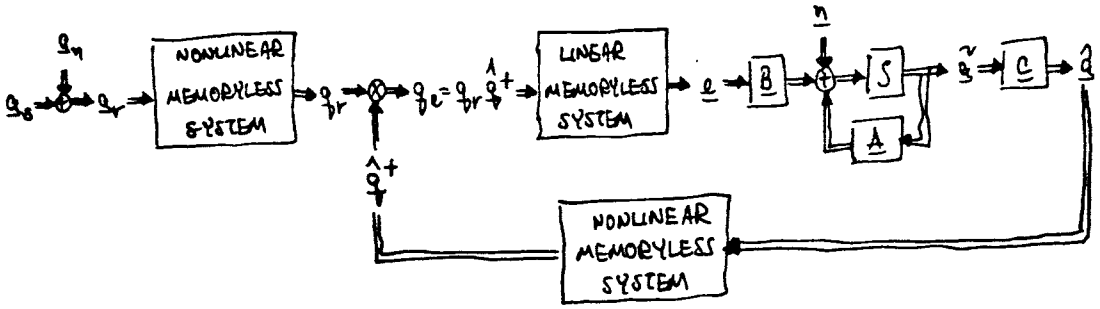

FIGURE 3.13
QUATERNION ATTITUDE ESTIMATION IN THE PRESENCE OF NOISE -- CONSTANT ORIENTATION IN SPACE

where $\underline{a}_n$ arises from sensor measurements, $\underline{n}$ from amplification and modulation as in the direction cosine case.

The received quaternion is:

$$\underline{q}_r = [c(s_x + n'_x/2) + \hat{i}\, s(s_x + n'_x/2)]\,[c(s_y + n'_y/2) + \hat{j}\, s(s_y + n'_y/2)]$$

$$[c(s_z + n'_z/2) + \hat{k}\, s(s_z + n_z/2)]$$

Again, no methods are known for handling $\underline{a}_n$; from this point on it will be

assumed $\underline{a}_n = \underline{0}$, while $\underline{n}$ is a zero-mean white Gaussian random process, uncorrelated from one component to the next.

3.3.2.2. Fokker-Planck Analysis

For example one, including $\underline{n}$ in equation (3.35) shows

$$
\begin{aligned}
\dot{\hat{x}} &= B_x\{s(d_x/2)\, c(d_y/2)\, c(d_z/2) + c(d_x/2)\, s(s_y/2)\, s(d_z/2)\} + n_x \\
\dot{\hat{y}} &= B_y\{c(s_x/2)\, s(d_y/2)\, c(d_z/2) - s(d_x/2)\, c(s_y/2)\, s(d_z/2)\} + n_y \\
\dot{\hat{z}} &= B_z\{c(s_x/2)\, c(s_y/2)\, s(d_z/2) + s(s_x/2)\, s(d_y/2)\, c(d_z/2)\} + n_z
\end{aligned}
\tag{3.49}
$$

where

$$
E[\underline{n}(t)\,\underline{n}^T(s)] = \frac{1}{2}\,\delta(t-s)\begin{bmatrix} N_x & 0 & 0 \\ 0 & N_y & 0 \\ 0 & 0 & N_z \end{bmatrix}, \quad E[\underline{n}(t)] = \underline{0}
$$

The Fokker-Planck equation is straightforward to derive:

$$
\begin{aligned}
\frac{\partial}{\partial t}p &= -\frac{\partial}{\partial \hat{x}}(B_x e_x p) - \frac{\partial}{\partial \hat{y}}(B_y e_y p) - \frac{\partial}{\partial \hat{z}}(B_z e_z p) \\
&\quad + \frac{1}{2}\left[\frac{N_x}{2}\frac{\partial^2 p}{\partial \hat{x}^2} + \frac{N_y}{2}\frac{\partial^2 p}{\partial \hat{y}^2} + \frac{N_z}{2}\frac{\partial^2 p}{\partial \hat{z}^2}\right]
\end{aligned}
\tag{3.50}
$$

$$p = p[\hat{\underline{q}}(t) \mid \underline{q}_r, [t_0, t)]$$

The initial condition and boundary conditions are

$$
p[\hat{\underline{q}}(t_0)] = \delta(\hat{\underline{q}} - \underline{q}_0)\,; \quad p[\hat{\underline{q}}(t) \mid \underline{q}_r, [t_0, t)] = p[\hat{\underline{q}}(t) + (4\pi a, 4\pi b, 4\pi c) \mid \underline{q}_r, [t_0, t)]
\tag{3.51}
$$

$$a, b, c = 0, \pm 1, \pm 2, \ldots$$

Three assumptions are made

i) $\underline{a}_r = \underline{a}_s = \underline{0}$, the actual angles $\underline{a}_r$ are all zero

ii) $N = N_x = N_y = N_z$, the noise covariance is identical in all three axes,

iii) $B_x = B_y = B_z = B$, identical gain in all three error amplifiers

then the steady-state Fokker-Planck equation can be written quite simply:

$$3.52) \quad \frac{\partial}{\partial t} p = \underbrace{\frac{\partial}{\partial \hat{x}}\left[\frac{N}{4}\frac{\partial p}{\partial \hat{x}} + B\ell_x p\right]}_{①} + \underbrace{\frac{\partial}{\partial \hat{y}}\left[\frac{N}{4}\frac{\partial p}{\partial \hat{y}} + B\ell_y p\right]}_{②} + \underbrace{\frac{\partial}{\partial \hat{\theta}}\left[\frac{N}{4}\frac{\partial p}{\partial \hat{\theta}} + B\ell_z p\right]}_{③}$$

If the solution is assumed to be p_1, where

$$3.53) \quad p_1 = C \exp \frac{8B}{N}\left[c(x/2)\, c(y/2)\, c(z/2) - s(x/2)\, s(y/2)\, s(z/2)\right]$$

C = normalization constant

then the first and third terms in (3.52) are zero, but not the second. On the other hand, if the solution is assumed to be p_2, where

$$3.54) \quad p_2 = C \exp\left\{\frac{8B}{N}\left[c(x/2)\, c(y/2)\, c(z/2) + s(x/2)\, s(y/2)\, s(z/2)\right]\right\}$$

C = normalization constant

then the second term in (3.52) is zero, but not the first or third. Even though the solution (3.52) seems within reach, no solution was found.

For example two, including amplifier noise $\underline{n}$, (3.47) now becomes

$$\dot{\hat{\varphi}}_x = B_x\left\{s\left(\frac{\varphi_{rx}-\hat{\varphi}_x}{2}\right) c\left(\frac{\varphi_{ry}-\hat{\varphi}_y}{2}\right) c\left(\frac{\varphi_{rz}-\hat{\varphi}_z}{2}\theta\right)\right\} + n_x = B_x \ell_x + n_x$$

$$3.55) \quad \dot{\hat{\varphi}}_y = B_y\left\{c\left(\frac{\varphi_{rx}+\hat{\varphi}_x}{2}\right) s\left(\frac{\varphi_{ry}-\hat{\varphi}_y}{2}\right) c\left(\frac{\varphi_{rz}-\hat{\varphi}_z}{2}\theta\right)\right\} + n_y = B_y \ell_y + n_y$$

$$\dot{\hat{\varphi}}_z = B_z\left\{c\left(\frac{\varphi_{rx}+\hat{\varphi}_x}{2}\right) c\left(\frac{\varphi_{ry}+\hat{\varphi}_y}{2}\theta\right) s\left(\frac{\varphi_{rz}-\hat{\varphi}_z}{2}\theta\right)\right\} + n_z = B_z \ell_z + n_z$$

The Fokker-Planck equation is identical in form to (3.50). Again, assume $\underline{\varphi}_r = \underline{0}$, $N_x = N_y = N_z = N$, and $B_x = B_y = B_z = B$, so that the steady state Fokker-Planck equation becomes:

3.56) $$0 = \frac{\partial}{\partial t} p = \frac{\partial}{\partial \hat{\varphi}_x}\left[\frac{N}{4}\frac{\partial p}{\partial \hat{\varphi}_x} + Bps(\hat{\varphi}_x/2)c(\hat{\varphi}_y/2)c(\hat{\varphi}_z/2)\right] + \frac{\partial}{\partial \hat{\varphi}_y}\left[\frac{N}{4}\frac{\partial p}{\partial \hat{\varphi}_y} + Bpc(\hat{\varphi}_x/2)s(\hat{\varphi}_y/2)c(\hat{\varphi}_z/2)\right] + \frac{\partial}{\partial \hat{\varphi}_z}\left[\frac{N}{4}\frac{\partial p}{\partial \hat{\varphi}_z} + Bc(\hat{\varphi}_x/2)c(\hat{\varphi}_y/2)s(\hat{\varphi}_z/2)\right]$$

$$p = p[\hat{\underline{\varphi}} \mid q_r, [t_0, t \to \infty)]$$

The solution to this equation is

3.57) $$p(\hat{\underline{\varphi}} \mid q_r, [t_0, t \to \infty)) = C \cdot \exp\left\{\frac{8B}{N} c(\hat{\varphi}_x/2)c(\hat{\varphi}_y/2)c(\hat{\varphi}_z/2)\right]$$

where C is a normalization constant, chosen such that

3.58) $$\int_{\hat{\varphi}_x=-2\pi}^{2\pi}\int_{\hat{\varphi}_y=-2\pi}^{2\pi}\int_{\hat{\varphi}_z=-2\pi}^{2\pi} p[\hat{\underline{\varphi}} \mid q_r, [t_0, t \to \infty)]\, d\hat{\varphi}_x\, d\hat{\varphi}_y\, d\hat{\varphi}_z = 1$$

If $|\hat{\varphi}_x| \ll 1$, $|\hat{\varphi}_y| \ll 1$, $|\hat{\varphi}_z| \ll 1$,

3.59) $$p \cong C \exp\left\{\frac{8B}{N}\left[1 - \frac{1}{8}(\hat{\varphi}_x^2 + \hat{\varphi}_y^2 + \hat{\varphi}_z^2)\right]\right.$$

which appears Gaussian with variance $(N/2B)$.

To keep the steady-state error variance small, B should be chosen such that

$$|N/2B| \ll 1$$

Recall that in the linearized analysis of the model, B corresponds to bandwidth. Speaking intuitively, the larger the bandwidth B the smaller the steady-state

error variance; this is analogous to the situation in an angle modulation communications system, where by increasing the system bandwidth noise effects are suppressed.

At this point, the steady-state Fokker-Planck equation has been explicitly solved for a special set of circumstances, a quaternion implementation of a particular estimation procedure. Why not return to the direction cosine implementation of this estimation process and solve the steady-state Fokker-Planck equation under the same set of circumstances as was just done?

In fact, this was attempted, but the attempt was unsuccessful. The reason for this failure is apparently fundamental, based on the observation that the observation spaces for direction cosines and quaternions are essentially different vector spaces. Recall the underlying parameter space for both estimation procedures is a real Euclidean three-dimensional vector space. However, the direction cosine observation space and the quaternion observation space are real Euclidean vector spaces, of dimension nine and four, respectively. Next, elements in the observed direction cosine matrix and components of the observed quaternion are functions of sines and cosines of the three angles to be estimated; the explicit relationship between each observed quaternion component and the elements in the observed direction cosine matrix, or between each element in the observed direction cosine matrix and the observed quaternion components is straightforward to work out but algebraically complex (this relationship reflects the fact that, loosely speaking, a quaternion when squared becomes a direction cosine). Finally, since the observation

spaces are different in each case, the actual details of the estimation procedure are different; for the particular example considered here, the demodulators differ for the direction cosine case from those in the quaternion case. If it could be shown that each estimation procedure was an optimum procedure, then perhaps it could be shown that the two estimation procedures were equivalent; however, the rule for estimating angles discussed here is a heuristic one, and it is not at all clear what the optimum estimation procedure should be, so it is not surprising that the two demodulators are different.

In summary, while it was fortuitous that the Fokker-Planck equation could be solved under a special set of circumstances in the quaternion case, it is not at all clear why this good fortune should carry over under the same special set of circumstances to the direction cosine case.

3.3.2.3. Angle Estimate Skipping

The next page shows the results of a computer simulation of example one with amplifier noise included (equation 3.49), with $\underline{a}_r = (60^o, 0^o, -60^o)$. Note that two of the estimates of these angles are initially close to the correct estimate, and then skip by 2π radians, while the third estimate always remains close to the correct angle. Some of the qualitative issues associated with estimates of angles skipping have been discussed earlier (3.2.2.3), and will not be repeated here. No bounds on how frequently the estimates might skip are known at the present time.

Figure 3.14

An Example of Angle Estimate Skipping--Constant Orientation in Space--Quaternion Implementation of Attitude Estimation Method

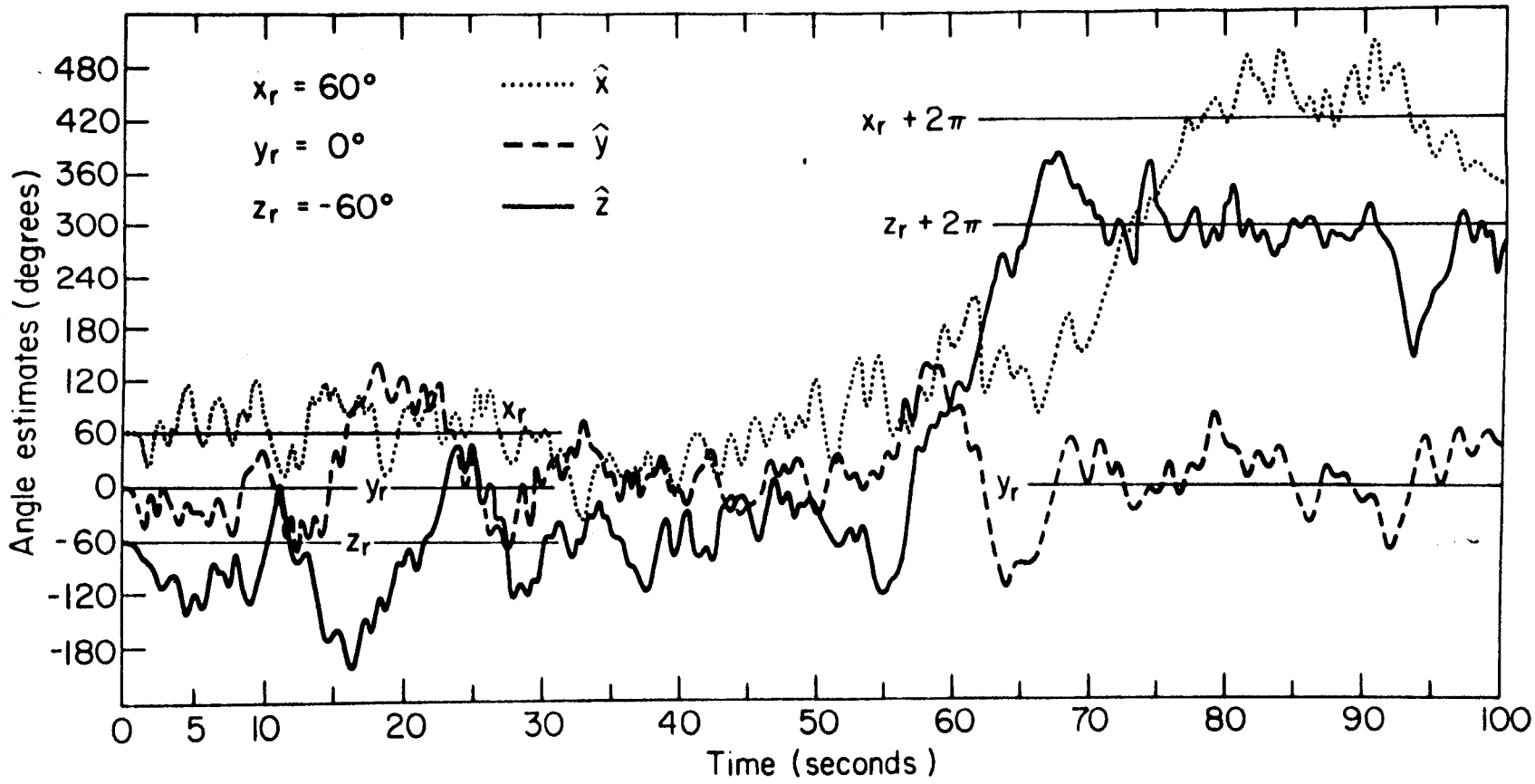

3.4. Summary

This chapter developed a new method for estimating the three angles which specify the spatial orientation of a rigid body, given noisy sensor measurements. Two ways to implement this method, one based on direction cosines, the other on quaternions, were discussed for two specific examples, fixed orientation in space and constant rate of change of the three angles. The theoretical deterministic performance limits of each implementation were covered: first, an analysis of the dynamics of each implementation (assuming samll estimation errors) was carried out, and second, the steady state and stable equilibrium points of each method were discussed. When noise was included in each implementation, the theoretical stochastic performance limits were quite difficult to pin down; in particular, while Fokker-Planck equations could be derived for angle estimation error a posteriori probability density functions under certain simplifying assumptions about the nature of the observation noise, these equations could rarely be solved. However, for a special set of simplifying assumptions, with a quaternion based method for estimating the unknown phases of the three angles which change at a constant known rate with time, the Fokker-Planck equation was explicitly solved for the steady state error probability density function.

Chapter Four

Solar Pressure Attitude Control

4.1. Introduction

A brief overall description of two possible synchronous orbit communication satellites is now presented, before proceeding to a detailed description of the attitude control dynamics of each design. Both satellites orient themselves in space using torques generated from solar or sunlight pressure.

The sketches on the next two pages show two possible designs for an air traffic control satellite that would be in synchronous orbit over the North Atlantic. Each design has two sets of solar cell panels and a central antenna-electronics body, with three solar sails attached to each solar panel for attitude control. In both designs the antenna rotates about its central shaft every twenty four hours, minus a factor due to the earth's annual motion about the sun; in Design I the solar panels rotate about their shafts once each year, while in Design II the panels wobble from plus 23.5 degrees (with respect to the antenna shaft) to minus 23.5 degrees and back again once each year. The attitude control problem is to point the antenna earthward and the solar panels sunward, aligning two prescribed body axes which is equivalent to three axis control of the solar panels and a prescribed motion of the antenna with respect to the panels.

The technological constraints involved in these designs are now sketched extremely quickly. First, thermal design is simplified for the solar cell power plant since nominally only one surface faces the sun. Second, Design I involves a set of bearings for each panel which must rotate

FIGURE 4.1
DESIGN I

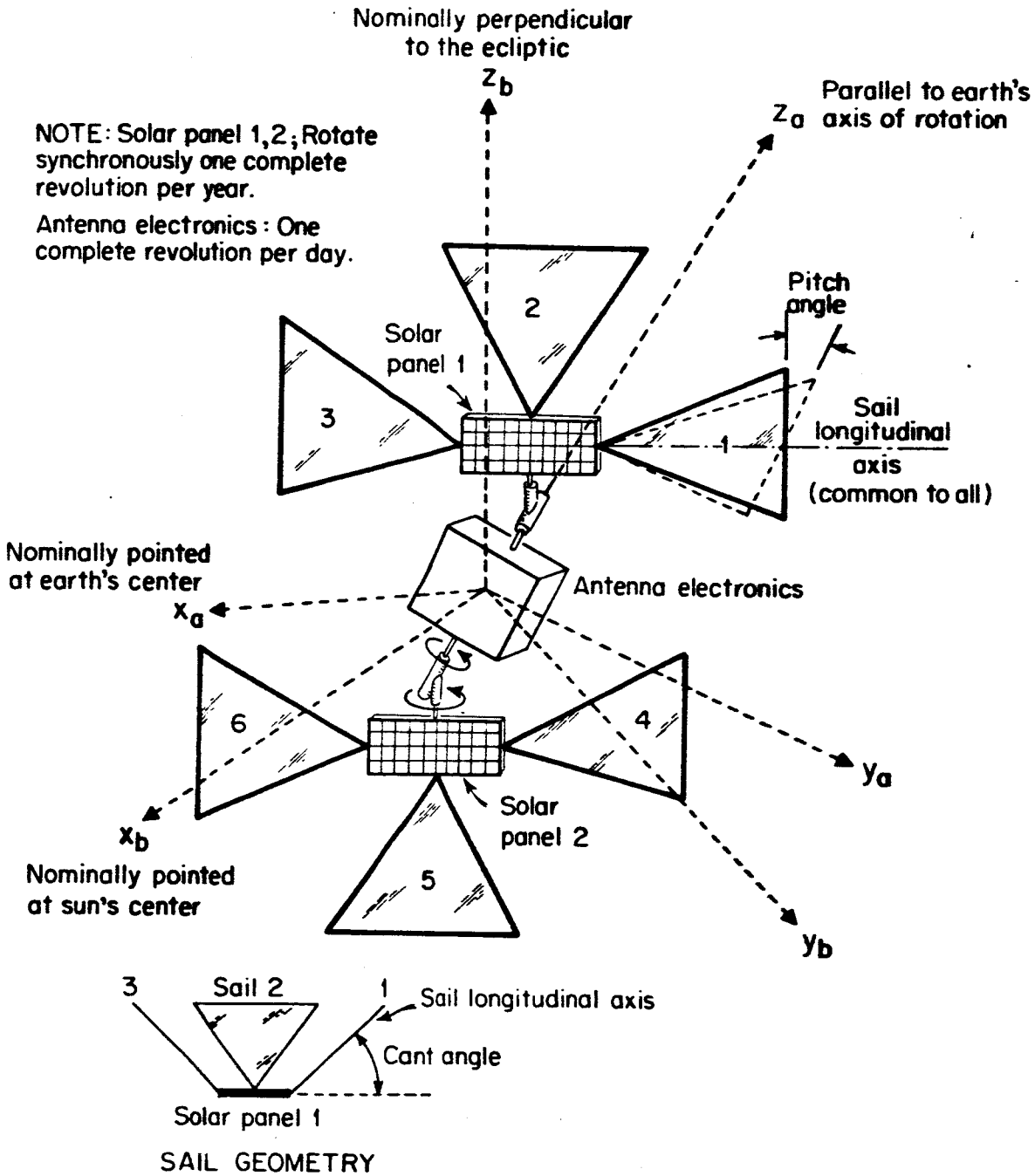

SAIL GEOMETRY

FIGURE 4.2
DESIGN II

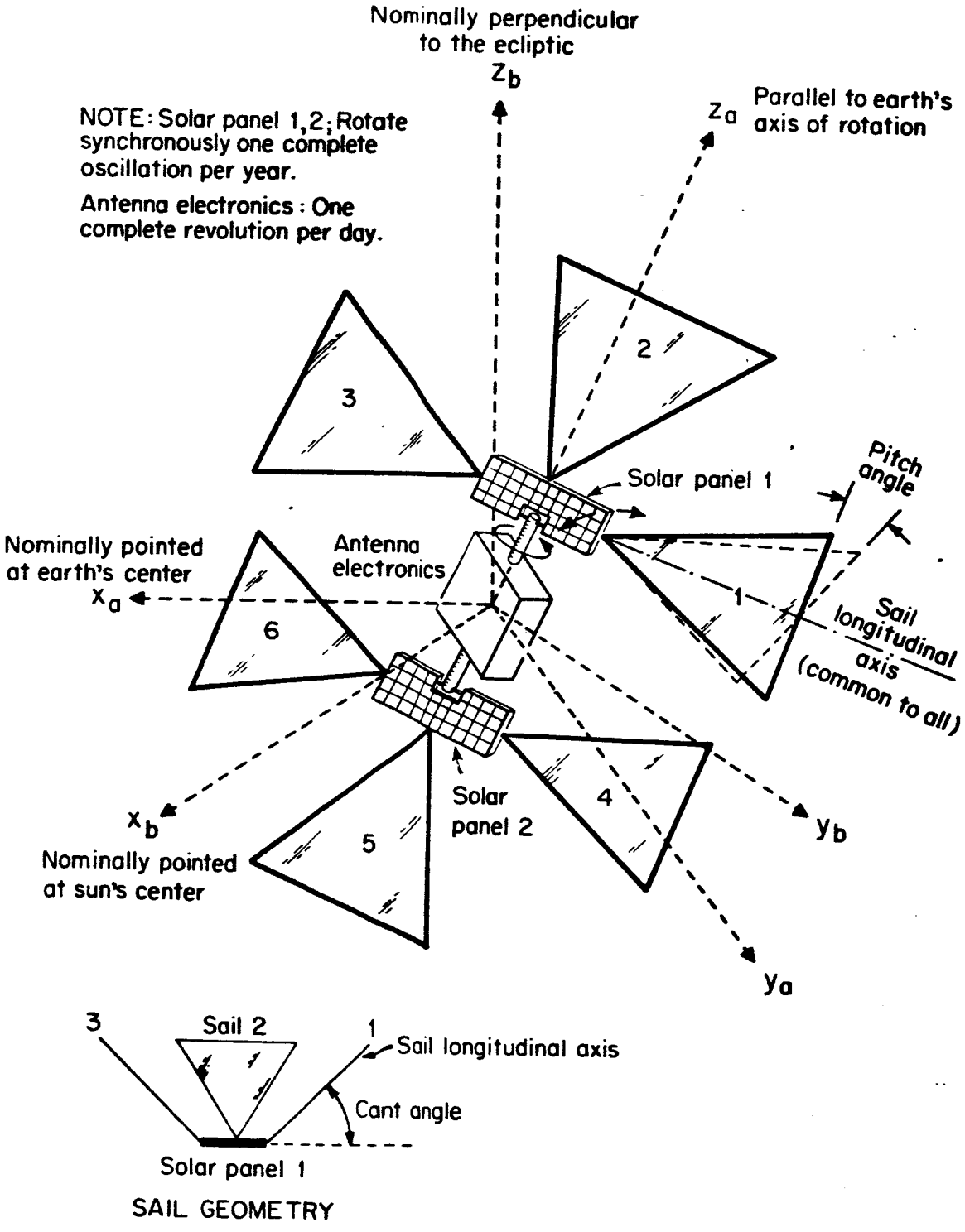

extremely slowly in space while passing DC electric power from the solar cells to the antenna electronics; Design II circumventsthis potential problem, because its solar panel need only be a spring capable of plus-minus 23.5 degree motion. Third, the power systems for both designs contain solar cells and batteries (for use when the satellite is in earth shadow--seventy two minutes is the longest shadow duration, twice a year (Goddard (56)). Fourth, structural problems are complicated by possible sail flexing and bending. For a much more thorough coverage of these and other technological problems, the reader is referred to the bibliography (Abel (53), Fleischer (55), Goddard (57), Likins (58) MacLellan (59), M.I.T. (60)). This report will concentrate on the attitude control dynamics of Designs I and II from here on, not on the systems engineering aspects of communications satellites.

4.2. Derivation of Equations of Motion

Assume the solar panels and antenna (in Designs I and II) are ideal rigid bodies with massless interconnecting shafts and solar sails, and the solar panels are identical and rotate in unison about their respective shafts. Fix an inertial right-handed coordinate frame at the center of the sun, with its z-axis normal to the ecliptic and its x-axis pointing at the center of mass of the earth once a year, at the winter solstice. From the previous discussion on Newtonian mechanics, the dynamical equations of motion for the center of mass of either design are

4.1) $\frac{d}{dt}\,\underline{P} = \underline{F} \qquad \frac{d}{dt}\,M = 0$

4.2) $\frac{d}{dt}\,(t\underline{P} - M\dot{\underline{R}}_{cm}) = tF$

where $\underline{P}$ = momentum of center of mass in inertial coordinates

M = total satellite mass

$\underline{F}$ = external forces acting on center of mass in inertial coordinates

The center of mass kinematical equations of motion for either design are

4.3) $\frac{d}{dt}\,\underline{R}_{cm} = \underline{V}_{cm}$

where $\underline{R}_{cm}$ = position of center of mass in inertial coordinates

$\underline{V}_{cm}$ = velocity of center of mass in inertial coordinates

Quite an extensive body of literature exists for these equations, in classical celestial mechanics as well as modern guidance and control theory. It was felt any work done here would not be a significant contribution to this area. From this point on, solar pressure attitude dynamics will be the main concern, with center of mass dynamics left for future work.

The angular momentum equations of motion for either solar cell panel are:

$$\frac{d}{dt}\,(\underline{I}_p\,\underline{w}_p) + \underline{w}_p \times (\underline{I}_p\,\underline{w}_p) = \underline{N}_{sails} + \underline{N}_{ant \rightarrow panel}$$

where $\underline{I}_p$ = solar panel inertia tensor in body-fixed coordinates

$\underline{w}_p$ = panel angular velocity with respect to inertial coordinates

$\underline{N}_{sails}$ = sail torque on panel due to attached sails

$\underline{N}_{ant \rightarrow panel}$ = antenna reaction torque on panel

Similarly, the angular momentum equations of motion for the antenna are:

$$4.5) \quad \frac{d}{dt}\left[\underline{I}_{ab}\left(\underline{w}_{ab} + \underline{w}_{p}\right)\right] + \underline{w}_{p} \times \left[\underline{I}_{ab}\left(\underline{w}_{ab} + \underline{w}_{p}\right)\right] = \underline{N}_{panels \rightarrow ant}$$

where $\underline{I}_{ab}$ = antenna inertia tensor in body-fixed coordinates

$\underline{w}_{ab}$ = antenna angular velocity in body-fixed coordinates

$\underline{N}_{panels \rightarrow ant}$ = total panel reaction torque

Adding these two equations, and using the fact reaction torques are equal and opposite, the total angular momentum equation of motion is found to be

$$4.6) \quad \frac{d}{dt}\left[\left(\underline{I}_{ab} + 2\underline{I}_{p}\right)\underline{w}_{p} + \underline{I}_{ab}\,\underline{w}_{ab}\right] + \underline{w}_{p} \times \left[\left(\underline{I}_{ab} + 2\underline{I}_{p}\right)\underline{w}_{p} + \underline{I}_{ab}\,\underline{w}_{ab}\right] = \underline{N}_{sails}$$

where $\underline{N}_{sails}$ = total sail torque generated by all six sails

A final kinematical equation is needed to describe how the direction cosines from body-fixed coordinates to inertial coordinates evolve with time:

$$4.7) \quad \frac{d}{dt}\,\underline{D}_{i}^{b} = \underline{D}_{i}^{b}\,\underline{W}_{i}^{b} \qquad \underline{W}_{i}^{b} = \begin{bmatrix} 0 & -w_z & w_y \\ w_z & 0 & -w_x \\ -w_y & w_x & 0 \end{bmatrix} \qquad \underline{w}_{p} = \begin{bmatrix} w_x \\ w_y \\ w_z \end{bmatrix}$$

where $\underline{D}_{i}^{b}$ = 3 x 3 direction cosine matrix from body-fixed coordinates to inertial coordinates

Equations 4.6) and 4.7) completely specify the attitude dynamics of Designs I and II. The inertia tensors of each design as well as a precise explanation of all coordinate frames and coordinate transformations are detailed in separate appendices.

4.3 Linearization of Equations of Motion

When the direction cosines are perturbed slightly from their nominal values, it can be shown (Goldstein(10))

$$4.9) \quad \underline{\dot{D}}^{b} \cong \underline{D}_{nom}\,(\underline{I}+\underline{E}),\ \underline{E} = \begin{bmatrix} 0 & e_z & -e_y \\ -e_z & 0 & e_x \\ e_y & -e_x & 0 \end{bmatrix}$$

$$\underline{D}_{nom} = \begin{bmatrix} \cos\psi & -\sin\psi & 0 \\ \sin\psi & \cos\psi & 0 \\ 0 & 0 & 1 \end{bmatrix} \qquad \psi = \dot{\psi}(t-t_o) + \psi_o,\ \dot{\psi} = \frac{2\pi}{365} \text{ rad/day}$$

where $\underline{D}_{nom}$ = nominal direction cosine matrix from body-fixed coordinates to inertial coordinates

$\underline{I}$ = 3 x 3 identity matrix

(e_x, e_y, e_z) = rotational errors about actual x, y and z body-fixed axes, respectively with respect to each nominal (body-fixed) axis

Using this, it is easy to show the actual angular velocity of the body-fixed frame with respect to an inertial frame, and its corresponding angular velocity, can be written as

$$4.10) \quad \underline{w}_p \cong \underline{w}_{nom} + \underline{D}_{nom}\,\dot{\underline{e}}$$

$$4.11) \quad \dot{\underline{w}}_p \cong \dot{\underline{w}}_{nom} + \underline{w}_{nom} \times \underline{D}_{nom}\,\dot{\underline{e}} + \underline{D}_{nom}\,\ddot{\underline{e}}$$

where

$$\underline{e} = \begin{bmatrix} e_x \\ e_y \\ e_z \end{bmatrix} \quad \underline{w}_{nom} = \begin{bmatrix} 0 \\ 0 \\ -\dot{\psi} \end{bmatrix} \quad \dot{\underline{w}}_{nom} = \begin{bmatrix} 0 \\ 0 \\ 0 \end{bmatrix}$$

Sail torque can be expanded in a series, including only the nominal sail torque and a first order perturbation:

$$4.12) \quad \underline{N}_{sails} \cong \underline{N}_{nom} + \underline{D}_{nom}\ \underline{N}_{body}$$

where $\underline{N}_{nom}$ = nominal sail torque (hopefully zero, as will be shown)

$\underline{N}_{body}$ = sail torque beyond nominal torque, in body-fixed axes

Substituting 4.9) - 4.12) into the total equations of motion, including only terms to first order in linearized variables, and equating nominal trajectory variables to each other and perturbational variables to each other, the linearized equations of motion are found to be:

$$\underline{I}_{sat}(\underline{w}_{nom} \times \underline{D}_{nom}\,\dot{\underline{e}} + \underline{D}_{nom}\,\ddot{\underline{e}}) + 2(\underline{W}_{nom}\,\underline{I}_{pm} - \underline{I}_{pm}\,\underline{W}_{nom})\,\underline{D}_{nom}\,\dot{\underline{e}}$$

$$4.13) \quad +(\underline{W}^{a}_{b}\,\underline{I}_{ab} - \underline{I}_{ab}\,\underline{W}^{a}_{b})\,\underline{D}_{nom}\,\dot{\underline{e}} + \underline{w}_{nom} \times \underline{I}_{sat}\,\underline{D}_{nom}\,\dot{\underline{e}} + \underline{D}_{nom}\,\dot{\underline{e}} \times (2\underline{I}_{pm}\,\underline{w}_{nom} +$$

$$\underline{I}_{ab}\,(\underline{W}^{a}_{b} + \underline{w}_{nom})) \cong \underline{D}_{nom}\ \underline{N}_{body}$$

where $\underline{I}_{sat} = \underline{I}_{ab} + 2\underline{I}_{p}$

$$\underline{W}_{nom} = \begin{bmatrix} 0 & -\dot{\psi} & 0 \\ \psi & 0 & 0 \\ 0 & 0 & 0 \end{bmatrix} \quad \underline{W}^{a}_{b} = \begin{bmatrix} 0 & w_{az} & -w_{ay} \\ -w_{az} & 0 & w_{ax} \\ w_{ay} & -w_{ax} & 0 \end{bmatrix} \quad \underline{w}^{a}_{b} = \begin{bmatrix} w_{ax} \\ w_{ay} \\ w_{az} \end{bmatrix}$$

and $\underline{I}_{pm}$ and $\underline{I}_{ab}$ are inertia tensors defined in an appendix.

Two simplifying assumptions can now be made:

i) $$\underline{I}_{sat}\,\underline{D}_{nom}\,\ddot{\underline{e}} \gg \underline{I}_{sat}\,(\underline{w}_{nom} \times \underline{D}_{nom}\,\dot{\underline{e}}) + 2(\underline{W}_{nom}\,\underline{I}_{pm} - \underline{I}_{pm}\,\underline{W}_{nom})\,\underline{D}_{nom}\,\dot{\underline{e}}$$

$$- 2\,\underline{I}_{p}\,\underline{w}_{nom} \times \underline{D}_{nom}\,\dot{\underline{e}} + \underline{w}_{nom} \times \underline{I}_{sat}\,\underline{D}_{nom}\,\dot{\underline{e}}$$

or, in words, the gyroscopic coupling of the satellite angular momentum vector with the angular momentum due to the annual rotation of the solar panels about their shafts, is neglected. Note each term on the right hand side of the inequality has a 365 day periodic component, while hopefully the term on the left hand side has most of its energy at much higher frequencies.

ii) $\underline{I}_{sat}\,\underline{D}_{nom}\,\ddot{\underline{e}} \gg (\underline{W}^{a}_{b}\,\underline{I}_{ab} - \underline{I}_{ab}\,\underline{W}^{a}_{b})\,\underline{D}_{nom}\,\dot{\underline{e}} + \underline{D}_{nom}\,\dot{\underline{e}} \times \underline{I}_{ab}\,(\underline{w}^{a}_{b} + \underline{w}_{nom})$

or in words, the gyroscopic coupling of the satellite angular momentum vector with the angular momentum due to the daily rotation of the antenna about its shaft, is neglected. Each term on the right hand side of the inequality has a 24 hour periodic component, while hopefully the term on the left hand side has most of its energy at much higher frequencies.

Both statements can be summarized: it is assumed the sail torques can correct gyroscopic disturbance torques caused by antenna rotation about its shaft once a day, + solar panel rotation about their shafts. These assumptions will be checked later.

The approximate equations of motion for the linearized variables are:

4.14) $\underline{I}_{sat}\,\underline{D}_{nom}\,\ddot{\underline{e}} \cong \underline{D}_{nom}\,\underline{N}_{body}$

4.4. Sensor Measurements

4.4.1. Linearized Sensor Measurements

Provided all pointing errors are small, earth sensors and sun sensors detect the center of the earth and sun, respectively, in body-fixed coordinates. Since $\underline{e}$ is defined as the pointing error of actual body-fixed axes with respect to nominally sun-pointing coordinates, the components of $\underline{e}$ have the following physical significance

i) e_x -- rotation about the body-fixed x-axis, rotation about the sun line

ii) e_y -- rotation about the body-fixed y-axis, moving up-down with respect to the center of the sun

iii) e_z -- rotation about the body-fixed z-axis, moving right-left with respect to the center of the sun

assuming $|e_x| \ll 1$, $|e_y| \ll 1$, $|e_z| \ll 1$. Sun sensors measures e_y and e_z directly, but provide no information about e_x.

Earth sensors must be used to find e_x indirectly. Consider the direction cosines from the nominally earth pointing coordinate frame to antenna principal axes frame, $\underline{D}_a^e$

4.15) $$\underline{D}_a^e \cong \underline{I} + \underline{E}', \quad \underline{E}' = \begin{bmatrix} 0 & -\tilde{e}'_z & \tilde{e}'_y \\ \tilde{e}'_z & 0 & -\tilde{e}'_x \\ -\tilde{e}'_y & \tilde{e}'_x & 0 \end{bmatrix}$$

where $(\tilde{e}'_x, \tilde{e}'_y, \tilde{e}'_z)$ = rotation errors of actual antenna principal axes with respect to nominal earth-pointing axes

and $|\tilde{e}'_x| \ll 1$, $|\tilde{e}'_y| \ll 1$, $|\tilde{e}'_z| \ll 1$ is assumed. Using standard Euler

angles to go from antenna principal axes to body-fixed axes (see Appendix), it can be shown:

$$
\begin{aligned}
e_x &= \tilde{e}'_z\,(\sin\psi\cos\varphi + \cos\psi\cos\theta\sin\varphi) - \tilde{e}'_y\sin\theta\sin\varphi \\
4.16)\quad e_y &= \tilde{e}'_z\,(\sin\psi\sin\varphi + \cos\psi\cos\theta\cos\varphi) - \tilde{e}'_y\sin\theta\cos\varphi \\
e_z &= \tilde{e}'_z\cos\psi\sin\theta - \tilde{e}'_y\cos\theta
\end{aligned}
$$

Since $\tilde{e}'_y$ and $\tilde{e}'_z$ are observable using earth sensors, they can be used to calculate e_x; as a bonus, earth sensor measurements provide a check on e_y and e_z measurements, and vice versa. These statements are valid provided the trigonometric weighting terms in 4.16) are not zero.

Two effects complicate sensor measurements. First, both sensor noise and additive Gaussian amplifier noise corrupts the measurements. Second, since solar pressure dynamics are extremely slow, it is probably unnecessary to continuously monitor satellite attitude, but rather to sample it at a rate much faster than that of any disturbances. Equation 4.14) is a continuous time differential equation; in order to approximate it by a discrete time difference equation, the following state variables are defined

$$4.17a)\quad \underline{e}_1(kT) = \underline{e}(kT)$$

$$4.17b)\quad \underline{e}_2(kT) = \underline{e}(kT) - \underline{e}\,[(k-1)T]$$

$$4.17c)\quad \underline{e}_3(kT) = \underline{D}_{nom}^{-1}(kT)\,\underline{I}_{sat}^{-1}(kT)\,\underline{D}_{nom}(kT)\,\underline{N}_{body}(kT)$$

where $k = 1, 2, 3, \ldots$

T = sampling period

and it is implicitly assumed the samples are taken at equally spaced time intervals. If it is assumed the sails exert no torque along the nominal

trajectory, then $\underline{e}_3(kT)$ is approximately constant, and the difference equation approximation to 4.14) can be written as

$$4.18) \quad \begin{bmatrix} \underline{e}_1(kT) \\ \underline{e}_2(kT) \\ \underline{e}_3(kT) \end{bmatrix} = \begin{bmatrix} \underline{I} & \underline{I} & \underline{I} \\ \underline{0} & \underline{I} & \underline{I} \\ \underline{0} & \underline{0} & \underline{I} \end{bmatrix} \begin{bmatrix} \underline{e}_1[(k-1)T] \\ \underline{e}_2[(k-1)T] \\ \underline{e}_3[(k-1)T] \end{bmatrix}$$

where $\underline{0}$ = 3 x 3 all zero matrix

$\underline{I}$ = 3 x 3 identity matrix

The sensor noise is assumed zero (as in Chapter Three), while the amplifier noise adds to the observations:

$$4.19) \quad \underline{y}(kT) = [\underline{I} \ \underline{0} \ \underline{0}] \begin{bmatrix} \underline{e}_1(kT) \\ \underline{e}_2(kT) \\ \underline{e}_3(kT) \end{bmatrix} + \underline{n}(kT)$$

where $\underline{n}(kT)$ = samples of (amplifier noise) stationary Gaussian random process sample function

$\underline{y}(kT)$ = sensor measurements corrupted by amplifier noise

If a minimum mean square error estimate of each of the state variables is desired, given noisy observations $\underline{y}(kT)$, a discrete time Kalman filter can be used.

One approach to suboptimal estimation of $\underline{e}_1(kT)$ and $\underline{e}_2(kT)$ is to assume the solar pressure dynamics, since they are extremely low frequency, will effectively low pass filter the noise; this is equivalent to ignoring the sensor noise entirely, and using for estimates of $\underline{e}_1(kT)$ and $\underline{e}_2(kT)$ equations (4.17a,b). Other examples of practical attitude estimation schemes can be found in MacLellan(59), Much(62), and Trudeau(68).

4.4.2. An Alternate Approach to Attitude Estimation

One major difficulty in using sun and earth sensors is that neither the roll-pitch-yaw angles, nor direction cosines or quaternions, are directly observable. However, if gyroscopes are used to measure angular velocity, then the direction cosines or quaternions are directly observable, and the results of Chapter III can be applied.

To see this, recall that if direction cosines are used to characterize orientation in space, then the differential equation which describes how the direction cosines evolve with time is

$$\frac{d}{dt}\begin{bmatrix} d_{11} & d_{12} & d_{13} \\ d_{21} & d_{22} & d_{23} \\ d_{31} & d_{32} & d_{33} \end{bmatrix} = \begin{bmatrix} 0 & -w_z & w_y \\ w_z & 0 & -w_x \\ -w_y & w_x & 0 \end{bmatrix} \begin{bmatrix} d_{11} & d_{12} & d_{13} \\ d_{21} & d_{22} & d_{23} \\ d_{31} & d_{32} & d_{33} \end{bmatrix}$$

On the other hand, if quaternions are used to characterize orientation in space, then the differential equation describing how the quaternion evolves with time is

$$\frac{d}{dt}\begin{bmatrix} a \\ b \\ c \\ d \end{bmatrix} = \frac{1}{2}\begin{bmatrix} 0 & -w_z & w_y & w_x \\ w_z & 0 & -w_x & w_y \\ -w_y & w_x & 0 & w_z \\ -w_x & -w_y & -w_z & 0 \end{bmatrix} \begin{bmatrix} a \\ b \\ c \\ d \end{bmatrix}$$

Since (w_x, w_y, w_z) are directly observable using gyroscopes, these equations can be integrated directly to provide all components of the direction cosine matrix or each component of the quaternion. Recall each component of the direction cosine matrix or quaternion was assumed observable in Chapter III; since that is now the case, the attitude estimation method developed there can be used to estimate the roll-pitch-yaw angles, and these angles can be used directly to define errors with respect to a nominal trajectory, just as with sun and earth sensors.

4.5. Solar Sail Torques

An appendix derives the exact torque generated by each sail, under the assumptions of no sail shadowing, no radiation falling on the rear of the sails, and small attitude pointing errors.

The force acting on a triangular sail such as in Designs I and II can be represented as a vector acting at a point two-thirds of the distance out the longitudinal sail axis, and this point is called the sail center of pressure (the distance from the sail hinge to the center of pressure will be called the center of pressure lever arm, or sail lever arm).

Solar pressure has three distinct components:

i) Reflected solar pressure, largest of the three, directed normal to the surface which sunlight strikes

ii) Absorbed solar pressure, next largest of the three, directed along the sun line

iii) Reradiated or thermal solar pressure, smallest of the three, directed normal to the surface which sunlight strikes

Three simplifying assumptions are now made:

i) Reflected solar pressure is the only contributor to sail torque

ii) $\sin b_k \cong b_k \qquad \cos b_k \cong 1 \qquad k \cong 1,2,\ldots 6$

where b_k = sail k pitch angle $= \{-b_o, b_o, \text{ or } 0\}$ $(b_o = 15^o)$

iii) $(\underline{n} \bullet \underline{s}) \cong (\underline{n}_k \bullet \underline{s}) \cong (\underline{n}_j \bullet \underline{s}) \qquad k,j = 1,2,\ldots 6$

where $\underline{n}_k$ = sail k normal, in body-fixed coordinates

$\underline{s}$ = sun vector in body-fixed coordinates

$\underline{n}$ = abbreviation for $\underline{n}_k$

or in other words, the projection of each sail's normal along the sun line is roughly the same. Using these assumptions, from the appendix it follows:

$$\underline{N}_{body} \cong A(1-E_s)\,(2I/c)\,(\underline{n}\cdot\underline{s})^2 \left\{ (b_1-b_3+b_4-b_6)\,\ell_s \cos(a) \begin{bmatrix}1\\0\\0\end{bmatrix} + (b_1+b_3+b_4+b_6)\,\ell_s \sin(a) \begin{bmatrix}0\\1\\0\end{bmatrix} - (b_2+b_5)\,\ell_s \sin(a) \begin{bmatrix}0\\0\\1\end{bmatrix} + \right.$$

$$\left. (b_1+b_3-b_4-b_6)\,r \begin{bmatrix}\sin\psi\\ \cos\psi\\ 0\end{bmatrix} + (b_3+b_6-b_1-b_4) \begin{bmatrix}0\\0\\y\end{bmatrix} + (b_2-b_5) \begin{bmatrix} z+h-\ell_s\cos a + 2r\sin(a)\\ 0\\ -r\cos a\end{bmatrix} \right\} \tag{4.21}$$

where A = area of sail (all sails assumed identical

E_s = emissivity of surface of sail

I = sunlight pressure constant = 1380 watts/meter^2

c = speed of light in vacuum

a = sail cant angle = 45^o degrees

ℓ_s = distance from sail hinge on solar panel to center of pressure of sail

r = radius of gyration of solar panel (see Appendix)

h = distance from antenna center of mass to solar panel center of mass (see Appendix)

y = half length of solar panel (see Appendix)

z = half width of solar panel (see Appendix)

and all vectors are measured in body-fixed coordinates. Three cases of interest now arise:

a) $b_1 = -b_3 = b_4 = -b_6 = b_o$, $b_2 = b_5 = 0$

4.22a) $$\underline{N}^a_{body} \cong A(1-E_s)(2I/c)\,(\underline{n}\cdot\underline{s})^2\{4b_o\ell_s\cos(a)\begin{bmatrix}1\\0\\0\end{bmatrix} - 4b_o y\begin{bmatrix}0\\0\\1\end{bmatrix} + 2r\sin(a)\sin\psi\begin{bmatrix}1\\0\\0\end{bmatrix}\}$$

b) $b_1 = b_3 = b_4 = b_6 = b_o$, $b_2 = b_5 = 0$

4.22b) $$\underline{N}^b_{body} \cong A(1-E_s)(2I/c)(\underline{n}\cdot\underline{s})^2\{4b_o\ell_s\sin(a)\begin{bmatrix}0\\1\\0\end{bmatrix} + 2r\sin(a)\sin\psi\begin{bmatrix}1\\0\\0\end{bmatrix}\}$$

c) $b_1 = b_3 = b_4 = b_6 = 0$, $b_2 = b_5 = -b_o$

4.22c) $$\underline{N}^c_{body} \cong A(1-E_s)(2I/c)(\underline{n}\cdot\underline{s})^2\{2b_o\ell_s\sin(a)\begin{bmatrix}0\\0\\1\end{bmatrix} + 2r\sin(a)\sin\psi\begin{bmatrix}1\\0\\0\end{bmatrix} - 2b_o z\begin{bmatrix}1\\0\\0\end{bmatrix}\}$$

If the sails are designed such that

$$\ell_s\cos(a), \ell_s\sin(a) \gg r\sin a, y, z$$

then x, y, and z torques can be generated in body-fixed axes, by cases a), b), and c) respectively. Sails 1, 3, 4 and 6 produce either x or y torques

at any instant, but not both simultaneously; sails 2 and 5 generate z torques.

If $\underline{I}_{sat}$ is assumed diagonal, then 4.14) become

$$4.23)\quad \ddot{\underline{e}} = \begin{bmatrix} I_{xx}^{-1}\cos^2\psi + I_{yy}^{-1}\sin^2\psi & 2(I_{xx}^{-1} - I_{yy}^{-1})\sin\psi\cos\psi & 0 \\ 2(I_{xx}^{-1} - I_{yy}^{-1})\sin\psi\cos\psi & I_{xx}^{-1}\sin^2\psi + I_{yy}^{-1}\cos^2\psi & 0 \\ 0 & 0 & I_{zz}^{-1} \end{bmatrix} \underline{N}_{body}$$

where

$$\underline{I}_{sat} = \begin{bmatrix} I_{xx} & 0 & 0 \\ 0 & I_{yy} & 0 \\ 0 & 0 & I_{zz} \end{bmatrix}$$

(see Appendix for correct expression for $\underline{I}_{sat}$)

Note that if an x torque is generated in body-fixed axes, the off-diagonal entries in the gain matrix for $\underline{N}_{body}$ above will couple this torque into the y axis. Cross coupling torques between x and y axes are unavoidable, because of the coordinate transformations between inertial and body-fixed axes. To minimize their effect, I_{xx} and I_{yy} must be chosen comparable to one another.

4.6. Solar Sail Control Law

At this point the analysis of the linearized equations of motion has been reduced to a previously solved problem. Two standard control laws will now be discussed (for more details, see Athans (54) and Flugge-Lotz (56)). Cross coupling torques will be assumed negligible from here on.

If it were possible to generate simultaneously three independent torques, the attitude error and its first derivative could be used in a control law

$$4.24) \quad \underline{N}_{body} = \underline{N}^{a}_{body} \ \text{sign}(e_x + k_x \dot{e}_x) + \underline{N}^{b}_{body} \ \text{sign}(e_y + k_y \dot{e}_y) + \underline{N}^{c}_{body} \ \text{sign}(e_z + k_z \dot{e}_z)$$

where

$$\text{sign}(x) = \begin{cases} +1 & x \geq 0 \\ -1 & x < 0 \end{cases}$$

Since x and y torques cannot simultaneously be generated, one possible modification to the above control law is

$$4.25) \quad \begin{aligned} &\text{If} \quad |e_x + k_x e_x| \geq |e_y + k_y e_y| \quad \text{generate x torque} \\ &\text{If} \quad |e_x + k_x e_x| < |e_y + k_y e_y| \quad \text{generate y torque} \end{aligned}$$

Finally, if a deadband is included in the control law for each axis, every "sign" function is replaced with a dbz

$$\text{dbz}(x) = \begin{cases} \text{sign}(x) & |x| \geq db \\ 0 & |x| < db \end{cases} \qquad db = \text{deadband}$$

Equations 4.24) and 4.25) with deadbands completely specify a possible control law for either Designs I or II. The gains k_x, k_y, k_z allow the designer to trade ringing and overshoot in the system transient response for the period of a limit cycle when the satellite is in its nominal trajectory (see Flügge-Lotz (56)). Another possible control law is the time optimal control law; a simple single axis control law is discussed in Athans (54).

4.7. Disturbance Torques

Five sources of disturbance torques, in addition to the cross-axis coupling torques already mentioned, can drive Designs I and II away from nominal attitude. The largest disturbance is due to the earth's gravitational field trying to align the satellite's longest axis along a line pointing to the earth's center of mass. The next largest disturbance is caused by sunlight reflecting, absorbing, and reradiating from the antenna. Third largest is caused by the satellite center of mass being misaligned. Fourth is micrometeoroid impact torques. Finally, the smallest disturbance torques are due to the satellite interacting with the earth's magnetic field; these magnetic torques are assumed negligible.

Gravitational torques on an arbitrary rigid body, or gravity gradient torques as they are referred to in the literature, are straightforward to calculate (see Nidney (65)). It can be shown

$$4.26) \quad \underline{N}^{e}_{\text{gravity gradient}} \cong 3w_o^2 \begin{bmatrix} 0 \\ -I_{xz} \\ I_{xy} \end{bmatrix}$$

where w_o = orbital frequency of satellite = $(2\pi/24)$ radians/hour

I_{xy}, I_{xz} = off diagonal elements in satellite inertia tensor computed in earth-pointing coordinates

$\underline{N}^{e}_{\text{gravity gradient}}$ = satellite gravity gradient torques in earth-pointing coordinates

$\underline{I}^{e}_{sat}$ = satellite inertia tensor in earth-pointing coordinates

$\underline{I}^{e}_{sat} = \underline{A}^{b}_{e}\ \underline{I}_{sat}\ \underline{A}^{e}_{b}$ $\qquad$ $\underline{A}^{e}_{b} = \underline{A}^{b\ T}_{e} = \underline{A}^{-1}_{e}$

$\underline{A}^{b}_{e}$ = direction cosines from body-fixed axes to earth pointing axes in body-fixed axes.

These torques can be written

4.27) $\underline{N}^{b}_{\text{gravity gradient}} \cong \underline{A}^{e}_{b}\ \underline{N}^{e}_{\text{gravity gradient}}$

and are plotted for Design I, in body-fixed axes, in Figure 4.3 under the assumption the satellite is moving in its nominal trajectory.

Sunlight pressure torques due to the antenna-electronics body are calculated explicitly in an appendix. The reflected and absorbed sunlight pressure torques are plotted in body-fixed axes in Figures 4.4 and 4.5; more information must be known before the reradiated torque can be calculated explicitly.

The calculation of center of mass misalignment torques, torques due to the center of mass of the satellite not coinciding with the center of mass of the antenna, is straightforward (Goddard (57)):

4.28) $\underline{N}_{cm} = \underline{R}_{a/cm} \times \underline{F}_{sails} + M_{sat}\left[2\underline{R}_{a/cm} \times (\underline{w}_{p} \times \underline{R}_{cm}) + \underline{R}_{a/cm} \times (\underline{w}_{a} \times \underline{R}_{cm})\right]$

where

$\underline{N}_{cm}$ = center of mass misalignment torques in body-fixed axes

$\underline{R}_{a/cm}$ = vector from antenna center of mass to actual satellite center of mass

Figure 4.3

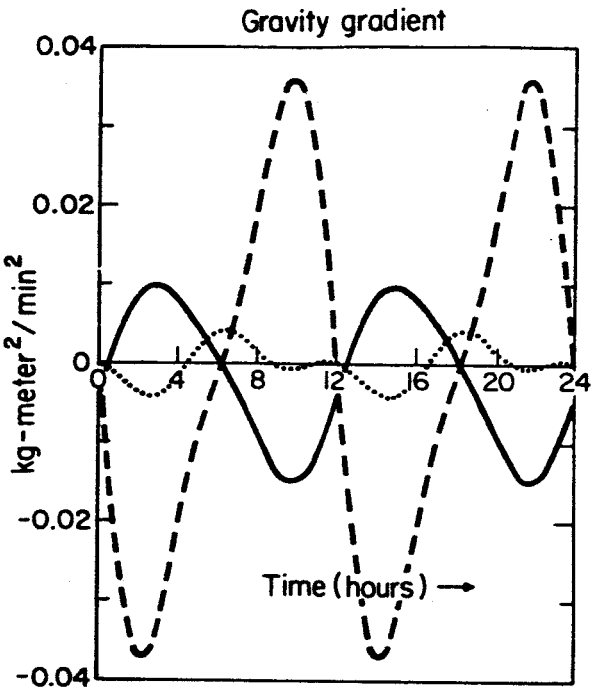

Figure 4.4

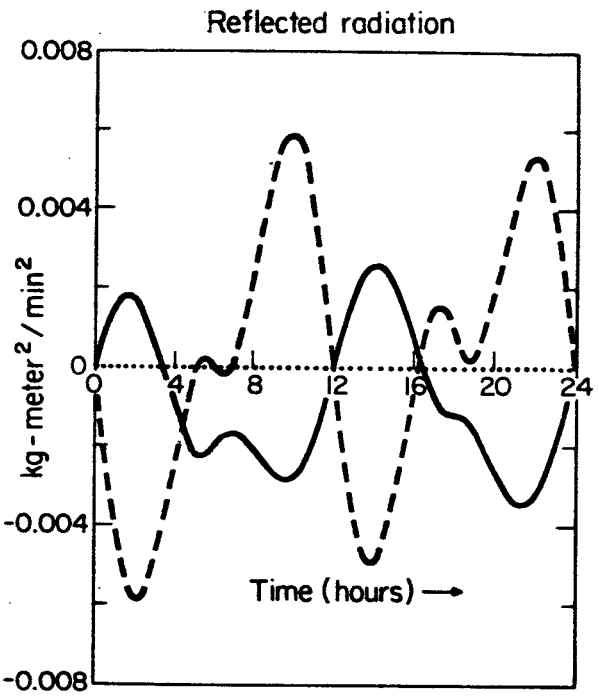

Figure 4.5

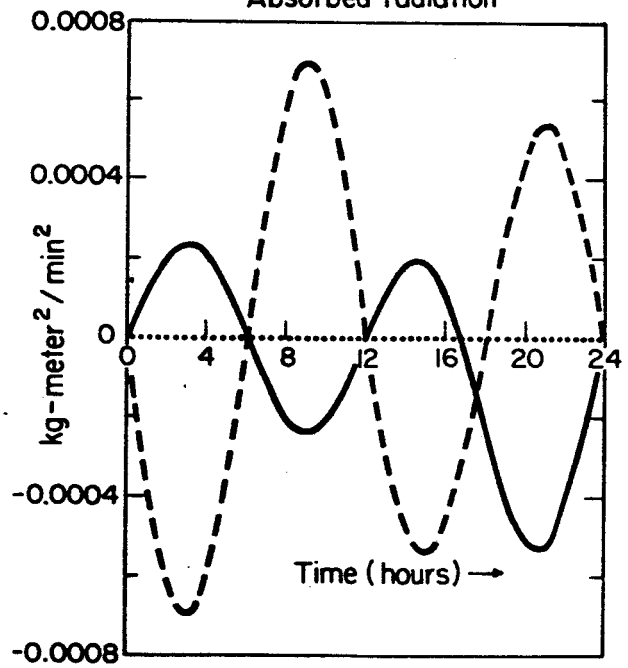

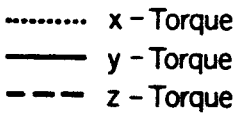

Figures 4.3-4.5

Nominal Disturbance Torques for Design I vs Time

$\underline{w}_p$ = satellite angular acceleration in body-fixed axes

$\underline{w}_a$ = antenna angular acceleration in body-fixed axes

A typical magnitude for $\underline{R}_{a/cm}$ is one quarter inch (Goddard (56)). Since sail torque is proportional to the sail center of pressure lever arm,

$$4.29) \qquad \underline{N}_{sails} \propto \ell_s A(1-E_s)(2I/c) \begin{Bmatrix} \sin(a) \\ \cos(a) \end{Bmatrix}$$

The sails must be designed such that the sail torque is much greater than the center of mass misalignment torque, that is,

$$\ell_s A(1-E_s)(2I/c) \begin{Bmatrix} \cos(a) \\ \sin(a) \end{Bmatrix} \gg M_{sat} \; |\underline{R}_{a/cm}|^2 [2|\underline{w}_p| + |\underline{w}_a|]$$

$$\ell_s \cos(a) \gg |\underline{R}_{a/cm}| \quad \text{and} \quad \ell_s \sin(a) \gg |\underline{R}_{a/cm}|$$

An analysis has been carried out to verify that if the sail cant and pitch angles are offset slightly from their nominal values, the resulting disturbance torques are negligible compared to the attitude correcting torques.

Finally, the largest expected micrometeoroid torques appears to be two orders of magnitude less than the attitude correcting torques and hence is negligible (Goddard (57), NASA – Naumann(64)).

4.8. Computer Simulation Results

As a check on the foregoing analysis, a computer program was written to simulate the dynamics and kinematics of either Designs I or II.

Figures 4.6 through 4.12 show the results of a simulation of Design I recovering from an initial pointing error. The initial error was due to the

satellite being rotated away from its nominal attitude by three successive rotations of ten degrees each, first about the z axis, then the y axis, and finally the x axis. Sun and earth sensor measurements are corrupted by additive Gaussian noise, and a sensor sampling rate of once each minute is used to determine the pointing error and its derivative (see 4.20)). The attitude control law described in 4.22) with a deadband is used to pitch the sails. Gravity gradient torques, antenna reflected and absorbed sunlight torques, and center of mass misalignment torques are included. Table 4.1 summarizes the numbers used for these simulations.

The simulation results lend credibility to the previous assumptions that gyroscopic coupling torques and cross-axis coupling torques are negligible compared to the sail attitude control torques. Note that for the example just discussed, the harmonic content of the error and its derivative is in the neighborhood of ten degrees per hour; this rate is much higher than the angular velocity of the solar panels about their shafts, but it is comparable to the angular velocity of the antenna about its shaft, roughly fifteen degrees per hour. Hence, there is some coupling between the angular momentum of the satellite and the angular momentum of the antenna, but the attitude control law is able to compensate for it.

The results presented here are representative of over fifty different simulations of the attitude control equations for both Designs I and II. Satellite transient response to pointing errors such as those just described were checked at eight equally spaced times of year (starting with December 21),

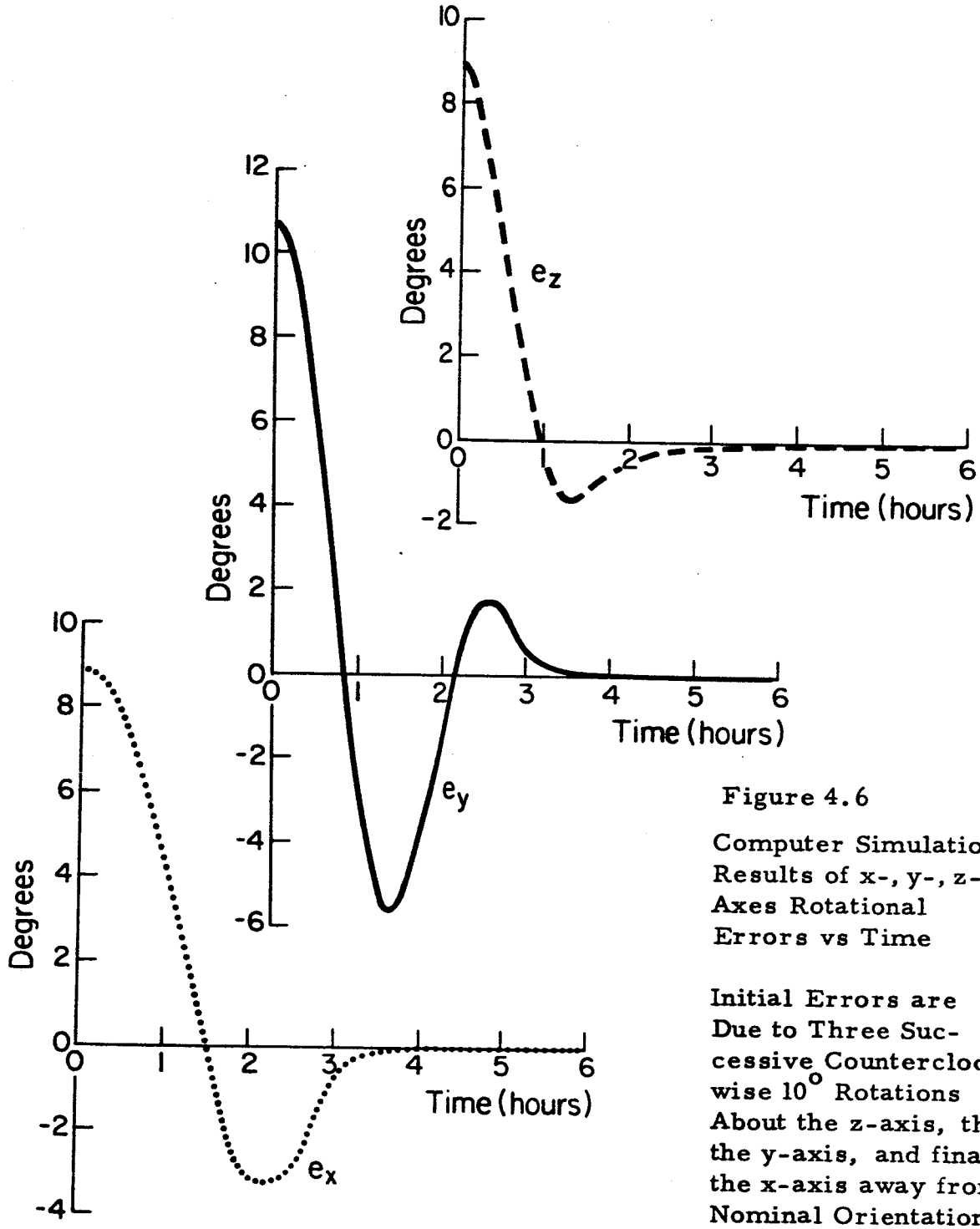

Figure 4.6

Computer Simulation Results of x-, y-, z-Axes Rotational Errors vs Time

Initial Errors are Due to Three Successive Counterclockwise 10° Rotations About the z-axis, then the y-axis, and finally the x-axis away from Nominal Orientation

Figure 4.7

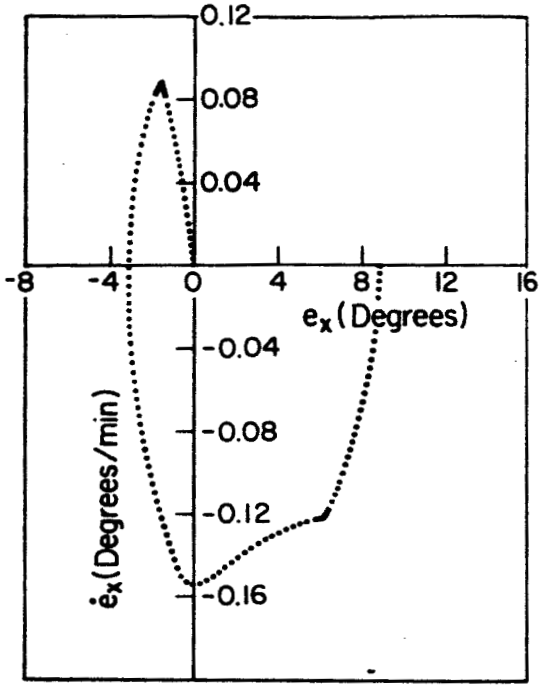

Figure 4.8

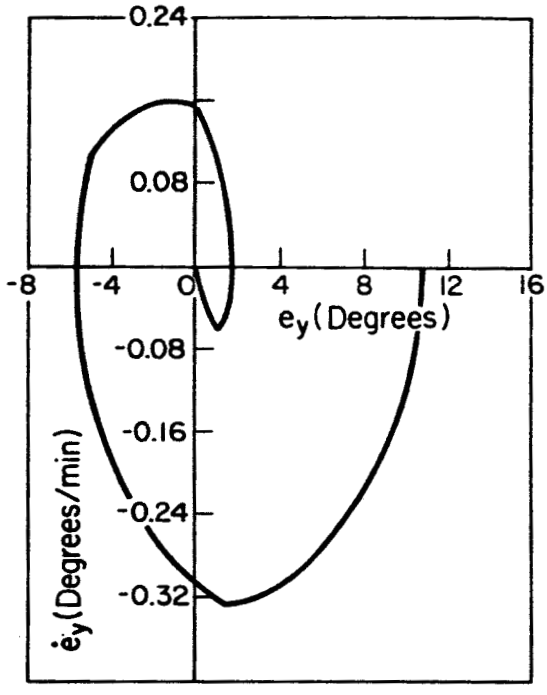

Figure 4.9

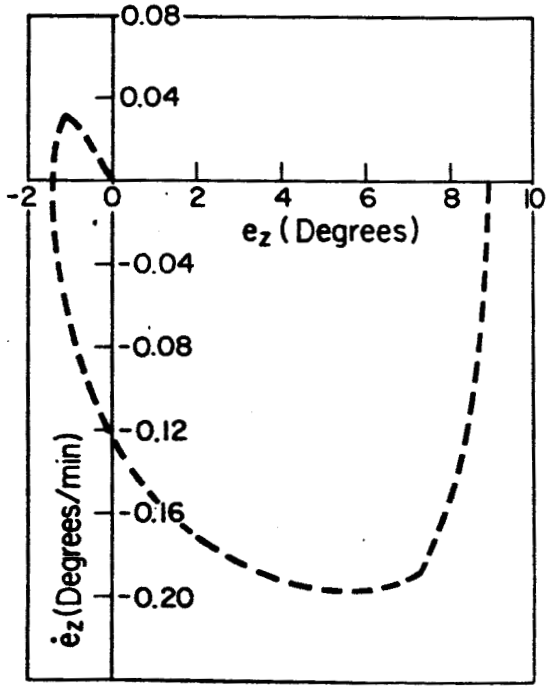

Figures 4.7-4.9

Computer Simulation Results of Design I--Phase Plane Plots of Rotational Error Derivatives vs Rotational Errors

Initial Errors are Due to Three Successive Counterclockwise 10^{o} Rotations about the z-axis, then the y-axis, and finally the x-axis away from Nominal Orientation

Figure 4.10

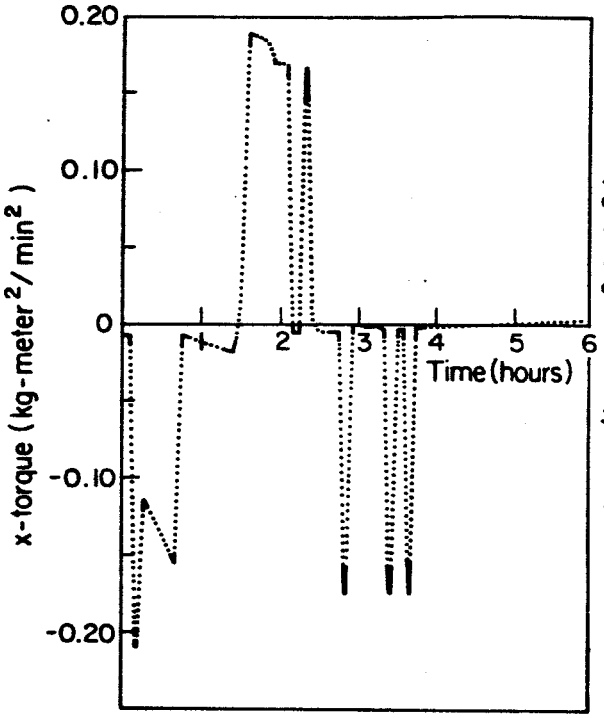

Figure 4.11

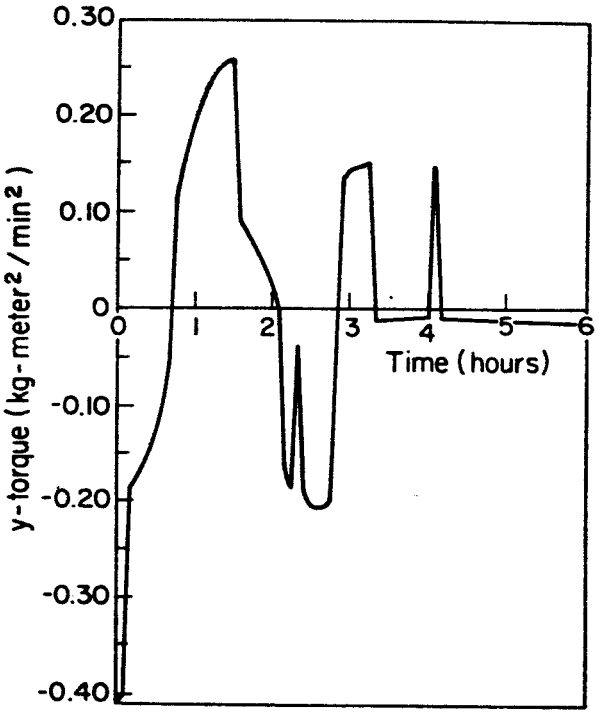

Figure 4.12

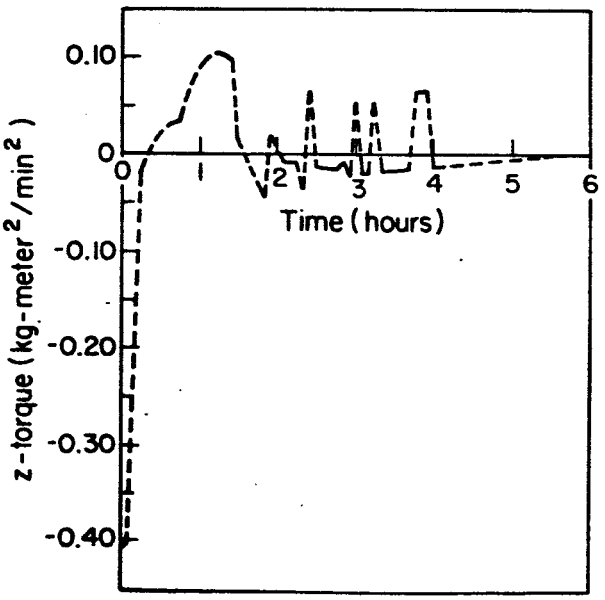

Figures 4.10-4.12

Computer Simulation Results of Design I--Solar Sail Torques vs Time

Initial Errors are due to Three Successive Counterclockwise 10^{o} Rotations about the z-axis, then the y-axis, and finally the x-axis away from Nominal Orientation

and at different initial times of day (midnight, six a.m., noon, and six p.m.). Finally, most runs were made with the sails misaligned in cant and pitch, the satellite center of mass misaligned, gravity gradient disturbance torques present, antenna sunlight pressure disturbance torques present, and sensor measurements corrupted by Gaussian noise. These simulation results verified the results of a theoretical analysis: When the satellite design parameters are perturbed slightly from their nominal values, and when disturbance torques act on the satellite the attitude control torques are sufficient to keep the satellite aligned along its nominal orientation to within attitude sensor noise limitations.

Figure 4.13

Design I -- Simulation Parameters

I. Inertia Tensor Components

A. Antenna Principal Axis Inertia Tensor Components

I_{axx} 300 kg-meter^2

I_{ayy} 225 kg-meter^2

I_{azz} 225 kg-meter^2

B. Solar Cell Body-fixed Axes Inertia Tensor Components

I_{xx} 964 kg-meter^2

I_{yy} 482 kg meter^2

I_{zz} 482 kg-meter^2

II. Sail Parameters

Sail area 3 meter^2

l_s - Center-of-pressure to sail hinge 5 meters

E_s 0.05 (dimensionless)

III. Control Law Parameters

x-axis deadband (same for all three axes) 0.1 degree

$K_x = K_y = 30$ (radians/min)$^{-1}$; $K_z = 40$ (radians/min)$^{-1}$

sensor noise (same for all three axes)

mean 0 degrees standard deviation 0.03 degrees

Cant angles

$a_k = 45$ degrees $k = 1,2,\ldots 6$

Pitch angles

$b_k = 15$ degrees $k = 1,2,\ldots 6$

IV. Dimensions

Center of mass misalignment

$\underline{r}_{a/cm} = (x_{a/cm}, y_{a/cm}, z_{a/cm})$ $x_{a/cm} = y_{a/cm} = z_{a/cm} =$

10 centimeters

Antenna (distance from center of mass to surfaces)

$r_{ax} = 0.725$ meters $r_{ay} = 0.5$ meters $r_{az} = 0.725$ meters

Antenna surface areas

$A_1 = A_6 = 2.05$ meter^2 $A_2 = A_3 = A_4 = A_5 = 1.45$ meters^2

Solar panel

r = 0.25 meter y = 0.25 meter

h = 1.0 meter z = 0.10 meter

V. Weight Breakdown (Goddard (57), M.I.T. (60))

A. Antenna-electronics

Antenna	25 lbs
Power control	23 lbs
Batteries	50 lbs
Electronics	80 lbs
Attitude control	25 lbs
Structure	25 lbs
Contingency	19 lbs
Total	247 lbs

B. Solar cells panels

Bearing drive	15 lbs
Solar cells	45 lbs
Electronics	10 lbs
Cables	8 lbs
Structure	25 lbs
Contingency	19 lbs
Total	122 lbs

APPENDIX A

Coordinate Frames and Coordinate Transformations

Five different coordinate frames are useful in discussing the attitude control dynamics of Designs I and II. Each of the following four coordinate frames have their origin at the satellite center of mass:

X_e-Y_e-Z_e--nominally earth-pointing coordinate frames, with the X_e-axis aimed at the center of mass of the earth, the Y_e-axis perpendicular to X_e and in the orbital plane, and the Z_e-axis parallel to the earth's axis of rotation

X_a-Y_a-Z_a--the antenna-electronics principal axes frame, nominally coincident with X_e-Y_e-Z_e

X_s-Y_s-Z_s--nominally sun-pointing coordinate frame, with the X_s-axis aimed at the center of the sun, the Y_s-axis perpendicular to X_s and parallel to the ecliptic, and Z_s-axis normal to the ecliptic

X_b-Y_b-Z_b--the body-fixed axes frame, parallel to the solar cell panel principal axes frame and nominally coincident with X_s-Y_s-Z_s

The fifth coordinate frame has its origin at the center of mass of the kth solar panel (see Figures 1 and 2):

X_{pk}-Y_{pk}-Z_{pk}--the principal axes frame for solar cell panel k, nominally parallel to X_s-Y_s-Z_s

Direction cosines from one coordinate frame to another are differentiated by a combination of mnemonic subscripts and superscripts. For example, the direction cosines from X_a-Y_a-Z_a to X_b-Y_b-Z_b are denoted by

$\underline{D}^a_b$ with the superscript "a" denoting antenna axes, the subscript "b" denoting body-fixed axes

The direction cosines from earth-pointing coordinates to sun-pointing coordinates can be expressed in terms of Euler angles:

$$\underline{D}^e_s = \begin{bmatrix} \cos\psi & \sin\psi & 0 \\ -\sin\psi & \cos\psi & 0 \\ 0 & 0 & 1 \end{bmatrix} \begin{bmatrix} 1 & 0 & 0 \\ 0 & \cos\theta & -\sin\theta \\ 0 & \sin\theta & \cos\theta \end{bmatrix} \begin{bmatrix} \cos\varphi & \sin\varphi & 0 \\ -\sin\varphi & \cos\varphi & 0 \\ 0 & 0 & 1 \end{bmatrix}$$

where

φ = daily orbital position of satellite

θ = angle of earth's axis of rotation with ecliptic

ψ = annual orbital position of satellite

or

$\psi = \dot{\psi}(t-t_o) + \psi_o$, $\dot{\psi} = 2\pi/(365 \cdot 24)$ radians/hour

$\theta = 23.5^o$

$\varphi = \dot{\varphi}(t-t_o) + \varphi_o$, $\dot{\varphi} = 2\pi/24$ radians/hour

t_o = initial time of day (midnight)

φ_o = initial position in orbit (side of earth away from sun)

ψ_o = initial time of year (December 21)

where all initial times are nominal times taken for convenience in the computer simulation of Designs I and II, and easily changed to other values.

If the antenna follows a preprogrammed drive with respect to the solar panels, then it is straightforward to find the angular velocity of the antenna in sun-pointing coordinates:

$$\underline{w}_{ab} = \begin{bmatrix} \cos\psi & \sin\psi & 0 \\ -\sin\psi & \cos\psi & 0 \\ 0 & 0 & 1 \end{bmatrix} \begin{bmatrix} 1 & 0 & 0 \\ 0 & \cos\theta & -\sin\theta \\ 0 & \sin\theta & \cos\theta \end{bmatrix} \begin{bmatrix} 0 \\ 0 \\ \dot{\varphi} \end{bmatrix} + \begin{bmatrix} 0 \\ 0 \\ \dot{\psi} \end{bmatrix}$$

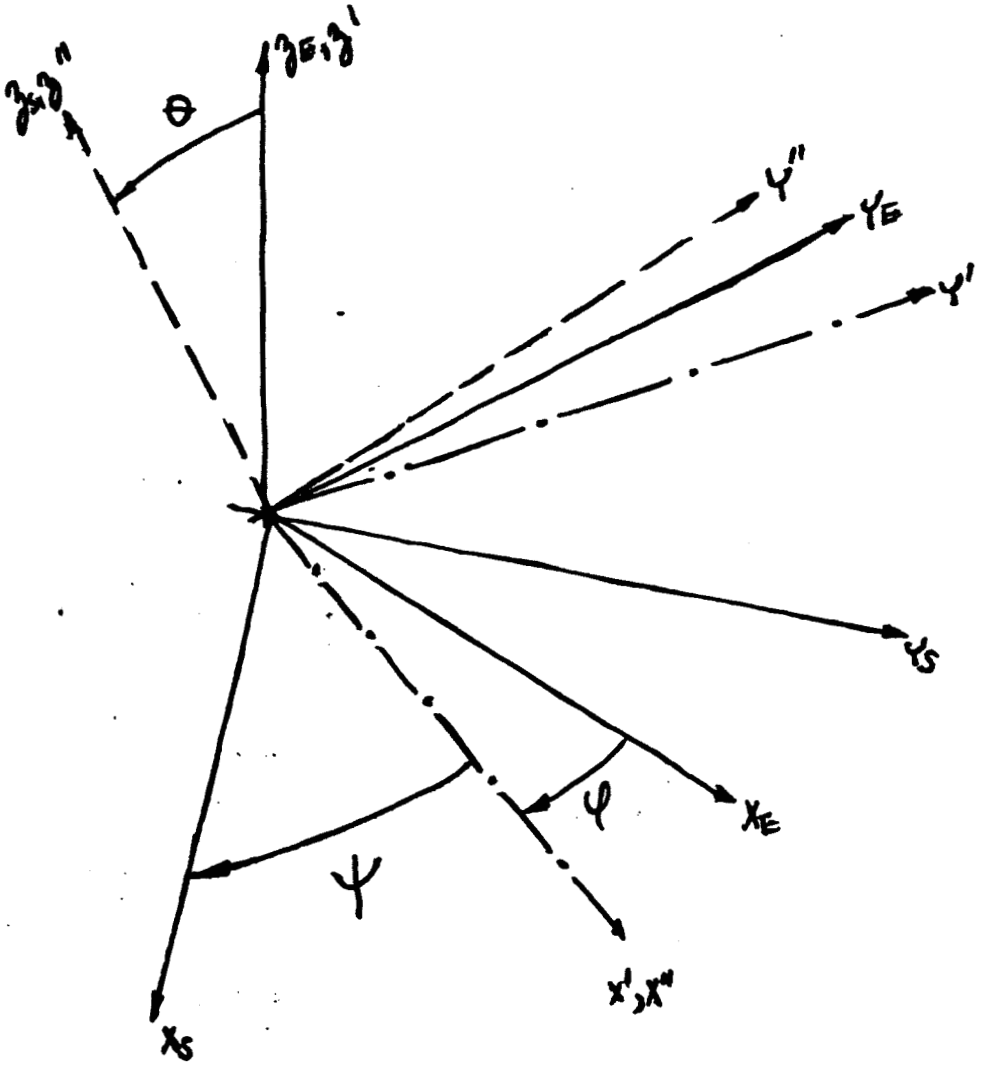

Figure A.1

Euler Angles From X_e-Y_e-Z_e to X_s-Y_s-Z_s

APPENDIX B

Inertia Tensors

In X_a-Y_a-Za the antenna-electronics inertia tensor is:

$$\underline{I}_{aa} = \begin{bmatrix} I_{axx} & 0 & 0 \\ 0 & I_{ayy} & 0 \\ 0 & 0 & I_{azz} \end{bmatrix}$$

In body-fixed axes X_b-Y_b-Z_b this becomes:

$$\underline{I}_{ab} = \underline{A}_b^a \, \underline{I}_{aa} \, \underline{A}_a^b \qquad \underline{A}_b^a = \underline{A}_a^{b\,-1} = \underline{A}_a^{b\,T}$$

In solar panel principal axes, X_{pk}-Y_{pk}-Z_{pk}, the kth solar panel inertia tensor is:

$$\underline{I}_{pk} = \begin{bmatrix} I_{pxx} & 0 & 0 \\ 0 & I_{pyy} & 0 \\ 0 & 0 & I_{pzz} \end{bmatrix}$$

In body-fixed axes X_b-Y_b-Z_b, for Design I, either solar panel inertia takes the form:

$$\underline{I}_p = \underline{I}_{pm} + \underline{I}_{pk}$$

$$\underline{I}_{pm} = m_p \, \underline{D}_{nom}^{I} \, \underline{I}_I \, \underline{D}_{nom}^{I\,-1}$$

$$\underline{I}_I = \begin{bmatrix} h^2 & 0 & -rh \\ 0 & r^2 + h^2 & 0 \\ -rh & 0 & r^2 \end{bmatrix}$$

m_p = solar cell panel mass

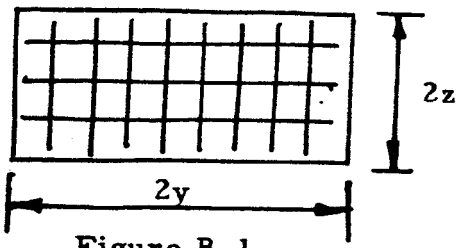

Figure B.1
Solar Panel Dimensions

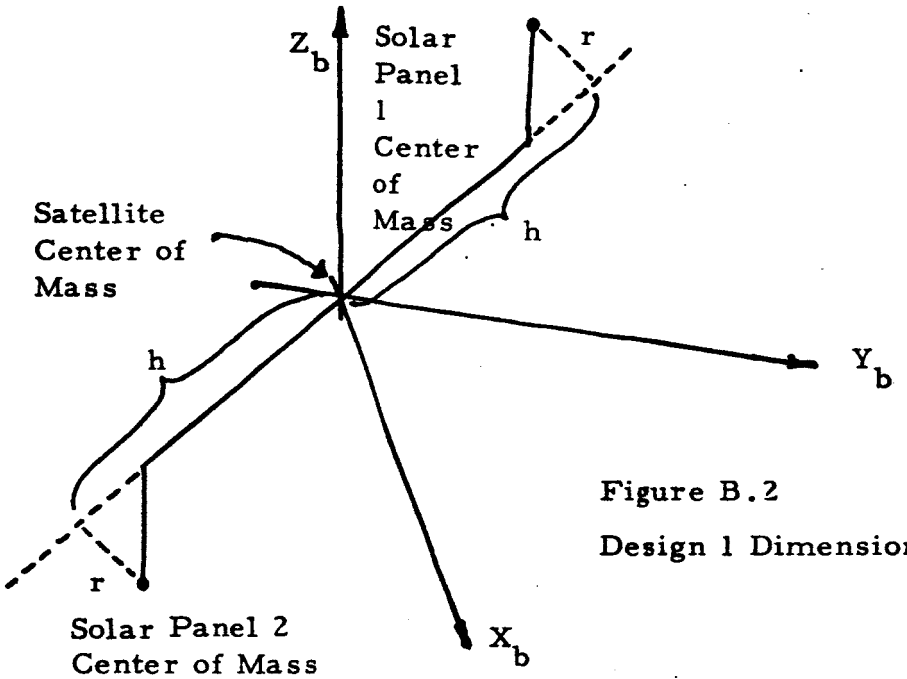

Figure B.2
Design 1 Dimensions

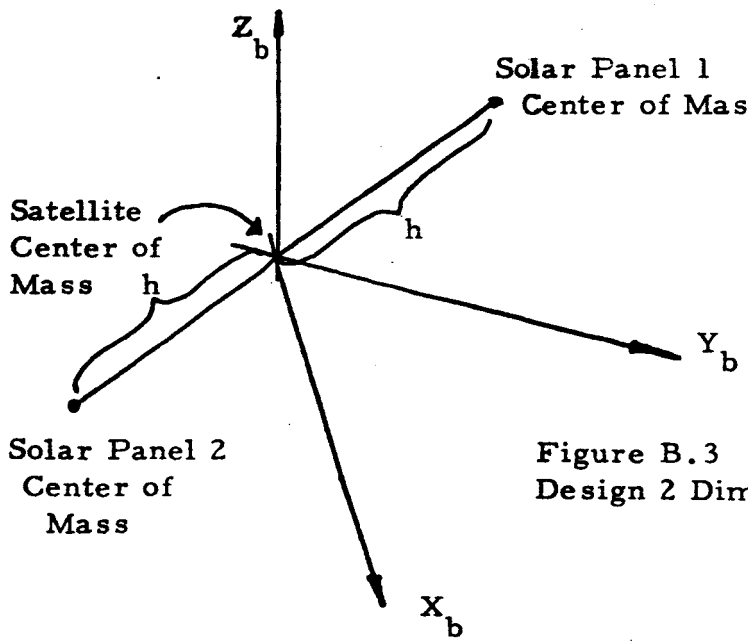

Figure B.3
Design 2 Dimensions

$$\underline{D}^{I}_{nom} = \begin{bmatrix} \cos\psi & -\sin\psi & 0 \\ \sin\psi & \sin\psi & 0 \\ 0 & 0 & 1 \end{bmatrix}$$

In body-fixed axes for Design II either solar panel inertia takes the form:

$$\underline{I}_{p} = \underline{I}_{pm} + \underline{I}_{pk}$$

$$\underline{I}_{pm} = m_p \, \underline{D}^{II}_{nom} \, \underline{I}_{II} \, \underline{D}^{II-1}_{nom}$$

$$\underline{I}_{II} = \begin{bmatrix} h^2 & 0 & 0 \\ 0 & h^2 & 0 \\ 0 & 0 & 0 \end{bmatrix}$$

$$\underline{D}^{II}_{nom} = \begin{bmatrix} \cos\gamma & 0 & \sin\gamma \\ 0 & 1 & 0 \\ -\sin\gamma & 0 & \cos\gamma \end{bmatrix} \qquad \sin\gamma = \sin\theta \sin\psi$$

Finally, the satellite inertia tensor becomes, in X_b-Y_b-Z_b:

$$\underline{I}_{sat} = \underline{I}_{ab} + 2\underline{I}_{p}$$

This is graphed as a function of time for Design I, starting at midnight, December 21, and continuing for twenty four hours, on the following page. Numbers to do the graph are taken from Table 4.1.

NOMINAL DESIGN I INERTIA TENSOR

IN SUN-POINTING COORDINATES

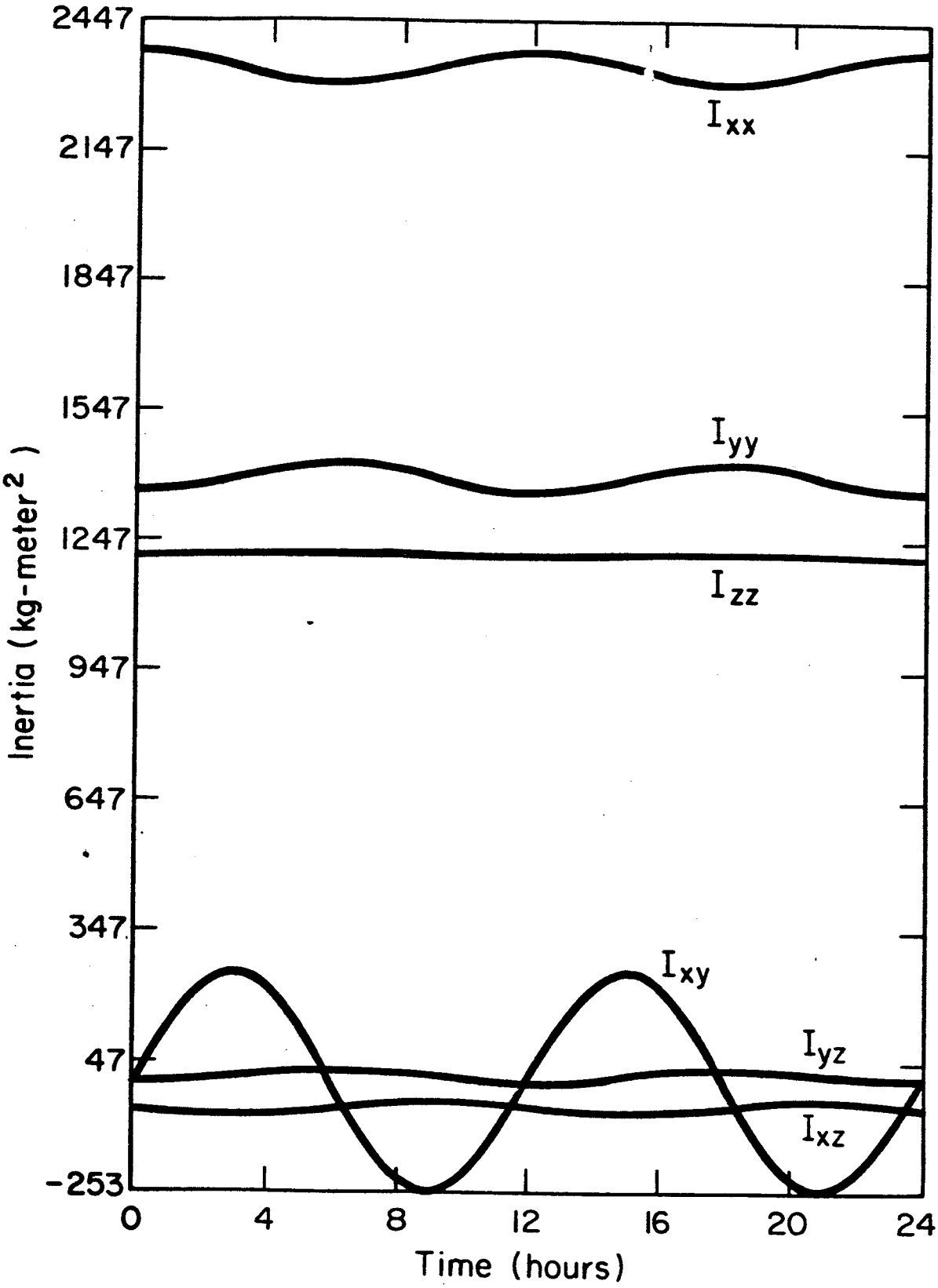

FIGURE B.4

APPENDIX C

Sail Torques

Sunlight pressure striking a surface generates a force with three physically distinct components:

$$\underline{F}_{sunlight} = \underline{F}_{reflected} + \underline{F}_{absorbed} + \underline{F}_{reradiated}$$

Only the reflected component will be dealt with here

$$\underline{F}_{reflected} = A(1-E_s)\,(2I/c)\,(\underline{n} \cdot \underline{s})^2\,(-\underline{n})$$

where

A = surface area

E = surface emissivity

I = sunlight pressure constant = 1380 watts/meter^2

c = speed of light in vacuum = 3×10^8 meters/sec

$\underline{s}$ = unit vector pointed at sun

$\underline{n}$ = unit vector normal outward from surface

The unit normal vectors for each sail in X_b-Y_b-Z_b are:

$$\underline{n}_k = \begin{bmatrix} \cos a_k & \cos b_k \\ \sin a_k & \cos b_k \\ & \sin b_k \end{bmatrix} \quad k = 1,4 \qquad \underline{n}_k = \begin{bmatrix} \cos a_k & \cos b_k \\ -\sin a_k & \cos b_k \\ & \sin b_k \end{bmatrix} \quad k = 3,6$$

$$\underline{n}_2 = \begin{bmatrix} \cos a_2 & \cos b_2 \\ & \sin b_2 \\ \sin a_2 & \sin b_2 \end{bmatrix} \qquad \underline{n}_5 = \begin{bmatrix} \cos a_5 & \cos b_5 \\ & \sin b_5 \\ -\sin a_5 & \cos b_5 \end{bmatrix}$$

where

a_k = cant angle with respect to x_b axis of sail k

b_k = pitch angle about longitudinal axis of sail k

The vectors from the satellite center of mass to the center of pressure of each sail are:

$$\underline{r}_1 = \begin{bmatrix} -r\cos\psi & -l_s \cdot \sin a_1 \\ r\sin\psi & +l_s \cdot \cos a_1 + y \\ & h \end{bmatrix} \qquad \underline{r}_4 = \begin{bmatrix} r\cos\psi & -l_s \cdot \sin a_4 \\ -r\sin\psi & +l_s \cdot \cos a_4 + y \\ & h \end{bmatrix}$$

$$\underline{r}_2 = \begin{bmatrix} -r\cos\psi & -l_s \cdot \sin a_2 \\ r\sin\psi & \\ h+z & +l_s \cdot \cos a_2 \end{bmatrix} \qquad \underline{r}_5 = \begin{bmatrix} r\cos\psi & -l_s \cdot \sin a_5 \\ -r\sin\psi & \\ -h-z & -l_s \cdot \cos a_5 \end{bmatrix}$$

$$\underline{r}_3 = \begin{bmatrix} -r\cos\psi & -l_s & \sin a_3 \\ r\sin\psi & -l_s & \cos a_3 - y \\ & h & \end{bmatrix} \qquad \underline{r}_6 = \begin{bmatrix} r\cos\psi & -l_s \cdot \sin a_6 \\ r\sin\psi & -l_s \cdot \cos a_6 \\ & h \end{bmatrix}$$

The torque generated by sail k is (in body-fixed axes):

$$\underline{T}_k = \underline{r}_k \times \underline{F}_k = A(1-E_s)\,(2I/c)\,(\underline{n}_k \cdot \underline{s})^2\,(\underline{n}_k \times \underline{r}_k) \qquad k = 1, \ldots 6$$

$$\underline{N}_{body} = \underline{T}_1 + \underline{T}_2 + \underline{T}_3 + \underline{T}_4 + \underline{T}_5 + \underline{T}_6 = \text{total sail torque}$$

and where the dot product of the sun pointing unit vector with each sail normal is carried out assuming all vectors are expressed in body-fixed axes.

APPENDIX D

Antenna Sunlight Disturbance Torques

A. Reflected Sunlight Pressure Torques

In antenna principal axes, vectors from the satellite center of mass to the surface of the antenna are:

$$\underline{r}_1 = -\underline{r}_6 = \begin{bmatrix} r_{ax} \\ 0 \\ 0 \end{bmatrix} \quad \underline{r}_2 = -\underline{r}_4 = \begin{bmatrix} 0 \\ -r_{ay} \\ 0 \end{bmatrix} \quad \underline{r}_3 = -\underline{r}_5 = \begin{bmatrix} 0 \\ 0 \\ -r_{az} \end{bmatrix}$$

The reflected sunlight force on each face of the antenna is

$$\underline{F}^r_{ka} = A_k(1-E_{sk})\,(2I/c)\,(\underline{s} \cdot \underline{n}_k)^2\,(-\underline{n}_k) \qquad k = 1,\ldots,6$$

where

A_k = surface area of face k, k = 1,...,6

E_{sk} = emissivity of surface k

$\underline{n}_k$ = unit normal vector outward from surface k in X_a-Y_a-Z_a

$\underline{s}$ = sun-pointing vector in antenna principal axes

The reflected sunlight torque due to each face is (in X_a-Y_a-Z_a)

$$\underline{T}^r_{ka} = \underline{r}_k \times \underline{F}^r_{ka} = A_k(1-E_{sk})\,(2I/c)\,(\underline{s} \cdot \underline{n}_k)^2\,(\underline{n}_k \times \underline{r}_k)$$

The total reflected sunlight torque due to the antenna in body-fixed axes X_b-Y_b-Z_b is then

$$\underline{T}^r_{ant} = \underline{A}^a_b\,\underline{T}^r_{a\,\text{total}} \qquad \underline{T}^r_{\text{total}} = \underline{T}^r_{1a} + \underline{T}^r_{2a} + \underline{T}^r_{3a} + \underline{T}^r_{4a} + \underline{T}^r_{5a} + \underline{T}^r_{6a}$$

B. Absorbed Sunlight Pressure Torques

Sunlight being absorbed by a surface it strikes causes a force to be generated.

$$\underline{F}_{absorbed} = A\ B\ (I/c)\ (\underline{s} \cdot \underline{n})\ (-\underline{s})$$

where

A = surface area of surface

B = absorptivity of surface

I = solar pressure constant = 1380 watts/meter^2

$\underline{c}$ = speed of light in vacuum = 3×10^8 meters/sec

$\underline{s}$ = unit vector pointed at sun

$\underline{n}$ = unit normal vector outward from surface

The absorbed sunlight pressure force on each face of the antenna in antenna principal axes is then:

$$\underline{F}^a_{ka} = A_k\ B_k\ (I/c)\ (\underline{s} \cdot \underline{n})\ (-\underline{s})$$

where

B_k = absorptivity of surface k

The absorbed sunlight torque due to surface k in antenna axes is:

$$\underline{T}^a_{ka} = \underline{r}_k \times \underline{F}^a_{ka} = A_k\ B_k\ (I/c)\ (\underline{s} \cdot \underline{n}_k)\ (\underline{s} \times \underline{r}_k)$$

The total absorbed sunlight torque due to the antenna is the vector sum of the individual surface torques.

C. Reradiated Sunlight Pressure Torques

Sunlight being reradiated by a surface it strikes generates a force:

$$\underline{F}_{reradiated} = A\,(I_R/c)\,(-\underline{n})$$

where

A = Surface area of surface

I_R = intensity of reradiated sunlight

c = speed of light in vacuum = 3×10^8 meters/sec

$\underline{n}$ = unit normal vector outward from surface

To find I_R, the temperature on the surface must be found as a function of time, then the Stefan-Boltzmann formula must be used to find I_R:

$$I_R = E_s\, T^4(t)\, \sigma$$

E_s = emissivity of

σ = Stefan-Boltzmann constant

T = surface temperature

Final Note: When sunlight does not strike a surface, there is no reflected or absorbed force. Each of the forces in sections A and B for a given surface are multiplied by a function which is one when the surface is struck by sunlight and zero when it is not; this shadowing factor was included in the graphs of the reflected and absorbed antenna sunlight torques (Figures 4.4 and 4.5).

Chapter Five

Summary and New Directions

5.1. Summary

The principal theme of this research program has been rigid body mechanics, as applied to space satellites. The study was broken down into three sections.

The first section developed a four-dimensional space-time formulation of Newtonian mechanics. The equations of motion for a particle, a point with mass m, were found to be:

$$\frac{d}{dt} p_x = F_x \qquad \frac{d}{dt}(y_o p_z - z_o p_y) = y_o F_z - z_o F_y \qquad \frac{d}{dt}(t_o p_x - m x_o) = t_o F_x$$

$$\frac{d}{dt} p_y = F_y \qquad \frac{d}{dt}(z_o p_x - x_o p_z) = z_o F_x - x_o F_z \qquad \frac{d}{dt}(t_o p_y - m y_o) = t_o F_y$$

$$\frac{d}{dt} p_z = F_z \qquad \frac{d}{dt}(x_o p_y - y_o p_x) = x_o F_y - y_o F_x \qquad \frac{d}{dt}(t_o p_z - m z_o) = t_o F_z$$

$$\frac{d}{dt} m = 0$$

where (x_o, y_o, z_o) are the spatial coordinates of the particle, (p_x, p_y, p_z, m) is the linear momentum of the particle, and (F_x, F_y, F_z) are the forces acting on the particle, with all variables measured in a right-handed Cartesian inertial coordinate frame at the same instant of time t_o. The first four equations describe how the time rate of change of the linear momentum is related to forces, while the last six describe how the time rate of change of the total angular momentum of the particle, the moment about the space-time origin of the linear momentum, is related to forces. When no forces act on the particle, the four components of the linear momentum and the six components of the total angular momentum are all constant. Noether(21) showed through a Lagrangian

formulation of mechanics as well as a calculus of variations argument that these are the only ten quantities conserved when no forces act on the point mass; the formulation of mechanics presented here complements this viewpoint, and is perhaps more straightforward and offers greater physical insight into the nature of the conservation laws.

The second section developed a new method for estimating the three angles which specify the spatial orientation of a rigid body, from observations of direction cosines and quaternions. The method presented is analogous to phase-locked-loop phase estimation, but is a generalization to three dimensions of phase-lock techniques, and is not simply three "one-dimensional" phase-locked loops. Two ways to implement this method, one based on direction cosines, the other on quaternions, were discussed for two specific examples, fixed orientation to space and constant rate of change of the three angles. The theoretical deterministic performance limits of each implementation were addressed: first, an analysis of the dynamics of each implementation for small estimation errors was carried out, and second, the steady state and stable equilibrium points of each scheme were discussed. When noise was included in each implementation the theoretical stochastic performance limits were quite difficult to pin down; in particular, Fokker-Planck equations could be derived for each example under certain simplifying assumptions about the nature of the noise, but they could not be solved. However, for a special set of conditions, with a quaternion based method for estimating the unknown phases of the three angles as the angles change at a constant known rate with

time, the Fokker-Planck equation was solved explicitly for the steady state error probability density. All theoretical analyses, both deterministic and stochastic, were backed up by extensive computer simulation.

The third section was concerned with the attitude control dynamics of two specific communication satellites, each using sunlight pressure to generate attitude control torques. Large reflecting surfaces, called solar sails, were attached to each satellite; by canting the sails in different directions, sunlight pressure torques were produced which corrected pointing errors. The equations of motion for each design were derived, and then linearized about a nominal trajectory, and the linearized equations were analyzed using standard linear system theory techniques. The attitude of each design was determined from sun and earth sensor measurements. A heuristic bang-bang control law which governed when and how to cant the sails was developed. Five types of disturbance torques were identified, the largest of which is due to the earth's gravitational field, and were shown to be much smaller than sunlight pressure attitude control torques. Extensive computer simulation of the total equations of motion for each design, typically with a small initial pointing error, confirmed the theoretical analysis of the linearized equations of motion.

5.2. New Directions

Several topics for further research are now outlined. These topics are grouped into the same three areas discussed in the main body of this report, in keeping with the central theme of developing a greater understanding into space satellite dynamics with applications to sunlight pressure attitude control.

1. Deterministic Rigid Body Mechanics

At the present time a mathematically rigorous theory of finite-dimensional linear systems exists, which has found wide application to many practical problems (e.g., problems arising in engineering and physics). At the same time, a mathematically rigorous theory of rigid body mechanics does not yet exist, but it would be useful in the design of practical attitude control systems for space satellites. Just as linear system theory has both qualitative and quantitative aspects, so would a theory for rigid body mechanics.

A qualitative theory of rigid body mechanics would presumably draw on differential geometry and differentiable manifold theory, Lie algebras and Lie groups, as well as geometry and topology, in addressing such issues as controllability and observability of a space satellite, as well as questions of stability. One example in which such a theory might prove of immediate use is the design of control laws for despinning space satellites from high spin rates just after injection into earth orbit down to much lower spin rates. A second example where this type of theory might find immediate application is in the question of the stability of a dual-spin space satellite.

A quantitative theory of rigid body mechanics would be concerned with at least two areas. The first is the application of digital computers and numerical techniques to questions such as numerical integration of rigid body equations of motion and optimal control laws for arbitrary space satellites. The second area is complex variable analysis. Elliptic functions and action angle variables play a key role in classical quantitative rigid body mechanics;

Hua(35) and Klein and Sommerfeld(16) have indicated this role might be more significant than previously expected. Many problems in complex variable theory are analytically intractable, and perhaps can be solved numerically.

Finally, how these threads of both qualitative and quantitative rigid body mechanics can be knotted together into a unified theory of rigid body mechanics, which would complement and lend insight to each other, remains to be seen.

2. Stochastic Rigid Body Mechanics

A natural extension of a deterministic theory of rigid body mechanics is to allow position, linear and angular momentum, and forces to be characterized as random processes. One example of this was discussed in the section on attitude estimation, where it was observed that both direction cosines and quaternions could be considered as matrix exponentials of random processes. Three broad areas for further research into random processes and rigid body mechanics are now outlined:

i) Several extensions of the work presented here, estimating the three angles which specify the orientation in space of a rigid body, come to mind. First, can the method presented here be extended to estimate the three angles if, for example the angular velocity is an arbitrary function of time, rather than the two specific examples discussed. Second, can that branch of information theory known as rate distortion theory be used to provide ultimate performance limitations for estimating the three angles in the two specific examples already

discussed, much as this theory has been used to point out performance limitations in phase-locked-loop phase estimation (see Van Trees(47)). Third, how do quantization of observations (either direction cosines or quaternions) affect performance. Fourth, how is performance affected by sampling the observations at discrete instants of time, as compared to continuously observing spatial attitude.

ii) A precise mathematical characterization of random processes found in rigid body mechanics is needed; since the problems encountered in mechanics are frequently nonlinear, mathematical rigor should aid in this characterization. Ito(36) and McKean(41) have carried out some preliminary work in this area. To be of practical use, their work must be related to observations made by actual attitude sensors; the section on solar pressure attitude control discussed sun and earth sensors, which are not yet adequately theoretically characterized, and which are not covered by Ito's or McKean's work. Another question of practical interest is how a force, which is a random process (e.g., disturbance torques in a gyroscope based attitude sensing scheme) influences attitude estimation (e.g., the three roll-pitch-yaw angles discussed earlier).

iii) A large body of mathematical literature exists on partial differential equations and properties of their solutions, both qualitative and quantitative. In particular, the Fokker-Planck equation has been extensively studied, as has abstract harmonic analysis, and the relationship of solutions of partial differential equations to representations of those Lie groups and Lie algebras associated with spatial orientations. How this literature might help answer the question of what the optimal attitude estimation procedure is for processing noisy observations of space satellite orientation remains to be seen (see Evans(30)).

3. Sunlight Pressure Attitude Control

The intent of the third section of this report was to demonstrate the feasibility of a particular example of three-axis attitude control which used sunlight pressure to generate attitude control torques. Two specific designs were discussed, but perhaps there are other designs than those presented here which take better advantage of the technological constraints associated with space satellite design. The question of whether or not light weight rigid solar sails with the correct surface properties can actually be built has never been adequately answered; an adequate answer would be to actually construct and test in space a satellite which used torques generated by sunlight striking solar sails to control its attitude., and to the best of the author's knowledge, this has not been done for any earth orbiting space satellite. In particular,

one question that must be answered is how serious is sail flexing and bending apt to be and how much might this inference with attitud: control dynamcis. Finally, can the same sails used for attitude control be used to station a synchronous equatorial orbit satellite over one spot on the earth's equator, in spite of irregularities in the earth's gravitational field.

Bibliography

A. Theoretical Rigid Body Mechanics

1. R. Abraham, Foundations of Mechanics, W. A. Benjamin, N.Y. (1967)

2. E. Bessel-Hagen, "Über Die Erhaltungssätze Der Elektrodynamik," Math. Ann., 84, pp. 258-276 (1921)

3. E. Cartan, "Sur Les Varietes A Connexion Affine et la Theorie de la Relativite Generalisee," Ann. Ec. Norm. (3), 40, pp. 329-359 (1923)

4. E. Cartan, Geometrie Des Espaces de Riemann, Gauthier-Villars, Paris (1946)

5. H. B. G. Casimir, Rotation of a Rigid Body in Quantum Mechanics, J. B. Wolter's, the Hague, The Netherlands (1931)

6. C. Chevalley, Theory of Lie Groups I, Princeton Univ. Press, Princeton, N.J. (1946)

7. H. Flanders, Differential Forms, Academic Press, N.Y. (1963)

8. V. Fock, "Zur Theorie Des Wasserstoffsatoms," Zeit, Physik, 98, pp. 145-154 (1936)

9. H. Freudenthal, H. de Vries, Linear Lie Groups, Academic Press, N.Y. (1969)

10. H. Goldstein, Classical Mechanics, Addison-Wesley, Reading, Mass. (1950)

11. W. Greub, Multilinear Algebra, Springer-Verlag, N.Y. (1967)

12. Y. Hagihara, Celestial Mechanics, Vol. I: Dynamical Principles and Transformation Theory, M.I.T. Press, Cambridge, Mass. (1970)

13. S. Helgason, Differential Geometry and Symmetric Spaces, Academic Press, N.Y. (1962)

14. N. Jacobson, Lie Algebras, Wiley Interscience, N.Y. (1962)

15. F. Klein, Vorlesungen Über Höhere Geometrie, Springer, Berhn (1962)

16. F. Klein, A. Sommerfeld, Theorie Des Kreisels, Teuber, Leipzig (1897)

17. S. MacLane, G. Birkhoff, Algebra, MacMillan, London (1967)

18. G. McCarty, Topology, McGraw-Hill, N. Y. (1967)

19. J. Moser, "Regularization of Kepler's Problem and the Averaging Method on a Manifold," Comm. Pure Appl. Math. 23, pp. 609-636 (1970)

20. E. Nelson, Tensor Analysis, Math. Notes, Princeton Univ. Press, Princeton, N. J. (1967)

21. E. Noether, "Invariante Variations Problems," Gott. Nachr., pp. 235-357 (1918)

22. R. Penrose, "Structure of Space-Time," in Battelle Rencontres, 1967 Lectures in Mathematics and Physics, C. deWitt, J. Wheeler (Eds.), W. A. Benjamin, N. Y. pp. 121-235 (1968)

23. A. Saenz, "On integrals of Motion of the Runge Type in Classical and Quantum Mechanics," U. of Michigan, Ph.D. Physics Dissertation (June, 1949)

24. H. Samelson, "Topology of Lie Groups," Bull. Am. Math. Soc., 58, pp. 2-37 (1952)

25. H. Samelson, Notes on Lie Algebras, Van Nostrand Reinhold, N. Y. (1969)

26. A. Trautman, "Noether Equations and Conservation Laws," Comm. Math. Phys., 6, pp. 248-261 (1967)

27. F. Warner, Foundations of Differentiable Manifolds and Lie Groups Scott Foresman, Glenview, Illinois (1971(

28. E. Whittaker, Analytical Dynamics of Particles and Rigid Bodies, Cambridge University Press, London (1965)

B. Attitude Estimation

29. S. Bochner, "Positive Zonal Functions on Spheres," Proc. Nat. Acad. Sci. U.S.A., 40, pp. 1141-1147 (1954)

30. J. Evans, "Chernoff Bounds on the Error Probability for the Detection of Non-Gaussian Signals," M.I.T. Elec. Eng. Sc.D. Dissertation (June, 1971)

31. P. Frost, T. Kailath, "An Innovations Approach to Least-Squares Estimation--Part III: Nonlinear Estimation in White Gaussian Noise," I.E.E.E. Trans. Auto. Con., AC-16, pp. 217-226 (1971)

32. H. Furstenberg, "A Poisson Formula for Semi-Simple Lie Groups," Ann. Math., 77, pp. 335-386 (1963)

33. R. Gangoli, "On the Construction of Certain Diffusions on a Differentiable Manifold," Z. Wahrscheinlichkeitstheorie, 2, pp. 406-419 (1964)

34. T. Hida, "Canonical Representations of Gaussian Processes and Their Applications," Mem. Col. Sci., Univ. Kyoto (A), 33, 1, pp. 109-166 (1960)

35. I. K. Hua, Harmonic Analysis of Functions of Several Complex Variables in the Classical Domains, Trans. Math. Mon., Vol. 6, A.M.S., Providence, R. I. (1963)

36. K. Ito, "Brownian Motion in a Lie Group," Proc. Japan Acad., 26, pp. 4-10 (1950)

37. K. Ito, H. McKean, Diffusion Processes and Their Sample Paths, pp. 269-276, Academic Press, N.Y. (1965)

38. K. Ito, "The Brownian Motion and Tensor Fields on Riemannian Manifold," Proc. Int. Cong. Math., Djursholm, Sweden, pp. 536-539 (1962)

39. A. Jazwinski, Stochastic Processes and Filtering Theory, Academic Press, N. Y. (1970)

40. S. Karlin, J. McGregor, "Classical Diffusion Processes and Total Positivity," J. Math. Anal. Appl., 1, pp. 163-183 (1960)

41. H. McKean, "Brownian Motions on the 3-Dimensional Rotation Group," Mem. Col. Sci., Univ. Kyota (A), 33, 1, pp. 25-38 (1960)

42. H. McKean, "Brownian Motion With a Several-Dimensional Time," Theory Prob. Appl., 8,4, pp. 335-354 (1963)

43. H. McKean, "The Bessel Motion and a Singular Integral Equations," Mem. Col. Sci., Univ. Kyoto (A), 33,2, pp. 317-322 (1960)

44. H. McKean, Stochastic Integrals, Academic Press, N.Y. (1969)

45. F. Perrin, "Mouvement Brownien de Rotation," Ann. Ec. Norm. (3), 45, pp. 1-51 (1928)

46. D. Snyder, The State Variable Approach to Continuous Estimation, M.I.T. Press, Cambridge, Mass. (1969)

47. H. Van Trees, Detection Estimation, and Modulation Theory, Part II: Nonlinear Modulation Theory, Wiley, N. Y. (1971)

48. A. Viterbi, Principles of Coherent Communication, McGraw Hill, N. Y. (1966)

49. E. Wong, J. Thomas, "On Polynomial Expansions of Second Order Distributions," J.S.I.A.M., 10, pp. 507-516 (1962)

50. E. Wong, "The Construction of a Class of Stationary Markoff Processes," Proc. Symp. Appl. Math., Vol. 16, Stochastic Processes in Mathematical Physics and Engineering, A.M.S., Providence, R. I. (1964)

51. E. Wong, Stochastic Processes in Information and Dynamical Systems, McGraw Hill, N. Y. (1971)

52. A. Yaglom, "Second Order Homogeneous Random Fields," Proc. Fourth Berkeley Symp. Math. Stat. Prob., Vol. 2, Contributions to Probability Theory, J. Neyman (ed.), U. Cal. Press, Berkeley (1961)

C. Solar Pressure Attitude Control

53. J. Abel, "Attitude Control and Structural Response Interaction," JPL Report 32-1461 (1970)

54. M. Athans, P. Falb, Optimal Control, McGraw Hill, N. Y. (1966)

55. G. Fleischer, "Multi-Rigid Body Attitude Dynamics Simulation," JPL Report 32-1516 (1971)

56. I. Flugge-Lotz, Discontinuous and Optimal Control, McGraw Hill, N. Y. (1968)

57. Goddard Space Flight Center, "A Conceptual Study of a UHF-VHF Hybrid Satellite for a Delta Launch Vehicle," Internal Memo (1970)

58. P. Likins, "Dynamics and Control of Flexible Space Vehicles," JPL Report 32-1329 (1970)

59. D. C. MacLellan, H. A. MacDonald, P. Waldron, H. Sherman, "Lincoln Experimental Satellites 5 and 6," AIAA 3rd Com. Sat. Conf., Los Angeles, California, 6-8 April 1970

60. M.I.T. Center for Space Research, "Electrically-Steerable L-Band Satellite Antenna," Report 70-8 (1970)

61. W. E. Morrow, ed., "Satellite Communications--Special Issues," Proc. IEEE, 59, 2 (1971)

62. C. Much, N. Smith, F. Floyd, E. Swenson, "LES-8/9 Attitude Control System Numerical Simulation," M.I.T. Lincoln Lab. Tech. Note 1971-10 (1971)

63. National Aeronautics and Space Administration, Spacecraft Radiation Torques, NASA SP-8027 (1969)

64. R. Naumann, "The Near Earth Meteoroid Environment," NASA TN D-3717 (1966)

65. R. Nidney, "Gravity Torque on a Satellite of Arbitrary Shape," ARS Journal, 30, 2, p. 203 (1960)

66. L. Nguyen, "Three Axis Orientation and Stabilization of a Probe Using Solar Pressure," M.I.T. CSR Report T-70-4 (1970)

67. R. Sohn, "Attitude Stabilization by Means of Solar Radiation Pressure," ARS Journal, 29, 5, p. 368 (1959)

68. N. Trudeau, F. Sarles, B. Howland, "Visible Light Sensors for Circular Near Equatorial Orbits," AIAA 3rd Com. Sat. Conf., Los Angeles, Cal., 6-8 April 1970

Biographical Note

Barton W. Stuck was born in [redacted], on [redacted]. He attended Grosse Pointe High School in Grosse Pointe, Michigan, graduating 2nd out of a class of 781 in 1964. He received the degrees of Bachelor of Science and Master of Science, both in Electrical Engineering, from M.I.T. in 1969, and the Electrical Engineer degree from M.I.T. in 1970. During the 1968-69 school year he was supported in his studies by a Katherine Tuck Scholarship. From 1969 to 1972 he was a Teaching Assistant in the Electrical Engineering Department, except for the summer of 1971 and the spring term of 1972, when he held National Science Foundation Traineeships.

His summer job experience includes work at the Bendix Research Laboratories in 1966, IBM Systems Development Division in 1967, M.I.T. Lincoln Laboratory in 1968, Hughes Aircraft Company in 1969, and M.I.T. Lincoln Laboratory in 1970.